
TÜRKİYE CUMHURİYETİ'NİN YÜZÜNCÜ YILI
ADVANCES IN AUTOMOTIVE AND MATERIAL ENGINEERING: INNOVATIONS IN DESIGN, MANUFACTURING AND PERFORMANCE
Editör
Hasan Köten
BİDGE

BIDGE Publications

Advances in Automotive and Material Engineering: Innovations in Design, Manufacturing, and Performance

Editor: Prof. Dr. Hasan Köten

ISBN: 978-625-372-443-6

Page Layout: Gözde YÜCEL

1st Edition:

Publication Date: 25.12.2024

BIDGE Publications,

Certificate No: 71374

www.bidgeyayinlari.com.tr - bidgeyayinlari@gmail.com

Krc Bilişim Ticaret ve Organizasyon Ltd. Şti.

Güzeltepe Mahallesi Abidin Daver Sokak Sefer Apartmanı No: 7/9 Çankaya / Ankara

Content

CHAPTER I

A Numerical Approach to Simulatıon of the Bolt-Spring Connections of Vehicle Seat for Collisions

Mehmet ÇALIŞKAN[1]
Murat KARABEKTAŞ

1. Introduction

The automotive industry now plays an important role in developed and developing countries. This can be seen by the way that countries that have a say in the automotive sector are giving increasing importance to technological development in the industry in order to expand their market share (Eraslan, Cibelek &Polat, 2014). A strong automotive sector is seen as one of the common characteristics of industrialized countries. In order for the automotive industry to sustain this active power, products with added value should be developed and improved, that is, they should have advantages in terms of technology, design, and safety. This

[1] Prof. Dr., Sakarya Uygulamalı Bilimler Üniversitesi, Teknoloji Fakültesi, Makine Mühendisliği Bölümü ORCID ID: 0000-0002-7835-9414

shows the importance of R&D (Research and Development) activities.

Expectations from the automotive industry have increased greatly in recent times. One of the most important factors of this has been the increased importance given to outputs like security and design by individuals with increased economic welfare. However, legal regulations in areas such as security and the increase in the industry's know-how have also paved the way for rapid progress. This dynamic system is required to develop continuously, acting fast with regards to the new innovations and quickly introducing the new product alternatives to the customer. With all this, a significant effort is required in the design and verification phases of a successful product development process for an optimized. Nowadays, the design of a car, the development of this design with the help of analysis programs, and the construction of the mass production stages of the created design prototype have become a rather complicated process. The legislations of the leading countries in the industry have guided the important strides made in the history of automobile development. A standard is defined as; a number of definitions and conditions set up to achieve and maintain the compatibility, efficiency, and specified quality levels of parts, materials or processes (Budynas & Nispett, 2020). Manufacturers are constantly under pressure as states regularly update the minimum standards that cars should have. The legislation of developing countries is generally based on the legislation of the countries that have completed their development in this field. For example, in Europe, UNECE (United Nations Economic Commission for Europe) regulations apply. These regulations are taken as a reference for vehicles that are to be sent to Europe post-production from any

country. These vehicles, which will be exported to the United States, must be able to meet the requirements under the "Federal Motor Vehicle Safety Standards and Rules" defined by the U.S. Department of Transportation For products that will be produced in large quantities (large batches and mass production), their technical and economic characteristics should be fully controlled before full capacity production. This type of production is done using samples and prototypes and often requires many development steps (Pahl, Beitz, Feldhusen & Grote, 2007).

In this case study, a vehicle seat was designed by going through the basic processes above. The vehicle seat is defined as "a structure that can be combined or separate from the vehicle structure, along with accessories designed for an adult person to sit." (Standard, ECE R17). To develop a successful vehicle seat, many inputs and restrictions need to be balanced, such as customer expectations, the requirements set by the vehicles the seat is to be used in and the countries it is to be sold in, ergonomics, impact on vehicle dynamics (driving etc.), whether products can be manufactured or be produced using an assembly line, appearance, weight, investment cost and cost per vehicle.

A seat is subjected to seat belt anchorage test, static loading test, energy distribution test, linear impactor, seat ingress/egress, seat endurance, and fatigue test, h point measurement, lumbar fatigue, structural fatigue, recliner and slide fatigue, sun visor fatigue, climatic for components and vibration anechoic chamber tests. We often can't easily grasp the events around us or solve the problems we face. That's why in order to solve a complex problem we try to make it more understandable by separating it into known or easier

sub-problems. In engineering applications, some problems are impossible to fully solve, and for such problems an approximate solution is accepted (Topcu & Tasgetiren, 1998).

The basic approach in the finite element method is a solution where complex problems are divided into simpler sub-problems, each of which is completely solved within itself. There are three basic attributes in this method. First, the geometrically complex solution region is divided into geometrically simple sub-regions called finite elements. Secondly, continuous functions in each element are considered to be linear combinations of algebraic polynomials. Lastly, obtaining the values of the defined equations that are continuous within each element is sufficient to solve the problem.

As the finite element method and computer technologies have evolved over time, they have become preferred by the industry as they are more accessible than physical tests in terms of costs. Using these technologies, the design stage of the project can be analyzed and optimized and results can be achieved at a minimum time. In this study, we will test the designed seat in a virtual dynamic collision simulation using the finite element method. The findings will then be compared to the criteria that would have to be met in order to mass-produce the designed seat. There have been numerous studies that have conducted vehicle seat analysis using the finite element method (References 6-16).

Past studies have also shown that the vehicle seat design process is quite detailed and is time-consuming. In order to shorten this process, in this study, the selection process of bolts and nuts in

design was carried out with the help of the findings obtained as a result of FEA analyses.

2. Materials and method

Seat Design

The design was created using the ECE R17 regulation as a reference, which contains provisions about the approval of vehicles with regards to design, seats, seat fittings, and headrest locations. The Cad model of the seat was created using the CATIA V5 design program. Since this study was focused on the design structure of the seat and its analysis using finite elements were aimed at the structure design, no work was done on the surface symbolizing the sponge texture of the seat. Furthermore, because the study is a front-impact test and the sponge does not have a significant effect on this type of impact, the study was carried out without the sponge. The floor where the seat was fixed and the hair printed under the dummy's feet were designed and symbolized. With this, the foundation of the design was laid as the first stage. In the later stages, design-optimization and analysis progressed together. In order to strengthen the design, many revisions were made and dozens of simulations were performed. When building the design, one of the two symmetrical sides was designed first and then mirrored with the help of the required datum planes using the 'mirror' mode included in the CATIA V5. The details of some parts of the seat we created the CAD model as shown in Figure 1. The entire CAD design was designed based on the H point belonging to a passenger model vehicle. H point regulations are defined as the theoretical position of a passenger's buttocks or tail somas on the seat. This location is usually determined by car manufacturers and designs are made accordingly. In the study,

a standard dummy was used to represent a human. Rib structure was added to increase the strength in brackets. The ribs were shaped taking into account the direction of the incoming force. The basic foundation needed for the preparation of a finite element model is a geometric model prepared in a CAD program. The model is converted into a finite element model using a FEM program that can perform dynamic analysis. After this conversion process, which is the initial processing phase, dynamic analysis is calculated with the help of a solver. Using a final processor that interprets results, the results obtained from the solver are processed and interpreted. An FEA Model flowchart displays the programs used in our study as shown in Figure 2.

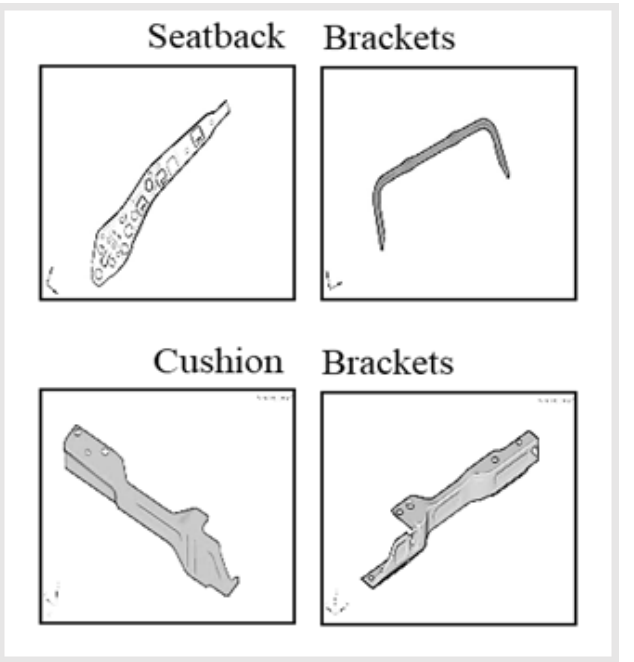

Fig. 1. FEA Model Preparation.

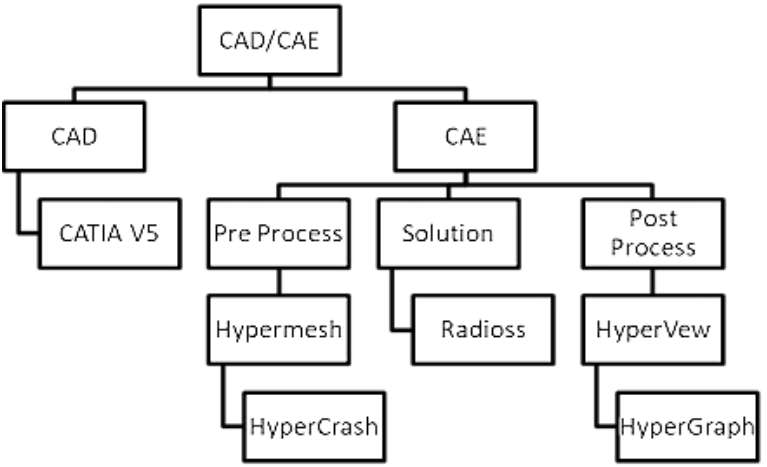

Fig. 2. Flow chart for the correction of the roll forming process design.

FEA Model

In the creation of the finite elements model, the stages can be roughly summarized as follows:

Since Hypermesh offers CATIA V5 data usage support, CAD data can be imported directly. Thus, the transition to the Hypermesh interface is made. Since the entire structure is in sheet-metal format, finite element models are made with the shell element type using midsurface for each piece. Then the mesh model is created. Properties are defined for each part. Property is where the information about the thickness of the material is found

Material identification is made after properties are defined. Material information can be entered either manually or by importing a ready material curve. In this study, some of a seating & interior

company’s ready-made material curves were used. Then, the rigid connection elements are defined. In this study, bolt-nut fasteners were selected and their strength was not checked. Spring element identification was made at these junctions. In other words, the possibility of deformation at those points was defined as not possible. The aim of this is to detect the force that will be on each connection point using the spring element and select the bolt or nut element accordingly, instead of trying different bolt-nut connections and wasting time. The front and side view of the FEA model is shown in Figure 3.

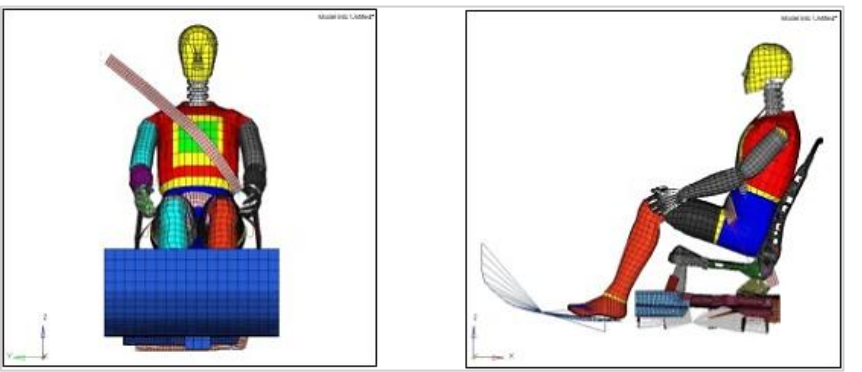

Fig. 3. The front and side view of the FEA model.

For this study, 2 types of the contact surface were identified. One is type 7, which we define as multi-usage, and the other is type 11, which we define as an edge to edge. Each contact acts as an element. Type 11 is used to identify beams, bars, and springs edge-to-edge. Then the data from Hypermesh is exported as a rad file, imported in HyperCrash and border conditions and surface contacts are defined. An important point here is that whichever unit system is used when working with Hypermesh, the same unit system should be defined while importing it to HyperCrash. To create the

acceleration function, it is possible to manually enter values in HyperCrash. It is also possible to import data either from a previously prepared acceleration function or from information received from a customer. In this study, it is used by importing the accelerator function used in the test of the same type of vehicle prepared before. Finally, the process of decoding the data is started on Radioss.

Data Inputs for Dynamic Collision Analysis

The Speed function entered into the program for the simulation is shown in Figure 4.

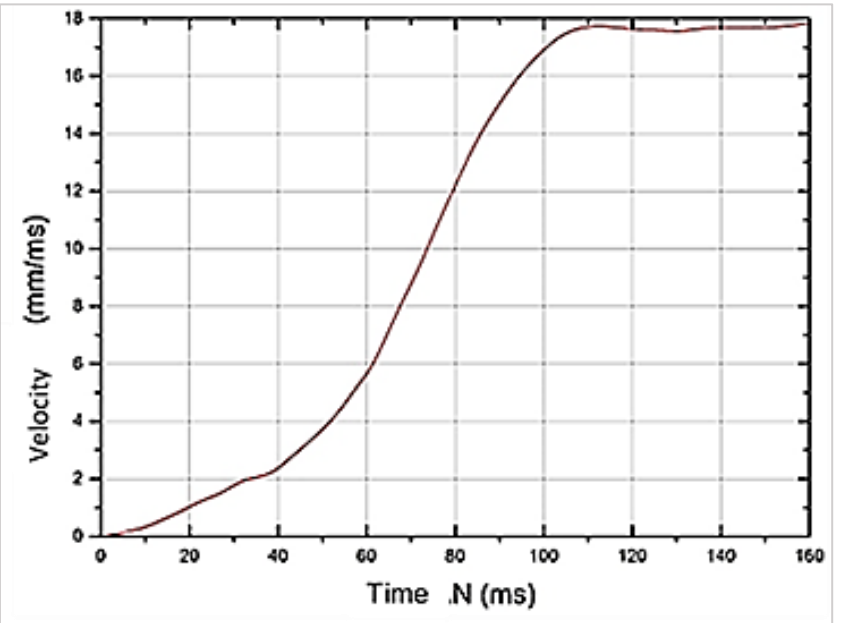

Fig. 4. Speed function entered into the program for the simulation.

The speed change above is defined as the first effect we want the seat to have after the physical collision. This speed corresponds to a speed of approximately 64 kilometers per hour.

3. Analysis results

Radioss program calculates the accuracy of each iteration step proportionally during FEA analysis, giving us information about the accuracy of the solution, and therefore, the inputs and boundary conditions. This rate is defined as a critical value of ±10%. Therefore, by questioning the number of errors that occur during the solution, we can see whether the work is at an acceptable level.

From the following graph, it can be seen that the number of errors is within the range of acceptable values and therefore our analysis has yielded a realistic result as seen in Figure 5. Our analysis shows photos of the seat and dummy's behaviour in different frames as shown in Figure 6.

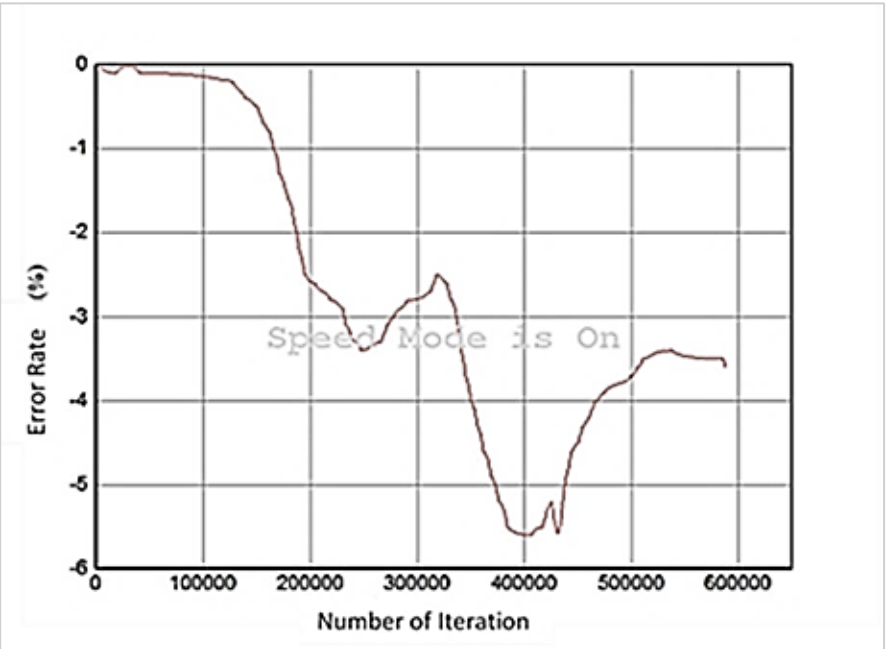

Fig. 5. Convergence graph.

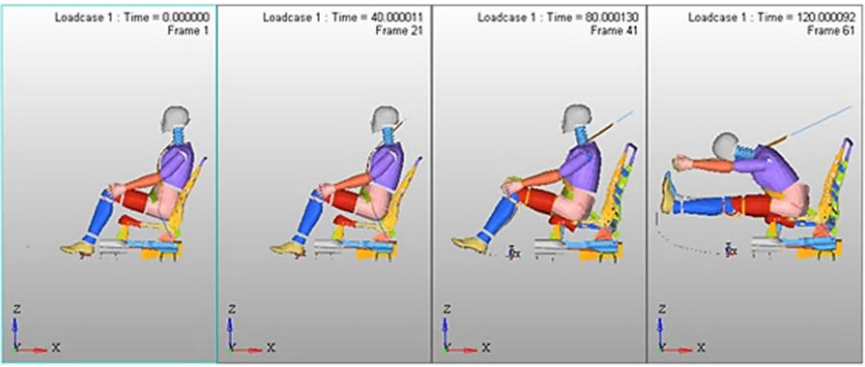

Fig. 6. The attitude of the seat and dummy at different times.

The plastic strain results of the seat from different perspectives are shown in Figure 7.

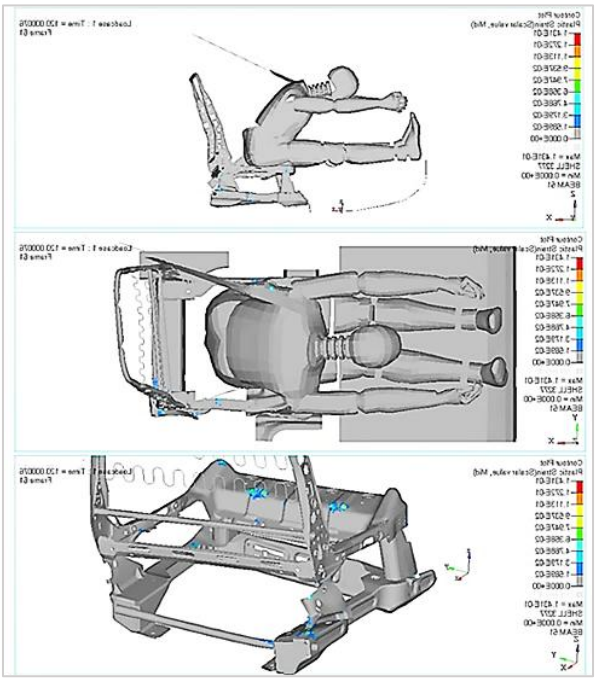

Fig. 7. The plastic strain results of the seat from different perspectives.

The first factor of accidents is undoubtedly human. Because of the fact that the car is the person who uses the vehicle or is affected by the accident of the vehicle, the car companies are constantly working on measures to mitigate the effects of accidents. These measures are defined as passive safety factors. One of the most important components in a seat is undoubtedly the seat belt and its ports. The load on seat belt ports, which have the duty to hold dummy as a passive safety factor due to the impact of a collision, is quite high. Seat belt anchorage points in the FEA model is shown in Figure 8.

Force-Time diagrams for the three points of seat belt anchorage is shown in Figure 9.

As can be noted in the following Figure 10, the area with the highest amount of deformation and displacement on the seat is the area where the seat belt port is connected to one of the brackets on the seat and its surroundings. This is why the design and material selection of these attachments becomes even more important. Change in the back area at the time of collision due to the force on the seat belt is shown in Figure 10.

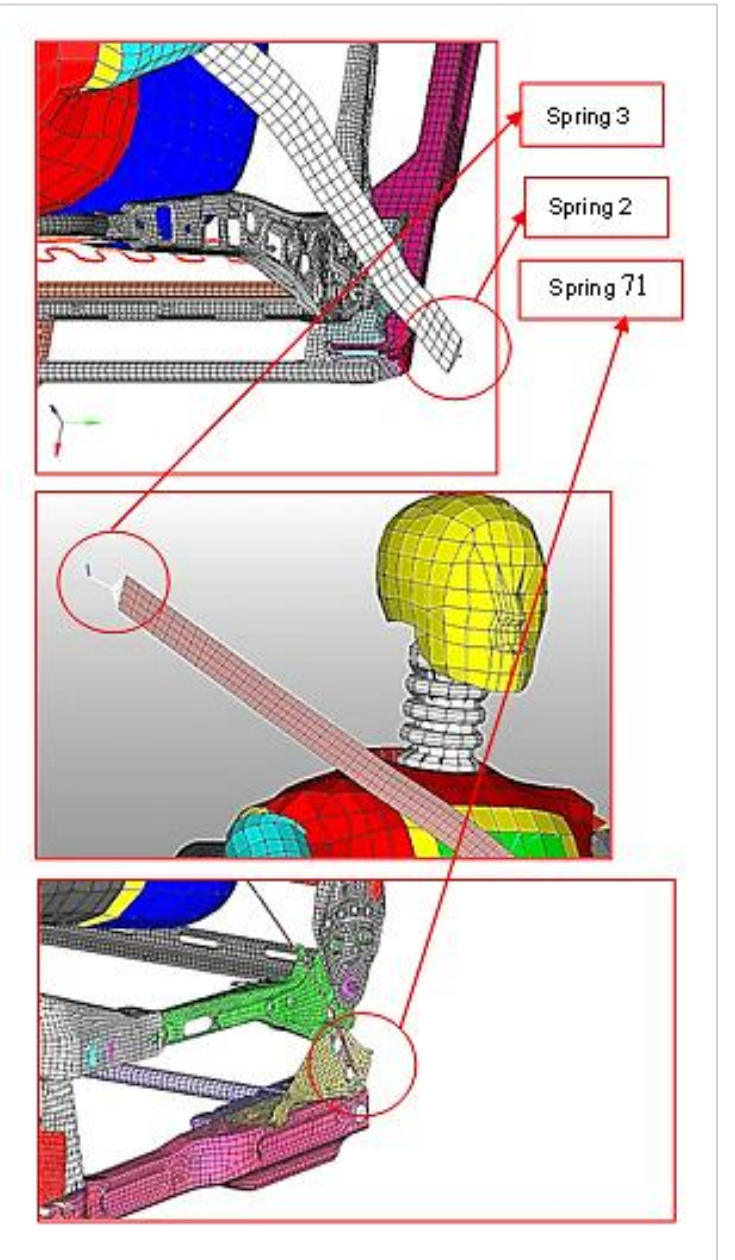

Fig.8. Seat belt anchorage points in the FEA model

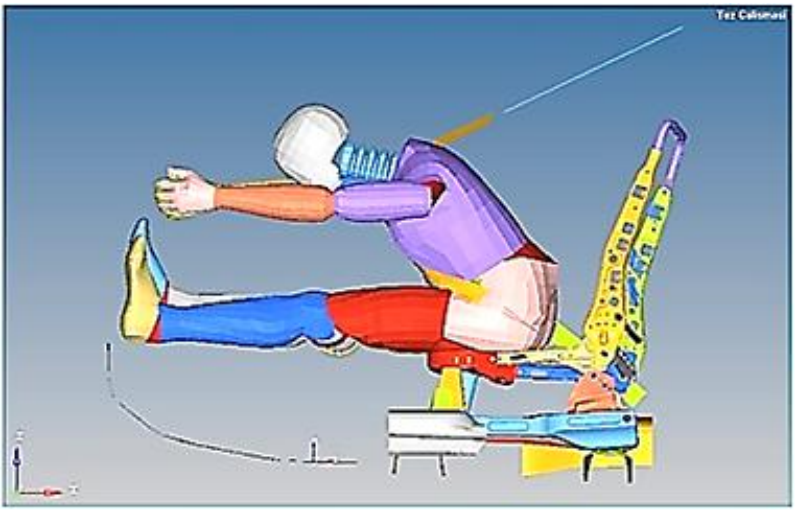

Fig. 9. Change in the back area at the time of collision due to the force on the seat belt.

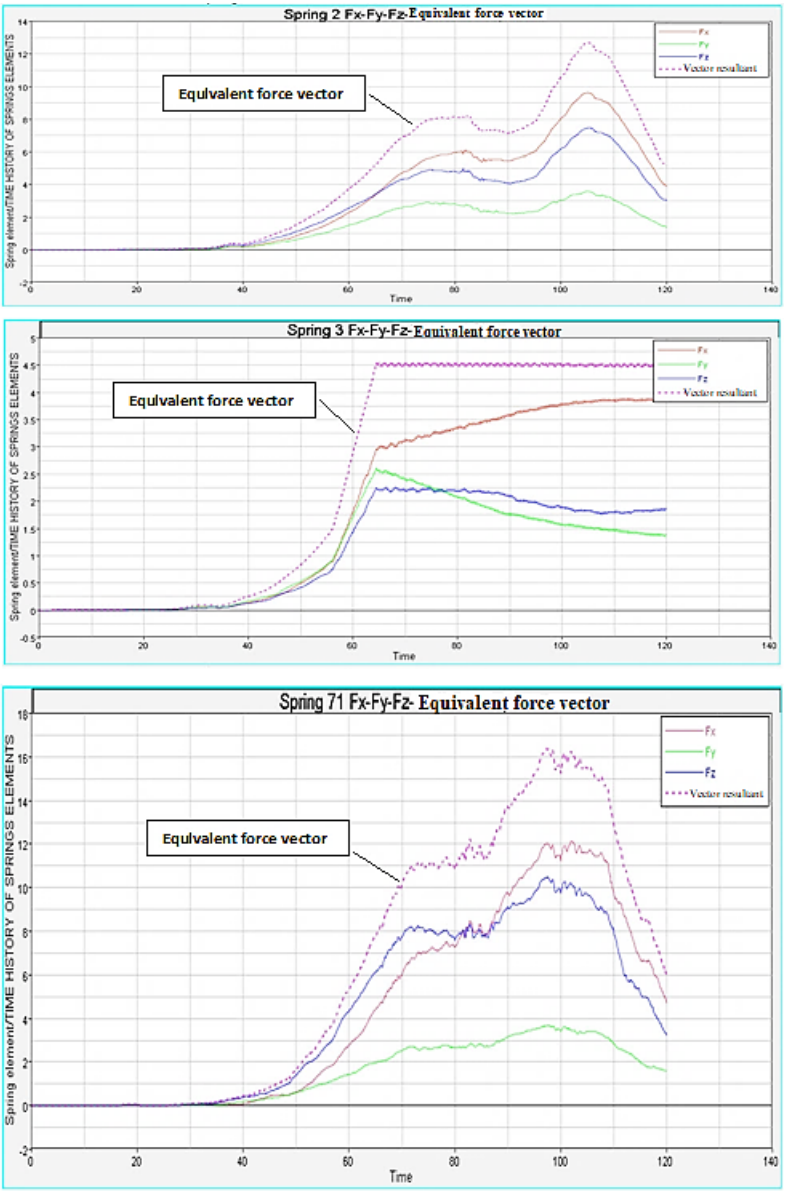

Fig. 10. Force-Time diagrams for the three points of seat belt anchorage.

As mentioned earlier, the strategy we used was to identify bolt-nut connections and accept those regions as rigid, then calculate in the incoming force to those regions to find the resultant force the chosen bolt-nut connection must resist. In other words, in this study, having moved away from the repetition of the trial-and-error method, we analyzed the amount of force coming on to the seat belt connection points, such as bolt-nut connections, and selected products accordingly. This saves us from having to conduct unnecessary repetitions and prevents us from choosing unnecessarily strong products.

The safety attachments are about the force in kN to the seat as much as the force coming to the vehicle ports. The x, y, and z in line with each chart mentioned above define the strength that our seat belt buckle and seat belt fabric must resist. When we examine the above results, the largest force on seat belt buckles is located at the seat belt attachments (≈17 kN). Therefore, the buckle mechanism and belt fabric should have the characteristics that can resist this force. As we have previously described, we have defined spring to bolt-nut ports, adopting rigid sequential and calculating incoming forces, a strategy to find the chip force that the bolt-nut connection must resist. For example, the strength of the force of the junction from springe 53337 is

about 10.5 kN. Therefore, the connection products to be selected for these points should be selected in capable of resisting these loads from each pedestrian. Load-time diagrams of right front floor connection spring and left front floor connection spring are given in Figure 11 and Figure 12 respectively.

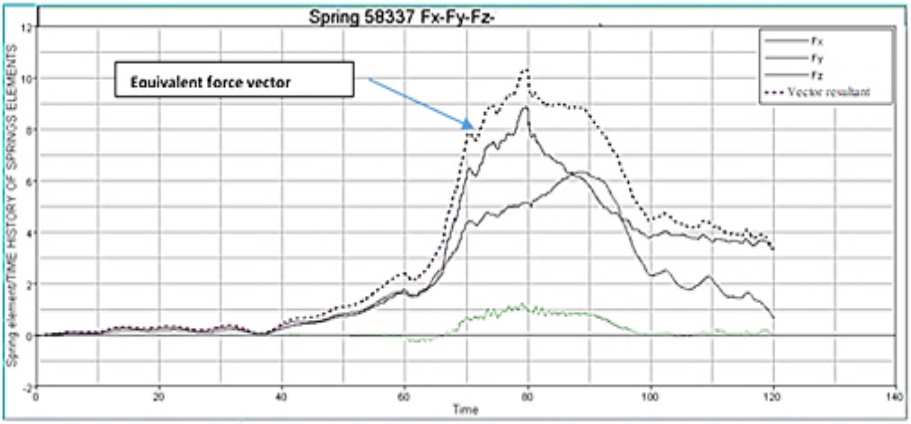

Fig. 11. Load-Time diagram of right front floor connection spring.

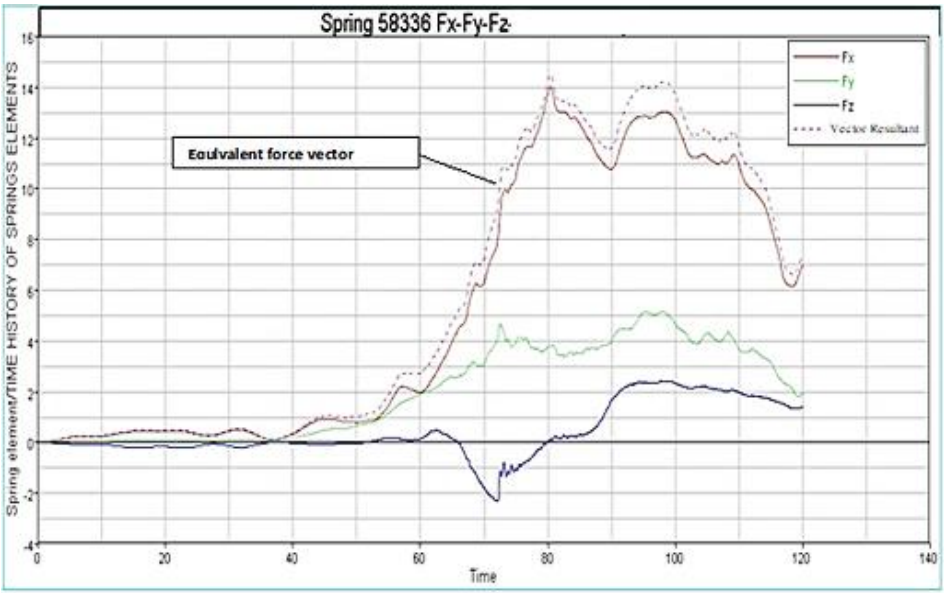

Fig. 12. Load-Time diagram of left front floor connection spring.

Right and left front floor connection spring in the FEA model is shown in Figure 13.

Fig. 13. Right and left front floor connection spring in the FEA model.

4. Discussions

As a result of the integrated execution of the design, optimization and analysis processes of the finite elements model, a number of design changes were made in our study, and after each of these changes, the finite elements model is analyzed and consistent analysis results were obtained in accordance with the acceptance criteria. Since there are no physical products of the study, there is no actual collision test result of this study. When we compare our study with the physical test findings obtained by seat manufacturers who design and conduct the same type of seats, our study is consistent and we have a prototype after physical testing of our study. When we were subjected to positive results.

In addition, an experimental seat test project carried out by a company supported our findings; bolt selection was made with the bolt-spring element simulation approach used in our study, and the results of the test confirmed the bolt-spring element simulation

approach and these are gratifying results that support the study. It has been observed in the entire product development process that a very small design change on the part can cause significant changes in the distribution of forces that act on the part in a positive or negative sense. Or changing the material selected for the part can contribute significantly to the force distribution on the part.

One of the most important points in our study is undoubtedly the approach shown to fasteners such as bolt-nuts. Bolt connections are defined as spring elements in our study. This approach has already shortened the trial-and-error process that is constantly encountered in the design and optimization process and reduced the number of elements used in the SEY model. Bolt-nut connections are considered spring elements and defined as rigid, and the equivalent forces acting on these elements are evaluated and appropriate bolt-nut elements are then selected. This way, the product development process becomes much more time-efficient. Also, this study once again proves the importance and necessity of finite element applications in design and optimization studies.

References

Eraslan M., Cibelek N., and Polat E., Bus Seat Development, 7th Automotive Technologies Congress, Bursa, Turkey, (2014).161-169,

Budynas R. G., and Nispett J. K, Shingley's Mechanical Engineering Design, 11th Ed. McGraw-Hill Education, NY, USA, (2020).

Pahl G., Beitz W., Feldhusen J., and Grote K. H, Engineering Design a Systematic Approach, Springer-Verlag, London, (2007).

ECE R17, Motor vehicles seats, seat fittings and headrest locations, Ankara, Turkey (2002).

Topcu M., and Tasgetiren S., Finite Element Method for Engineers, University of Pamukkale Press, no:7, Denizli (1998).

Sun G., Li G., Zhou S., Li H., Hou S., and Li Q., Crashworthiness design of vehicle by using multiobjective robust optimization, Structural and Multidisciplinary Optimization, (44),1,99-110, (2011).

Youn B. D., Choi K. K., Yang R. J., and Gu L., Reliability-based design optimization for crashworthiness of vehicle side impact, Structural and Multidisciplinary Optimization, 26, (2004) 272–283.

Yildiz R. A, and Solanki N. K., Multi-objective optimization of vehicle crashworthiness using a new particle swarm-based approach, International Journal of Advanced Manufacturing Technology, 59 (2012) 367–376.

Pickett K. A., Pyttel T., Payen F., Lauro N., Petrinic N., Werner H., and Christlein F., Failure prediction for advanced

crashworthiness of transportation vehicles. International Journal of Impact Engineering 30, (2004) 853–872.

Fang H., Rais-Rohani M., Liu Z. and Horstemeyer F. M., A comparative study of metamodeling methods for multiobjective crashworthiness optimization, Computers&Structures 83, (2005) 2121–2136.

Bois P. D., Chou C. C., Fileta B. B., Khalil B. T., King I. A., Mahmood F. H., Mertz J. H. and Wismans J., Vehicle crashworthiness and occupant protection. American Iron and Steel Institute Publications, Southfield, Michigan, (2004).

Hamza K., Hossoy I, Reyes-Luna J. F., and Papalambros P. Y., Combined maximization of interior comfort and frontal crashworthiness in preliminary vehicle design, International Journal of Vehicle Design, 35, (3), (2004) 167-185.

Hou S., Liu T., Dong D., and Han X., Factor screening and multivariable crashworthiness optimization for vehicle side impact by factorial design. Structural and Multidisciplinary Optimization, 49, (1), (2014) 147–167.

Fang H., Solanki K. and Horstemeyer F. M., Numerical simulations of multiple vehicle crashes and multidisciplinary crashworthiness optimization, International Journal of Crashworthiness, 10, (2), (2005).161-172.

Pedersen C. B. W., Crashworthiness design of transient frame structures using topology optimization, Comput. Methods Appl. Mech. Engrg. 193 (2004) 653–678.

Kim E., Fard M., and Kato K. A., seated human model for predicting the coupled human-seat transmissibility exposed to fore-

aft whole-body vibration, Applied Ergonomics, 84, 102929, (2020) 1-9.

Acknowledgement

We would like to thank Mr. Özgür Özlü (Mechanical Engineer MSc), who included this study in his master's thesis at Sakarya University of Applied Sciences, Department of Mechanical Engineering.

CHAPTER II

Effect of Mass and Size on CO2 Emission and Fuel Consumption in Curtain-Sided Semi-Trailer

Ahmet Serdar SERTER[1]

1. INTRODUCTION

Carbon dioxide (CO2) is an important heat-trapping gas, also known as a greenhouse gas, that comes from the extraction and burning of fossil fuels (such as coal, oil, and natural gas), from wildfires, and natural processes like volcanic eruptions (NASA,2024).

The Paris Agreement, shaping the framework of the post-2020 climate change regime, has paved the way for the implementation of new regulations and initiatives in various sectors around the world to minimize carbon emissions, fossil fuel use and other environmental impacts (T.C. Dışişleri Bakanlığı, n.d.).

[1] Makine Mühendisi, Koluman Otomotiv Endüstri A.Ş, Ar-Ge Departmanı, serdar.serter@koluman.com, Orcıd: 0009-0004-4320-7367

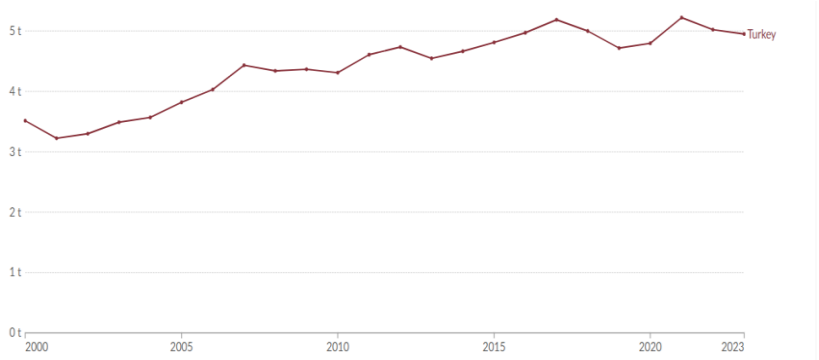

Figure 1. *Per capita CO_2 emissions (Global Carbon Budget,2024; Population based on various sources,2024)*

When we examine the trend of CO2 emissions per capita in Turkey over the years, we see that emissions have gradually increased starting around 2000 and peaked around 2015. This trend reflects the increasing carbon footprint in the country, especially due to industrialization and energy consumption. The values shown in the graph indicate that there has been a steady increase in CO2 emissions per capita and that Turkey's figures will reach around 5 tons per capita in 2023.

In this context, significant efforts are being made, particularly in the trailer category, including curtain-sided closed box, panel-sided closed box, and refrigerated closed box vehicles (O3 and O4 categories), to reduce carbon emissions by enhancing fuel efficiency.

The European Commission, to further its efforts to decrease fuel consumption and CO2 emissions, introduced the VECTO (Vehicle Energy Consumption Calculation Tool) simulation program, which came into effect under EU Regulation 2022/1362 as of January 1, 2024. By July 1, 2024, the use of this simulation

program became mandatory for trailer manufacturers (European Commission, 2022). VECTO provides a realistic and comprehensive simulation, particularly for trailers, by accounting for various parameters such as the effects of aerodynamic wings and side skirts, tire rolling resistance, air drag, weight, size, and inertia. The simulation requires manual input of the vehicle's superstructure dimensions, total height, and volume; changes in these parameters directly influence fuel consumption and carbon emissions.

Given the high fuel consumption and carbon emissions in the trailer category, the design process for vehicle dimensions and weight has become a critical focus area. This study simulates trailers with different dimensions and weights (closed box superstructures) using the VECTO program, comparing fuel consumption and carbon emission values. The results were analyzed to determine efficiency variations under different road conditions.

2. MATERIAL and METHOD

VECTO simulation program was used to compare the fuel consumption and carbon emission values according to the superstructure features of the vehicles. In the simulations, a standard curtainsider box trailer was used as a reference. Compared to the reference vehicle, the superstructure volumes of vehicles that are 1 meter shorter in length, 200 mm lower in height and 500 kg lighter in weight were calculated and simulation inputs were made according to these data.

Figure 2. *Curtain-sided Trailer*

(European Commission, 2022)

Data inputs for the vehicles are presented in Table 1 below:

Table 1. *Data Inputs of Curtain-sided Box Bodies*

Curtain-sided Box Bodies	**Standart**	1 m shorter lenght	200 mm lower height	500 kg lighter weight
External Length of the Body	13.950 m	12.950 m	13.950 m	13.950 m
External Width of the Body	2.550 m	2.550 m	2.550 m	2.550 m
External Height of the Body	2.900 m	2.900 m	2.700 m	2.900 m
Total Height of the trailer	4.000 m	4.000 m	4.000 m	4.000 m
Cargo Volume	103.2 m3	95.8 m3	99.6 m3	103.2 m3
Number of Axles	3	3	3	3
Trailer Type	DA	DA	DA	DA
Bodywork Type	Curtain-Sided	Curtain-Sided	Curtain-Sided	Curtain-Sided
Corrected Mass in Running Order	7200 kg	7200 kg	7200 kg	6700 kg
TPMLM Trailer	39000 kg	39000 kg	39000 kg	39000 kg
TPMLM Axle Assembly	27000 kg	27000 kg	27000 kg	27000 kg
Tyre/Rolling Resistance Coefficient	385/65 R22.5 – 4.0 N/kN	385/65 R22.5 – 4.0 N/kN	385/65 R22.5 – 4.0 N/kN	385/65 R22.5 – 4.0 N/kN

The data is organized according to the pavement characteristics and VECTO input parameters. The simulation results were analyzed to examine the effects of these parameters on fuel consumption and carbon emissions.

3. RESULTS

The VECTO simulation program provided average CO2 emissions and fuel consumption values for a curtain-sided trailer under loaded and unloaded conditions in three different scenarios: long-haul, regional delivery, and urban delivery. This enabled a detailed assessment of the trailer's performance under varying operational conditions. The calculations took into account parameters such as dimensions, weight, aerodynamic devices, and tire characteristics.

The standard curtain-sided trailer was simulated using the VECTO program under three different road conditions, both loaded and unloaded.

As seen in Figure 3, on long-haul routes, the fuel consumption is 22.6 l/100 km while CO_2 emission is 590 g/km when the vehicle is unloaded. On long-haul routes with a loaded vehicle, the fuel consumption is 30.1 l/100 km, and CO_2 emission is 789 g/km.

Long Haul		
Simulation Parameters		
Payload:	2600	kg
Total vehicle mass:	17547	kg
Average speed:	79.7	km/h
Fuel consumption:	22.6	l/100km
Fuel consumption:	0.0868	l/t-km
Fuel consumption:	0.00219	l/m³-km
Fuel consumption:	189	g/km
Fuel consumption:	72.5	g/t-km
Fuel consumption:	1.83	g/m³-km
CO2 emissions:	590	g/km
CO2 emissions:	227.0	g/t-km
CO2 emissions:	5.72	g/m³-km
Efficiency ratio:	0.995	km-based
Efficiency ratio:	0.995	t-km-based
Efficiency ratio:	0.878	m³-km-based
Reference ratio:	0.977	km-based

Long Haul		
Simulation Parameters		
Payload:	19300	kg
Total vehicle mass:	34247	kg
Average speed:	78.4	km/h
Fuel consumption:	30.1	l/100km
Fuel consumption:	0.0156	l/t-km
Fuel consumption:	0.00292	l/m³-km
Fuel consumption:	252	g/km
Fuel consumption:	13.1	g/t-km
Fuel consumption:	2.44	g/m³-km
CO2 emissions:	789	g/km
CO2 emissions:	40.9	g/t-km
CO2 emissions:	7.65	g/m³-km
Efficiency ratio:	0.992	km-based
Efficiency ratio:	0.992	t-km-based
Efficiency ratio:	0.875	m³-km-based
Reference ratio:	1.002	km-based

Figure 3. *Unloaded and Lodaded valuses on Long Haul*

As seen in Figure 4, on regional delivery routes, the fuel consumption is 23.7 l/100 km while CO_2 emission is 620 g/km when the vehicle is unloaded. On regional delivery routes with a loaded vehicle, the fuel consumption is 30.3 l/100 km, and CO_2 emission is 793 g/km.

Regional Delivery		
Simulation Parameters		
Payload:	2600	kg
Total vehicle mass:	17547	kg
Average speed:	60.7	km/h
Fuel consumption:	23.7	l/100km
Fuel consumption:	0.0911	l/t-km
Fuel consumption:	0.00230	l/m³-km
Fuel consumption:	198	g/km
Fuel consumption:	76.2	g/t-km
Fuel consumption:	1.92	g/m³-km
CO2 emissions:	620	g/km
CO2 emissions:	238.4	g/t-km
CO2 emissions:	6.01	g/m³-km
Efficiency ratio:	0.969	km-based
Efficiency ratio:	0.969	t-km-based
Efficiency ratio:	0.855	m³-km-based
Reference ratio:	0.980	km-based

Regional Delivery		
Simulation Parameters		
Payload:	12900	kg
Total vehicle mass:	27847	kg
Average speed:	60.0	km/h
Fuel consumption:	30.3	l/100km
Fuel consumption:	0.0235	l/t-km
Fuel consumption:	0.00294	l/m³-km
Fuel consumption:	253	g/km
Fuel consumption:	19.6	g/t-km
Fuel consumption:	2.45	g/m³-km
CO2 emissions:	793	g/km
CO2 emissions:	61.4	g/t-km
CO2 emissions:	7.68	g/m³-km
Efficiency ratio:	0.976	km-based
Efficiency ratio:	0.976	t-km-based
Efficiency ratio:	0.861	m³-km-based
Reference ratio:	0.994	km-based

Figure 4. *Unloaded and Lodaded valuses on Regional Delivery*

As seen in Figure 5, on urban delivery routes, the fuel consumption is 37.3 l/100 km while CO_2 emission is 976 g/km when the vehicle is unloaded. On urban delivery routes with a loaded vehicle, the fuel consumption is 52.5 l/100 km, and CO_2 emission is 1373 g/km.

Urban Delivery

Simulation Parameters

Payload:	2600	kg
Total vehicle mass:	17547	kg
Average speed:	26.2	km/h

Fuel consumption:	37.3	l/100km
Fuel consumption:	0.143	l/t-km
Fuel consumption:	0.00362	l/m³-km
Fuel consumption:	312	g/km
Fuel consumption:	119.9	g/t-km
Fuel consumption:	3.02	g/m³-km
CO2 emissions:	976	g/km
CO2 emissions:	375.4	g/t-km
CO2 emissions:	9.46	g/m³-km
Efficiency ratio:	0.961	km-based
Efficiency ratio:	0.961	t-km-based
Efficiency ratio:	0.848	m³-km-based
Reference ratio:	0.966	km-based

Urban Delivery

Simulation Parameters

Payload:	12900	kg
Total vehicle mass:	27847	kg
Average speed:	25.7	km/h

Fuel consumption:	52.5	l/100km
Fuel consumption:	0.0407	l/t-km
Fuel consumption:	0.00509	l/m³-km
Fuel consumption:	439	g/km
Fuel consumption:	34.0	g/t-km
Fuel consumption:	4.25	g/m³-km
CO2 emissions:	1373	g/km
CO2 emissions:	106.4	g/t-km
CO2 emissions:	13.31	g/m³-km
Efficiency ratio:	0.971	km-based
Efficiency ratio:	0.971	t-km-based
Efficiency ratio:	0.857	m³-km-based
Reference ratio:	0.977	km-based

Figure 5. *Unloaded and Lodaded valuses on Urban Delivery*

As shown in Figure 6, the average CO2 emissions for a standard curtain-sided trailer is 730 g/km, and the fuel consumption is 27.9 l/100 km. These values represent the baseline performance for the standard configuration under typical operating conditions.

Weighted Results		
Payload:	13842	kg
Fuel consumption:	27.9	l/100km
Fuel consumption:	0.0202	l/t-km
Fuel consumption:	0.00271	l/m³-km
Fuel consumption:	233.3	g/km
Fuel consumption:	16.9	g/t-km
Fuel consumption:	2.26	g/m³-km
CO2 emissions:	730	g/km
CO2 emissions:	52.8	g/t-km
CO2 emissions:	7.08	g/m³-km
Efficiency ratio:	0.991	km-based
Efficiency ratio:	0.991	t-km-based
Efficiency ratio:	0.874	m³-km-based

Figure 6. *Average Values of Standard Curtain-sided Trailer*

1-meter shorter length curtain-sided trailer was simulated using the VECTO program under three different road conditions, both loaded and unloaded.

As seen in Figure 7, on long-haul routes, the fuel consumption is 22.4 l/100 km while CO_2 emission is 587 g/km when the vehicle is unloaded. On long-haul routes with a loaded vehicle, the fuel consumption is 30.0 l/100 km, and CO_2 emission is 786 g/km.

Long Haul

Simulation Parameters

Payload:	2600	kg
Total vehicle mass:	17547	kg
Average speed:	79.7	km/h

Fuel consumption:	22.4	l/100km
Fuel consumption:	0.0862	l/t-km
Fuel consumption:	0.00234	l/m³-km
Fuel consumption:	187	g/km
Fuel consumption:	72.1	g/t-km
Fuel consumption:	1.96	g/m³-km
CO2 emissions:	587	g/km
CO2 emissions:	225.7	g/t-km
CO2 emissions:	6.13	g/m³-km
Efficiency ratio:	0.989	km-based
Efficiency ratio:	0.989	t-km-based
Efficiency ratio:	0.940	m³-km-based
Reference ratio:	0.977	km-based

Long Haul

Simulation Parameters

Payload:	19300	kg
Total vehicle mass:	34247	kg
Average speed:	78.5	km/h

Fuel consumption:	30.0	l/100km
Fuel consumption:	0.0156	l/t-km
Fuel consumption:	0.00314	l/m³-km
Fuel consumption:	251	g/km
Fuel consumption:	13.0	g/t-km
Fuel consumption:	2.62	g/m³-km
CO2 emissions:	786	g/km
CO2 emissions:	40.7	g/t-km
CO2 emissions:	8.20	g/m³-km
Efficiency ratio:	0.988	km-based
Efficiency ratio:	0.988	t-km-based
Efficiency ratio:	0.939	m³-km-based
Reference ratio:	1.002	km-based

Figure 7. *Unloaded and Lodaded Valuses on Long Haul*

As seen in Figure 8, on regional delivery routes, the fuel consumption is 23.6 l/100 km while CO_2 emission is 617 g/km when the vehicle is unloaded. On regional delivery routes with a loaded vehicle, the fuel consumption is 30.2 l/100 km, and CO_2 emission is 790 g/km.

Regional Delivery

Simulation Parameters

Payload:	2600	kg
Total vehicle mass:	17547	kg
Average speed:	60.6	km/h

Fuel consumption:	23.6	l/100km
Fuel consumption:	0.0907	l/t-km
Fuel consumption:	0.00246	l/m³-km
Fuel consumption:	197	g/km
Fuel consumption:	75.8	g/t-km
Fuel consumption:	2.06	g/m³-km
CO2 emissions:	617	g/km
CO2 emissions:	237.3	g/t-km
CO2 emissions:	6.44	g/m³-km
Efficiency ratio:	0.964	km-based
Efficiency ratio:	0.964	t-km-based
Efficiency ratio:	0.916	m³-km-based
Reference ratio:	0.980	km-based

Regional Delivery

Simulation Parameters

Payload:	12900	kg
Total vehicle mass:	27847	kg
Average speed:	60.2	km/h

Fuel consumption:	30.2	l/100km
Fuel consumption:	0.0234	l/t-km
Fuel consumption:	0.00315	l/m³-km
Fuel consumption:	252	g/km
Fuel consumption:	19.6	g/t-km
Fuel consumption:	2.63	g/m³-km
CO2 emissions:	790	g/km
CO2 emissions:	61.2	g/t-km
CO2 emissions:	8.25	g/m³-km
Efficiency ratio:	0.973	km-based
Efficiency ratio:	0.973	t-km-based
Efficiency ratio:	0.924	m³-km-based
Reference ratio:	0.994	km-based

Figure 8. *Unloaded and Lodaded Valuses on Regional Delivery*

As seen in Figure 9, on urban delivery routes, the fuel consumption is 37.3 l/100 km while CO_2 emission is 975 g/km when the vehicle is unloaded. On urban delivery routes with a loaded vehicle, the fuel consumption is 52.4 l/100 km, and CO_2 emission is 1372 g/km.

Urban Delivery

Simulation Parameters

Payload:	2600	kg
Total vehicle mass:	17547	kg
Average speed:	26.2	km/h

Fuel consumption:	37.3	l/100km
Fuel consumption:	0.143	l/t-km
Fuel consumption:	0.00389	l/m³-km
Fuel consumption:	312	g/km
Fuel consumption:	119.8	g/t-km
Fuel consumption:	3.25	g/m³-km
CO2 emissions:	975	g/km
CO2 emissions:	375.1	g/t-km
CO2 emissions:	10.19	g/m³-km
Efficiency ratio:	0.960	km-based
Efficiency ratio:	0.960	t-km-based
Efficiency ratio:	0.912	m³-km-based
Reference ratio:	0.966	km-based

Urban Delivery

Simulation Parameters

Payload:	12900	kg
Total vehicle mass:	27847	kg
Average speed:	25.7	km/h

Fuel consumption:	52.4	l/100km
Fuel consumption:	0.0406	l/t-km
Fuel consumption:	0.00547	l/m³-km
Fuel consumption:	438	g/km
Fuel consumption:	34.0	g/t-km
Fuel consumption:	4.58	g/m³-km
CO2 emissions:	1372	g/km
CO2 emissions:	106.3	g/t-km
CO2 emissions:	14.33	g/m³-km
Efficiency ratio:	0.971	km-based
Efficiency ratio:	0.971	t-km-based
Efficiency ratio:	0.922	m³-km-based
Reference ratio:	0.977	km-based

Figure 9. *Unloaded and Lodaded Valuses on Urban Delivery*

As shown in Figure 10, the average CO2 emission for 1-meter shorter length curtain-side trailer is 727 g/km and fuel consumption is 27.8 l/100 km.

Weighted Results		
Payload:	13842	kg
Fuel consumption:	27.8	l/100km
Fuel consumption:	0.0201	l/t-km
Fuel consumption:	0.00290	l/m³-km
Fuel consumption:	232.3	g/km
Fuel consumption:	16.8	g/t-km
Fuel consumption:	2.43	g/m³-km
CO2 emissions:	727	g/km
CO2 emissions:	52.5	g/t-km
CO2 emissions:	7.59	g/m³-km
Efficiency ratio:	0.986	km-based
Efficiency ratio:	0.986	t-km-based
Efficiency ratio:	0.937	m³-km-based

Figure 10. *Average Values of a 1-Meter Shorter Length Curtain-Sided Trailer*

200-millimeter lower height curtain-side trailer was simulated using the VECTO program under three different road conditions, both loaded and unloaded.

As seen in Figure 11, on long-haul routes, the fuel consumption is 22.0 l/100 km while CO_2 emission is 576 g/km when the vehicle is unloaded. On long-haul routes with a loaded vehicle, the fuel consumption is 29.7 l/100 km, and CO_2 emission is 776 g/km.

Long Haul

Simulation Parameters

Payload:	2600	kg
Total vehicle mass:	17547	kg
Average speed:	79.7	km/h

Fuel consumption:	22.0	l/100km
Fuel consumption:	0.0846	l/t-km
Fuel consumption:	0.00221	l/m³-km
Fuel consumption:	184	g/km
Fuel consumption:	70.7	g/t-km
Fuel consumption:	1.85	g/m³-km
CO2 emissions:	576	g/km
CO2 emissions:	221.4	g/t-km
CO2 emissions:	5.78	g/m³-km
Efficiency ratio:	0.970	km-based
Efficiency ratio:	0.970	t-km-based
Efficiency ratio:	0.887	m³-km-based
Reference ratio:	0.977	km-based

Long Haul

Simulation Parameters

Payload:	19300	kg
Total vehicle mass:	34247	kg
Average speed:	78.5	km/h

Fuel consumption:	29.7	l/100km
Fuel consumption:	0.0154	l/t-km
Fuel consumption:	0.00298	l/m³-km
Fuel consumption:	248	g/km
Fuel consumption:	12.8	g/t-km
Fuel consumption:	2.49	g/m³-km
CO2 emissions:	776	g/km
CO2 emissions:	40.2	g/t-km
CO2 emissions:	7.79	g/m³-km
Efficiency ratio:	0.976	km-based
Efficiency ratio:	0.976	t-km-based
Efficiency ratio:	0.892	m³-km-based
Reference ratio:	1.002	km-based

Figure 11. *Unloaded and Lodaded Valuses on Long Haul*

As seen in Figure 12, on regional delivery routes, the fuel consumption is 23.2 l/100 km while CO_2 emission is 608 g/km when the vehicle is unloaded. On regional delivery routes with a loaded vehicle, the fuel consumption is 29.9 l/100 km, and CO_2 emission is 781 g/km.

Regional Delivery

Simulation Parameters

Payload:	2600	kg
Total vehicle mass:	17547	kg
Average speed:	60.6	km/h

Fuel consumption:	23.2	l/100km
Fuel consumption:	0.0894	l/t-km
Fuel consumption:	0.00233	l/m³-km
Fuel consumption:	194	g/km
Fuel consumption:	74.8	g/t-km
Fuel consumption:	1.95	g/m³-km
CO2 emissions:	608	g/km
CO2 emissions:	234.0	g/t-km
CO2 emissions:	6.11	g/m³-km
Efficiency ratio:	0.951	km-based
Efficiency ratio:	0.951	t-km-based
Efficiency ratio:	0.869	m³-km-based
Reference ratio:	0.980	km-based

Regional Delivery

Simulation Parameters

Payload:	12900	kg
Total vehicle mass:	27847	kg
Average speed:	60.1	km/h

Fuel consumption:	29.9	l/100km
Fuel consumption:	0.0231	l/t-km
Fuel consumption:	0.00300	l/m³-km
Fuel consumption:	250	g/km
Fuel consumption:	19.4	g/t-km
Fuel consumption:	2.51	g/m³-km
CO2 emissions:	781	g/km
CO2 emissions:	60.6	g/t-km
CO2 emissions:	7.84	g/m³-km
Efficiency ratio:	0.962	km-based
Efficiency ratio:	0.962	t-km-based
Efficiency ratio:	0.879	m³-km-based
Reference ratio:	0.994	km-based

Figure 12. *Unloaded and Lodaded Valuses on Regional Delivery*

As seen in Figure 13, on urban delivery routes, the fuel consumption is 37.1 l/100 km while CO_2 emission is 972 g/km when the vehicle is unloaded. On urban delivery routes with a loaded vehicle, the fuel consumption is 52.3 l/100 km, and CO_2 emission is 1369 g/km.

Urban Delivery

Simulation Parameters

Payload:	2600	kg
Total vehicle mass:	17547	kg
Average speed:	26.2	km/h
Fuel consumption:	37.1	l/100km
Fuel consumption:	0.143	l/t-km
Fuel consumption:	0.00373	l/m³-km
Fuel consumption:	310	g/km
Fuel consumption:	119.4	g/t-km
Fuel consumption:	3.12	g/m³-km
CO2 emissions:	972	g/km
CO2 emissions:	373.8	g/t-km
CO2 emissions:	9.76	g/m³-km
Efficiency ratio:	0.957	km-based
Efficiency ratio:	0.957	t-km-based
Efficiency ratio:	0.874	m³-km-based
Reference ratio:	0.966	km-based

Urban Delivery

Simulation Parameters

Payload:	12900	kg
Total vehicle mass:	27847	kg
Average speed:	25.7	km/h
Fuel consumption:	52.3	l/100km
Fuel consumption:	0.0406	l/t-km
Fuel consumption:	0.00525	l/m³-km
Fuel consumption:	437	g/km
Fuel consumption:	33.9	g/t-km
Fuel consumption:	4.39	g/m³-km
CO2 emissions:	1369	g/km
CO2 emissions:	106.1	g/t-km
CO2 emissions:	13.74	g/m³-km
Efficiency ratio:	0.969	km-based
Efficiency ratio:	0.969	t-km-based
Efficiency ratio:	0.885	m³-km-based
Reference ratio:	0.977	km-based

Figure 13. *Unloaded and Lodaded Valuses on Urban Delivery*

As shown in Figure 14, the average CO2 emission for 200-millimeter lower height curtain-side trailer is 717 g/km and fuel consumption is 27.4 l/100 km.

Weighted Results

Payload:	13842	kg
Fuel consumption:	27.4	l/100km
Fuel consumption:	0.0198	l/t-km
Fuel consumption:	0.00275	l/m³-km
Fuel consumption:	229.1	g/km
Fuel consumption:	16.6	g/t-km
Fuel consumption:	2.30	g/m³-km
CO2 emissions:	717	g/km
CO2 emissions:	51.8	g/t-km
CO2 emissions:	7.20	g/m³-km
Efficiency ratio:	0.973	km-based
Efficiency ratio:	0.973	t-km-based
Efficiency ratio:	0.889	m³-km-based

Figure 14. Average Values of a 200-Millimeter Lower Height Curtain-Sided Trailer

500 kg lighter weight curtain-side trailer was simulated using the VECTO program under three different road conditions, both loaded and unloaded.

As seen in Figure 15, on long-haul routes, the fuel consumption is 22.3 l/100 km while CO_2 emission is 585 g/km when the vehicle is unloaded. On long-haul routes with a loaded vehicle, the fuel consumption is 29.9 l/100 km, and CO_2 emission is 783 g/km.

Long Haul

Simulation Parameters

Payload:	2600	kg
Total vehicle mass:	17047	kg
Average speed:	79.7	km/h

Fuel consumption:	22.3	l/100km
Fuel consumption:	0.0859	l/t-km
Fuel consumption:	0.00217	l/m³-km
Fuel consumption:	187	g/km
Fuel consumption:	71.8	g/t-km
Fuel consumption:	1.81	g/m³-km
CO2 emissions:	585	g/km
CO2 emissions:	224.9	g/t-km
CO2 emissions:	5.67	g/m³-km
Efficiency ratio:	0.985	km-based
Efficiency ratio:	0.985	t-km-based
Efficiency ratio:	0.869	m³-km-based
Reference ratio:	0.977	km-based

Long Haul

Simulation Parameters

Payload:	19300	kg
Total vehicle mass:	33747	kg
Average speed:	78.5	km/h

Fuel consumption:	29.9	l/100km
Fuel consumption:	0.0155	l/t-km
Fuel consumption:	0.00290	l/m³-km
Fuel consumption:	250	g/km
Fuel consumption:	13.0	g/t-km
Fuel consumption:	2.42	g/m³-km
CO2 emissions:	783	g/km
CO2 emissions:	40.6	g/t-km
CO2 emissions:	7.59	g/m³-km
Efficiency ratio:	0.984	km-based
Efficiency ratio:	0.984	t-km-based
Efficiency ratio:	0.868	m³-km-based
Reference ratio:	1.002	km-based

Figure 15. *Unloaded and Lodaded Valuses on Long Haul*

As seen in Figure 16, on regional delivery routes, the fuel consumption is 23.4 l/100 km while CO_2 emission is 613 g/km when the vehicle is unloaded. On regional delivery routes with a loaded vehicle, the fuel consumption is 30.0 l/100 km, and CO_2 emission is 785 g/km.

Regional Delivery

Simulation Parameters

Payload:	2600	kg
Total vehicle mass:	17047	kg
Average speed:	60.7	km/h

Fuel consumption:	23.4	l/100km
Fuel consumption:	0.0900	l/t-km
Fuel consumption:	0.00227	l/m³-km
Fuel consumption:	196	g/km
Fuel consumption:	75.3	g/t-km
Fuel consumption:	1.90	g/m³-km
CO2 emissions:	613	g/km
CO2 emissions:	235.6	g/t-km
CO2 emissions:	5.94	g/m³-km
Efficiency ratio:	0.957	km-based
Efficiency ratio:	0.957	t-km-based
Efficiency ratio:	0.844	m³-km-based
Reference ratio:	0.980	km-based

Regional Delivery

Simulation Parameters

Payload:	12900	kg
Total vehicle mass:	27347	kg
Average speed:	60.2	km/h

Fuel consumption:	30.0	l/100km
Fuel consumption:	0.0232	l/t-km
Fuel consumption:	0.00291	l/m³-km
Fuel consumption:	251	g/km
Fuel consumption:	19.4	g/t-km
Fuel consumption:	2.43	g/m³-km
CO2 emissions:	785	g/km
CO2 emissions:	60.8	g/t-km
CO2 emissions:	7.60	g/m³-km
Efficiency ratio:	0.966	km-based
Efficiency ratio:	0.966	t-km-based
Efficiency ratio:	0.852	m³-km-based
Reference ratio:	0.994	km-based

Figure 16. *Unloaded and Lodaded Valuses on Regional Delivery*

As seen in Figure 17, on urban delivery routes, the fuel consumption is 36.6 l/100 km while CO_2 emission is 957 g/km when the vehicle is unloaded. On urban delivery routes with a loaded vehicle, the fuel consumption is 51.7 l/100 km, and CO_2 emission is 1354 g/km.

Urban Delivery

Simulation Parameters

Payload:	2600	kg
Total vehicle mass:	17047	kg
Average speed:	26.2	km/h

Fuel consumption:	36.6	l/100km
Fuel consumption:	0.141	l/t-km
Fuel consumption:	0.00354	l/m³-km
Fuel consumption:	306	g/km
Fuel consumption:	117.6	g/t-km
Fuel consumption:	2.96	g/m³-km
CO2 emissions:	957	g/km
CO2 emissions:	368.0	g/t-km
CO2 emissions:	9.27	g/m³-km
Efficiency ratio:	0.942	km-based
Efficiency ratio:	0.942	t-km-based
Efficiency ratio:	0.831	m³-km-based
Reference ratio:	0.966	km-based

Urban Delivery

Simulation Parameters

Payload:	12900	kg
Total vehicle mass:	27347	kg
Average speed:	25.7	km/h

Fuel consumption:	51.7	l/100km
Fuel consumption:	0.0401	l/t-km
Fuel consumption:	0.00501	l/m³-km
Fuel consumption:	432	g/km
Fuel consumption:	33.5	g/t-km
Fuel consumption:	4.19	g/m³-km
CO2 emissions:	1354	g/km
CO2 emissions:	104.9	g/t-km
CO2 emissions:	13.12	g/m³-km
Efficiency ratio:	0.958	km-based
Efficiency ratio:	0.958	t-km-based
Efficiency ratio:	0.845	m³-km-based
Reference ratio:	0.977	km-based

Figure 17. *Unloaded and Lodaded Valuses on Urban Delivery*

As shown in Figure 18, the average CO2 emission for 500 kg lighter weight curtain-side trailer is 724 g/km and fuel consumption is 27.7 l/100 km.

Weighted Results		
Payload:	13842	kg
Fuel consumption:	27.7	l/100km
Fuel consumption:	0.0200	l/t-km
Fuel consumption:	0.00268	l/m³-km
Fuel consumption:	231.4	g/km
Fuel consumption:	16.7	g/t-km
Fuel consumption:	2.24	g/m³-km
CO2 emissions:	724	g/km
CO2 emissions:	52.3	g/t-km
CO2 emissions:	7.02	g/m³-km
Efficiency ratio:	0.982	km-based
Efficiency ratio:	0.982	t-km-based
Efficiency ratio:	0.867	m³-km-based

Figure 18. *Average Values of a 500 kg Lighter Weight Curtain-Sided Trailer*

4. CONCLUSION

In this study, the effects of changes in vehicle weight, length, and superstructure height on CO2 emissions and fuel consumption were analyzed. The results demonstrated that improvements in these parameters significantly contribute to enhancing energy efficiency and reducing environmental impacts.

A 500 kg reduction in vehicle weight decreased CO2 emissions by 0.82% and fuel consumption by 0.71%. The use of lightweight technologies offers a valuable opportunity for environmentally conscious applications in the transportation sector. A 1-meter reduction in vehicle length led to a 0.41% decrease in CO2 emissions and a 0.36% reduction in fuel consumption. This highlights the impact of vehicle dimensions on energy efficiency. A

200 mm reduction in superstructure height achieved the highest improvement, with CO2 emissions decreasing by 1.78% and fuel consumption by 1.79%. This finding indicates that optimizing superstructure height is a more effective strategy compared to other parameters.The strong relationship between aerodynamic improvements and reduced energy consumption and emissions is confirmed by this result.

The findings of this study reveal that innovations in vehicle design can effectively meet regulatory standards and sustainability goals. Notably, optimizing superstructure height has been identified as having greater improvement potential compared to other design parameters.

In conclusion, this study provides valuable insights for the development of environmentally friendly and energy-efficient designs in the automotive sector. Future research should comprehensively examine critical parameters such as superstructure height across different vehicle types and usage scenarios.

REFERENCE

European Commission. (2022) .*Regulation 2022/1362 Performance of heavy-duty trailers with regard to their influence on the CO2 emissions, fuel consumption*.Retrieved from https://eur-lex.europa.eu/legal-content/EN/2022/1362

European Commission. (2022). *Vehicle Energy Consumption Calculation Tool (VECTO)*. Retrieved from https://climate.ec.europa.eu/eu-action/transport/road-transport-reducing-co2-emissions-vehicles/vehicle-energy-consumption-calculation-tool-vecto_en

Global Carbon Budget (2024); Population based on various sources (2024). *Per capita CO_2 emissions.* Retrieved from https://ourworldindata.org/co2-and-greenhouse-gas-emissions

The National Aeronautics and Space Administration (NASA). (2024). *Carbon Dioxide*. Retrieved from https://climate.nasa.gov/vital-signs/carbon-dioxide/?intent=121

Turkish Ministry of Foreign Affairs. (n.d.). *The Paris Agreement*. Retrieved from: https://www.mfa.gov.tr/paris-anlasmasi.tr.mfa

CHAPTER III

Non-traditional Manufacturing Methods and Laser Hybrid Welding Technologies

Ferit ARTKIN[1]

Introduction

The term "non-traditional manufacturing processes" refers to a collection of procedures that eliminate surplus material using mechanical, thermal, electrical, chemical, or combinations of these energies; however, they do not employ sharp cutting tools, which are necessary for traditional manufacturing processes. Neither the tool nor the workpiece come into direct touch throughout this operation. It is challenging to use conventional machining techniques like turning, drilling, shaping, and milling on materials that are extremely hard and brittle. When typical machining techniques are neither

[1] Lect.Dr., Kocaeli University, Hereke Asimkocabiyik Vocational School, Department of Machinery and Metal Technologies, Machinery Programme, Kocaeli/Türkiye, Orcid: 0000-0002-8543-6334, artkinf@kocaeli.edu.tr

practical, acceptable, or cost-effective, non-traditional machining techniques also known as advanced manufacturing techniques are used.

Arc and laser welding are two welding techniques having been working for a long time in industrial manufacturing. There are features of both welding techniques that set them apart. Laser-arc hybrid welding process that combines these two approaches. Wide-gap welding and quicker welding may be accomplished in this application utilizing the advantages of both strategies. Furthermore, the arc in laser welding lowers the high cooling rate after welding, brittle phase development in the welding region.

Non-traditional Manufacturing Methods

Innovative and extremely specialized methods for shaping, forming, or modifying materials are provided by non-traditional manufacturing, commonly referred to as advanced machining methods or unconventional machining. Because of this, materials that are hard or impossible to process with conventional techniques may be worked on. Unconventional machining includes a range of methods, each suited to certain materials and applications, such as electrical discharge machining (EDM), laser cutting, abrasive waterjet machining, and ultrasonic machining. For the following reasons, traditional machining methods are not practical, satisfactory, or cost-effective:

- Chip formation and material removal may happen simultaneously, or there may be no chip creation at all.

- In order to remove material, NTM procedures often don't require mechanical energy.
- The tool in NTM does not have to be more durable than the material of the work item.
- It is challenging to clamp extremely hard, delicate materials for conventional machining.

Hard titanium alloys, nimonic alloys, and other high strength heat resistant (HSTR) alloys have been developed and utilized in the aircraft industry because of the necessity for great strength at high temperatures while retaining lightweight characteristics. Unconventional machining methods have surfaced due to the advancement of the development of cutting tools with hardness levels between 80 and 85 HRC, which were previously prohibitively expensive for machines employing standard techniques.

HSTR alloys, titanium, stainless steel (SST), nimonic alloys, ceramics, and semiconductors are essential components of many high-tech enterprises. Conventional machining techniques are no longer appropriate for these materials. Using conventional machining processes to produce and mill intricately formed components and similarly challenging-to-machine alloys in HSTR is time-consuming, expensive, and labor-intensive.

Classification of Non-Traditional Manufacturing Methods and Laser Hybrid Welding

Numerous techniques, such as Electrical Discharge Machining (EDM), Electrochemical Machining (ECM), Laser Cutting, Ultrasonic Machining, and Abrasive Waterjet Machining,

are included in non-traditional machining procedures. Each of these techniques has unique benefits for precision machining applications. Non-traditional manufacturing (NTM) processes are categorized based on the type of energy utilized to remove materials.

1. Mechanical Processes

- Ultrasonic Machining (USM)
- Water Jet Machining (WJM)
- Abrasive Jet Machining (AJM)
- Abrasive Water Jet Machining (AWJM)

2. Chemical Processes

- Chemical Milling (CHM)

3. Electrochemical Processes

- Electro Chemical Grinding (ECG)
- Electro Jet Drilling (EJD)

4. Electro-Thermal Processes

- Laser Beam Machining (LBM)
- Electron Beam Machining (EBM)

The Laser Hybrid Welding technique is one of these techniques, as is the Laser Beam Machining (LBM) technique. Additionally, the typical Gas Metal Arc Welding (GMAW) has the following characteristics.

Ultrasonic Machining (USM)

A non-traditional technique called ultrasonic machining creates tiny, round and non-circular lower than 1 mm by vibrating the cutting tool at a high frequency, which creates abrasive particles and impacts the workpiece.

Electrical Discharge Machining (EDM)

EDM, sometimes referred to as spark machining, removes material by localized melting or vaporization by using electrical energy to produce a spark that forms between a workpiece immersed in a dielectric fluid and a tool. EDM uses sparks to cut. In a jig immersed in a dielectric liquid, like kerosene, the workpiece is retained. The workpiece and an electrode (a continuous wire or a shaped form of graphite) are closest to one another when a power source generates quick electrical pulses that cause a discharge between them. The ability to manufacture any conductive material, regardless of its hardness, is one benefit of EDM. Another benefit implies that the workpiece does not undergo mechanical stresses since the wire does not come into touch with it (mechanical-engineering.com, 2024).

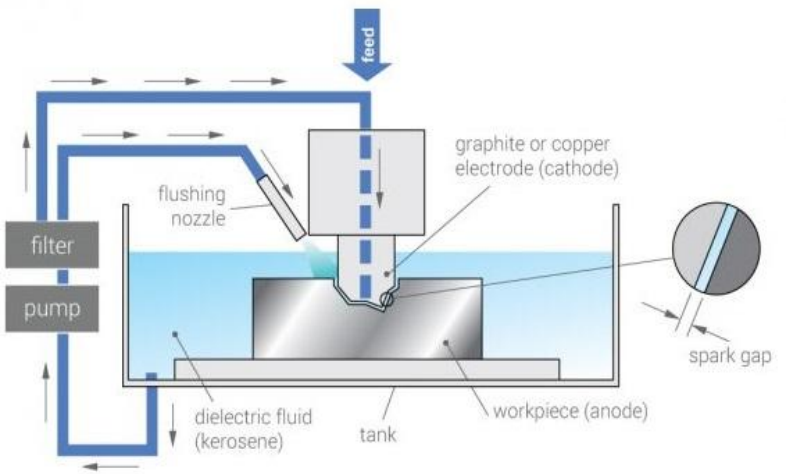

Figure 1. Electrical Discharge Machining (EDM) Diagram.

Electrochemical Machining (ECM)

ECM removes material off a workpiece surface by combining chemical and electrical energy in line with Faraday's

electrolytic law. It has an infinite uses conductive electrolytes such as NaCl.

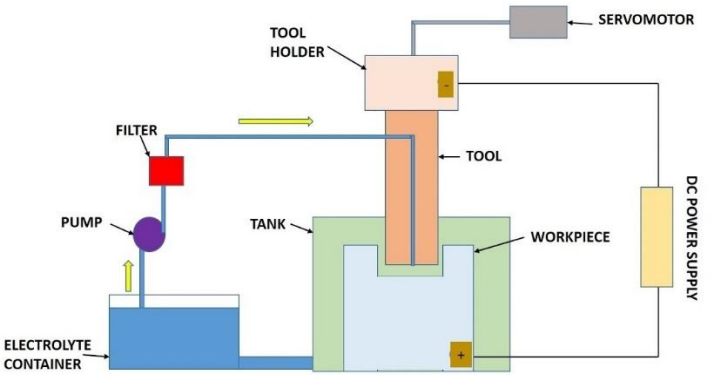

Figure 2. Electrochemical Machining (EDM) Diagram.

The ECM process involves pushing a negatively charged cutting tool (cathode) towards a positively charged workpiece (anode).

A pressurized electrolyte is introduced into the area of cutting at a predefined temperature. Between 80 and 800 microns (0.003 to 0.030 in.) isolates the workpiece from the cutting instrument. The tool simultaneously takes on the desired shape inside the workpiece as material is dissolved from it as electrons. This electrochemical process produces metal hydroxide, electrolytic solution (leadrp.net, 2024).

Water Jet Machining (WJM)

High-pressure water jets create a high-velocity water jet by transforming kinetic energy from pressure energy when they are directed through a convergent nozzle. Material removal is made

easier by the plastic deformation and fracture caused by this jet's impact on the workpiece.

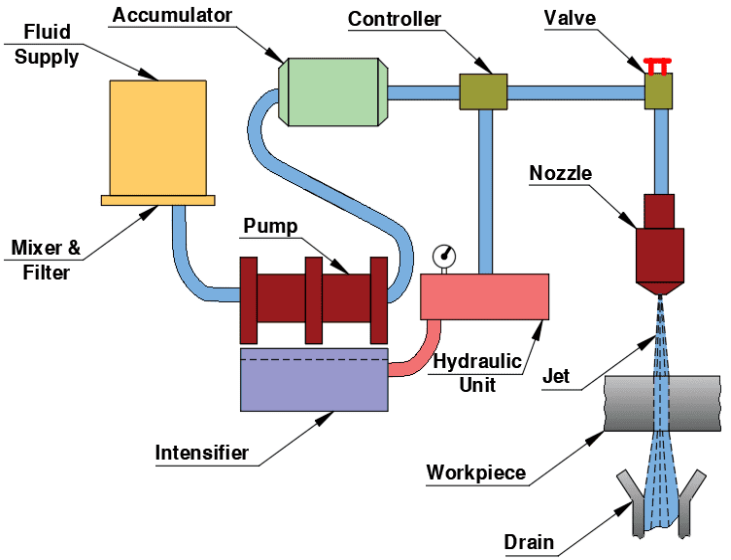

Figure 3. Water Jet Machining (WJM) Diagram.

The concept of water erosion is the foundation of waterjet machining (WJM). When a swift water jet strikes the surface, material is removed. Pure waterjet is used to process softer materials. AWJM, conversely, is a machining technique that uses abrasive particles combined with water to cut tougher materials.

Abrasive Water Jet Machining (AWJM)

As a development of WJM, AWJM adds abrasives to the high-velocity water jet to improve cutting capabilities. To improve material removal, abrasive particles are delivered at a rate of roughly 40-60%.

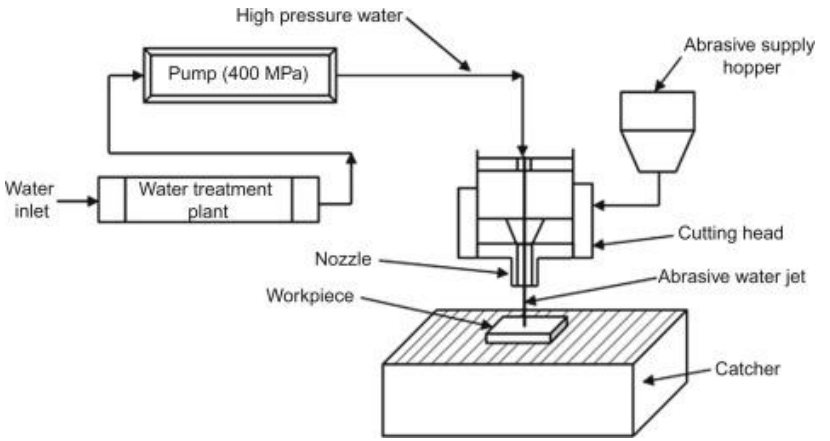

Figure 4. Sketch of abrasive-waterjet machining setup. (Krishna K. et al., 2018).

Materials that are composites, ceramics, rocks, concrete, titanium alloys, etc., are frequently cut using abrasive-waterjet machining (AWJM). The procedure uses the effects of a waterjet and abrasives. A setup schematic for AWJM is shown in Fig. 4. Pure water is pumped at extremely high pressures of 4000–6000 bar using a reciprocating pump, which is the primary component of an abrasive-waterjet arrangement. In the mixing chamber, a hopper introduces the abrasive particles into the waterjet. Cutting or machining composites, Kevlar polymer, hardened steels, and some ceramics is possible thanks to the combined impacts of waterjet and abrasives (M. Shukla, 2013).

Electron Beam Machining (EBM)

The thermal machining technique known as electron beam machining (EBM) uses high-velocity electrons focused into a narrow beam to quickly heat, melt, or evaporate the material. Applications for this procedure are numerous and include welding, annealing, cutting, and drilling.

EBM achieves remarkable precision in material removal by using high-voltage electricity to create a concentrated stream of fast electrons.

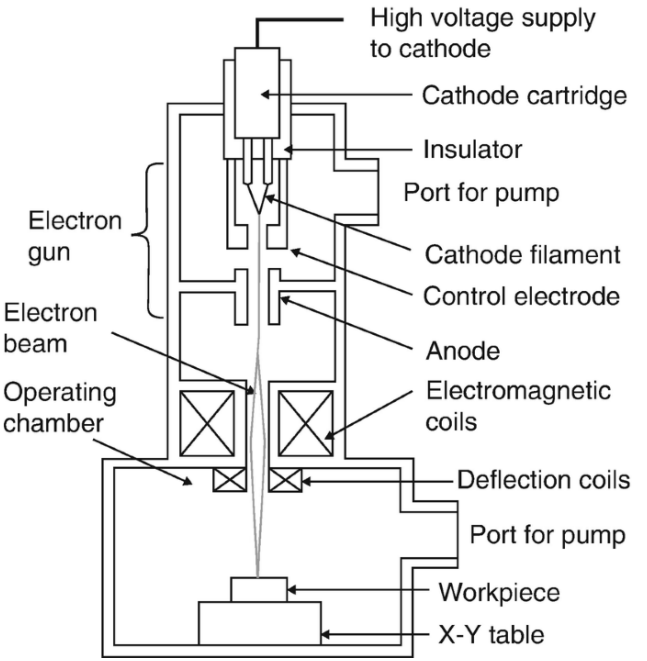

Figure 5. Electron Beam Machining setup.

When electrons move at high speeds, the majority of their kinetic energy is transformed into thermal energy a tightly focussed beam strike the workpiece surface. Since attempts to employ the electron beam as a machining tool were undertaken with the introduction of electron microscopy, this phenomena has been well understood. Electromagnetic focusing and deflection lenses make it simple to focus and deflect the beam. By altering the acceleration voltage, the power density may also be easily controlled. Thus, several kinds of thermal machining are made possible by the electron

beam. Because of this, it may be used in the industrial sector for high-precision welding with a deep fusion zone and quick, precise drilling (link.springer.com, 2024).

Laser Beam Machining (LBM)

Many industrial processes, such as heat treatment, welding, measuring, scribing, cutting, and drilling, depend on laser technology (Teixidor, D., et al., 2019).

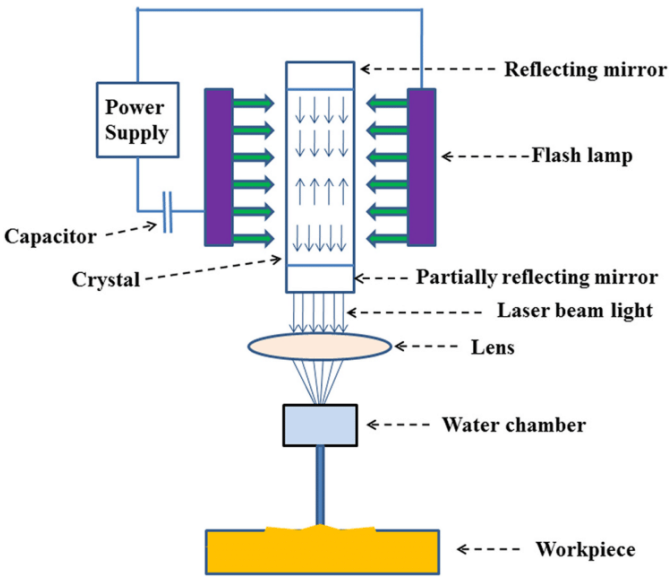

Figure 6. Laser Beam Machining (LBM) setup (Kumar, S., et al., 2021).

The phrase "laser" refers to the amplification of light by stimulated emission of radiation.Electrical energy is transformed into a highly coherent light beam by an optical transducer called a laser. A laser light beam differs from other types of light due to a number of characteristics. It is extremely collimated, meaning that the light rays in the beam are nearly perfectly parallel, and

monochromatic, meaning that the light may potentially have just one wavelength. Because of these characteristics, laser light may be focussed onto a small area using standard optical lenses, producing high power densities.

Laser beam machining (LBM) removes material by vaporization and ablation using light energy from a laser instrument. Figure 6 shows the LBM configuration. Solid-state lasers and carbon dioxide gas lasers are the two types of lasers utilized in LBM. The coherent light beam's energy is focused both optically and temporally in laser beam machining. Melting and evaporation, the light laser beam is pulsed such that the energy emitted causes an impulse against the work surface, causing the molten material to evacuate the surface quickly.

Laser Hybrid Welding (LHD) Technique

Innovative, hybrid, or combining many existing processes are examples of recent advancements in welding. Here, we'll discuss an example of one of these novel strategies. The laser beam and gas metal arc welding (GMAW) techniques are combined in a hybrid method called hybrid laser welding, which has been widely developed (Figure 7). This method makes use of a head that houses the GMAW gun and laser focusing optics. A keyhole is formed close to the puddle's leading edge by the laser beam. Additionally, hybrid methods that combine gas metal arc welding (GMAW) and laser have been developed for usage in fixed positions. The tools that were utilized to create the joint design are also no longer needed. The filler metal alloys are made especially to make the connection physically smooth.

LBW and GMAW processes have been combined to create laser-GMAW hybrid welding. Welding lightweight structures, particularly aluminum alloys, is a promising use for this combination.

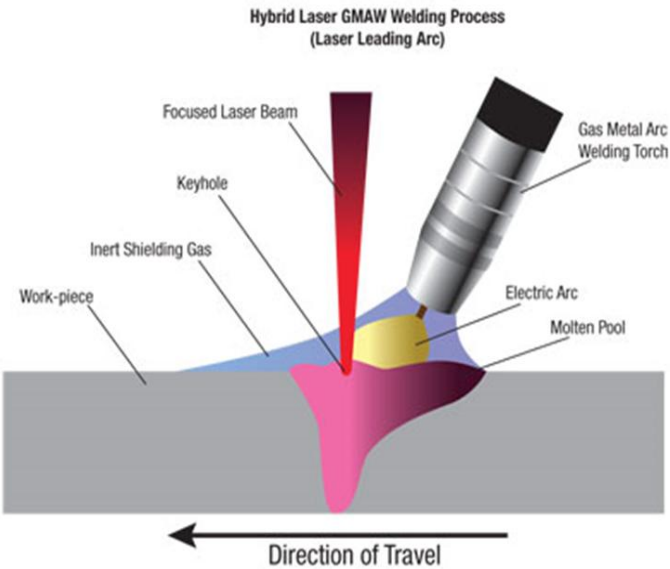

Figure 7. Hybrid Laser GMAW Welding Process.

This hybrid welding method is well acknowledged for its effectiveness, robustness, and adaptability. The main uses of LBW and GMAW can be greatly enhanced by combining a deep-penetrating laser beam with the high fillet feed of GMAW. This technique's primary advantages are minimal distortion, deep and steady weld penetration, quick filler metal addition, and strong gap-bridging ability. Compared to the LBW of some metals, such aluminum alloys, this hybrid technique permits substantially broader groove tolerances.

Types of Hybrid Laser Welding

Types of laser hybrid welding might be divided into three main groups. TIG, plasma arc, or MIG aided laser welding are the three primary forms of hybrid welding procedures, whose types differ according on thearc utilized. MIG, also referred to as hybrid laser welding, despite TIG aided laser welding being the first source to be studied.Third Harmonic Generation (THG).

Laser Hybrid MIG Welding

Electric arcs and laser beams have long been known to produce welds with numerous technical advantages of laser-only welds, including little distortion and deep penetration. Compared to laser welding alone, this method permits higher speeds, deeper penetration, and wider tolerance for conformance since the arc and laser travel in the same molten pool (see figure 8). Compared to laser procedures, hybrid laser-MIG welding enables better completion rates, lowers the necessary laser power, and greatly increases joint dependability. Hybrid welding is therefore more affordable than laser welding. while maintaining or even enhancing laser welding's technological benefits (Hügel H. et al. 2004; Steen, W. M., 2003; Seyffarth, P., et al., 2002).

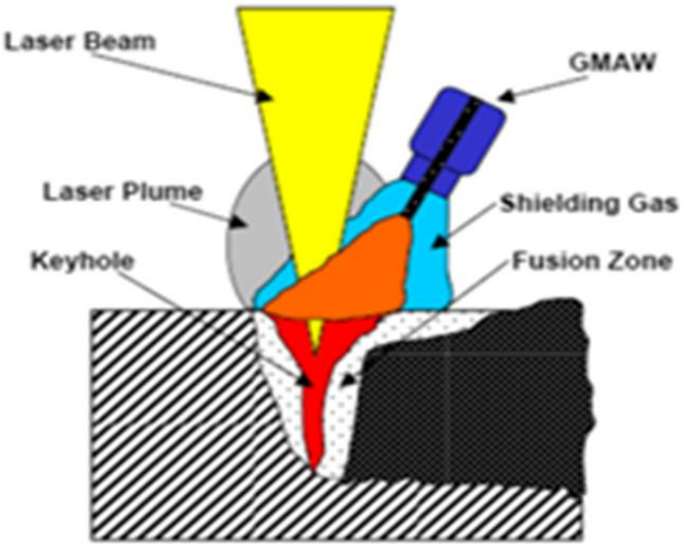

Figure 8. Hybrid Laser-MIG Welding Process.

Laser Hybrid TIG Welding

The initial proposal for laser-arc hybrid welding was made forty years ago (Steen and Eboo., 1978). When laser welding and traditional TIG welding are combined, laser-TIG hybrid welding offers excellent productivity, efficiency, and weld quality (Figure 9). Energy density and gradient can be precisely controlled, and the formation and characteristics of hard-to-weld materials like magnesium alloys are tightly managed, due to laser-TIG hybrid welding.

An arc and a low-power laser (about 400 W) are used in a novel hybrid welding energy loss issue that exists in today's welding process. The novel method has been discovered to have several benefits over laser or arc welding alone when it comes to magnesium

alloys, including rapid welding speed, deep penetration, and high-quality welds. The new method employs a laser of roughly 400 W, which is approximately one-fifth of high-power laser (about 2000 W)-arc hybrid welding, allowing for considerable energy savings and a large reduction in welding expenses.

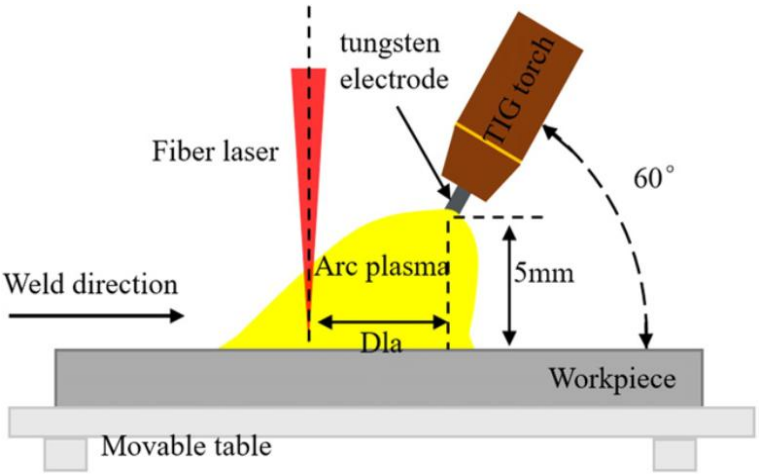

Figure 9. Schematic Diagram of Laser-Hybrid TIG Welding (Mu, Z., et al., 2019).

Laser Hybrid Plasma Welding

Laser-plasma arc (laser-PA) hybrid welding can decrease porosity and hot cracks, enhance weld appearance, and increase welding speed and tolerance to poor joint fit as compared to laser welding. Laser-PA can be used to add filler material in welding and surface alloying, furthermore to produce thin sheet joints, overlap joints of coated steels, and specific weld cavities at high speeds.

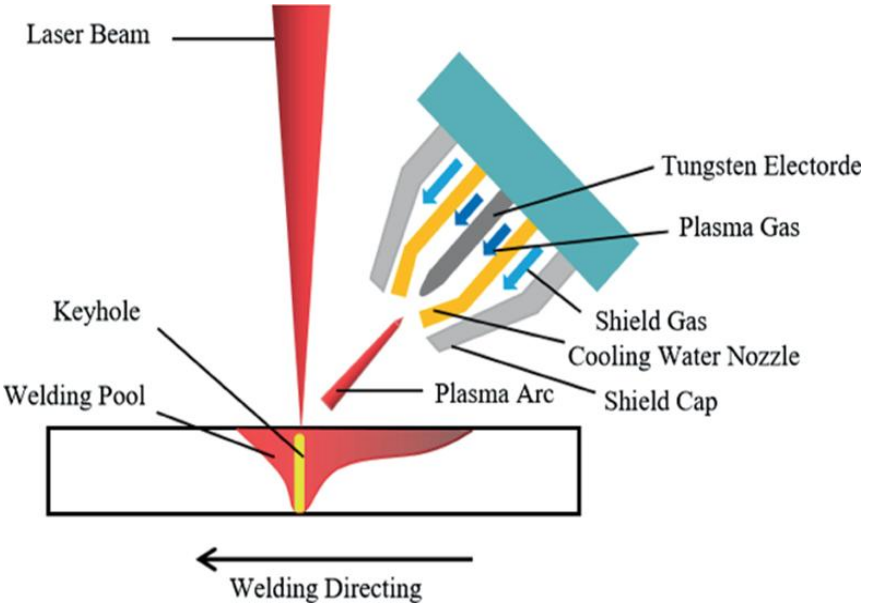

Figure 10. Laser-Hybrid Plasma Welding diagram.

Traditional plasma and laser equipment are combined in plasma-laser-hybrid welding technology will deliver an extremely cost-effective weld source. This new process's economic benefits include increased productivity, a quicker processing speed, and comparatively cheap equipment expenses. On the other hand, this recently created method can also enhance joint quality. In the plasma-laser-hybrid method, the PAW and LBW processes are combined.. In the laser PAW hybrid welding technique, the secondary heat source is a constricted plasma arc (Li, R., et al. 2024)

Advantages and Limitations of Laser Hybrid Welding Methods

The complementing effects of an electric arc and a laser beam in the same weld pool provide the laser arc hybrid welding

technology several advantages over laser and arc welding approaches.

- Fewer passes in a multi-pass weld joint;
- Narrow weld bead with tiny heat impacted zones;
- Higher welding speed and depth of penetration with better productivity
- Enhanced sidewall fusion results in increased weld bead stability.
- Better gap bridging capabilities; reduced susceptibility to workpiece tolerances; and access to all welding locations with the right parameter selection
- Welds a an assortment of metals reactive and highly reflective materials;
- Reduces deformation of the weld due to reduced heat input than arc welding;
- Filler materials help fill the joint gap and add alloying elements not possible with autogenous laser welding.

Despite its many advantages, the laser arc hybrid welding There are a number of disadvantages to utilizing this strategy, including:

- Compared to arc welding, the capital cost is quite expensive.,

- Proper part assembly and precise placement are necessary.
- A lot of process parameters need to be managed.
- More safety measures need to be implemented (Bappa A., 2018).

Disadvantages of Laser Hybrid Welding Methods

Expensive initial outlay, The initial cost of laser welding equipment is frequently high. The equipment's cost is increased by the sophisticated technology needed, including strong lasers, precise optics, cooling systems, and automation components.

Restricted Thickness While laser welding works well for thin to medium-thick materials. Because they can produce a wider weld cross-section, conventional welding methods like typically better suited to extremely thick materials.

Precision Joint Fit, The components' precise alignment and fit being joined are necessary for laser welding. Poor weld quality or partial fusion may arise from any joint misalignment or gaps. in the joint because the concentrated laser energy may not fill them as well as conventional filler-based welding methods.

Concerns about Safety Burns, fire risks, and laser exposure harm using strong laser systems. Inadequate safety measures, such wearing laser safety glasses, can result in irreversible eye injury from lasers' intense light.

Conclusion

In comparison to laser and arc welding, this hybridization effect causes a variety of process benefits, including superior gap bridging ability, deeper penetration, greater welding speed, improved process stability, and increased process efficiency.

Besides the specific control parameters for arc and laser welding, additional parameters must be defined when processes are hybridized. Only after the arc and laser welding procedures are appropriately coupled and the parameters are tuned can the intended advantages be realized. During laser arc hybrid welding, which creates the keyhole and offers deep penetration welding, laser power provides the primary source of heat.

Superior quality is produced using laser arc hybrid welding, welds with exceptional, acceptable mechanical attributes and improved fatigue characteristics. It greatly reduces the welds' porosity, fractures, and other flaws. The weld bead produced by laser arc hybrid techniques has more ductility than laser welding. Industrial uses have shown this method's potential for commercial use. The construction, pipeline, heavy engineering, energy, offshore, railway car, and container manufacturing sectors, as well as the aerospace industry, have also made using hybrid laser-arc welding

REFERENCES

https://leadrp.net/blog/what-is-electrochemical-machining-and-its-process-and-benefits/ Accessed 12 December 2024

https://link.springer.com/referenceworkentry/10.1007/978-3-662-53120-4_6480 Accessed 13 December 2024

https://mechanical-engineering.com/electro-discharge-machining-edm/ Accessed 12 December 2024

Hügel, H., C. Schinzel, Handbook of laser technology and applications, Vol. 3, Applications, Part D, Welding, edited by Colin E. Webb and Julian D.C. Jones, Bristol, Institute of Physics, 2004.

Krishna K. Saxena, Mattia Bellotti, Jun Qian, Dominiek Reynaerts, Bert Lauwers, Xichun Luo, Chapter 2 - Overview of Hybrid Machining Processes, Editor(s): Xichun Luo, Yi Qin, Hybrid Machining, Academic Press, 2018, Pages 21-41, ISBN 9780128130599, doi.org/10.1016/B978-0-12-813059-9.00002-6.

Kumar, Sanjay & Roy, Dijendra & Dey, Vidyut. (2021). A comprehensive review on techniques to create the anti-microbial surface of biomaterials to intervene in biofouling. Colloid and Interface Science Communications. 43. 100464.10.1016/j.colcom.2021.100464.

Li, R., Li, T. (2024). Laser-Arc Hybrid Welding. In: Advanced Welding Methods and Equipment. Springer, Singapore. https://doi.org/10.1007/978-981-97-4109-0_2

M. Shukla, Abrasive water jet milling BT, J.P. Davim (Ed.), Nontraditional Machining Processes: Research Advances, Springer, London (2013), pp. 177-203

Mu, Z., Chen, X., Zheng, Z., Huang, A., Pang, S., 2019. Laser cooling arc plasma effect in laser-arc hybrid welding of 316L stainless steel. International Journal of Heat and Mass Transfer 132, 861–870

Seyffarth, P., I. V. Krivtsun, Laser-arc processes and their applications in welding and material treatment, London, Taylor & Francis, 2002.

Steen, W.M, M. Eboo, J. Clarke, Arc augmented laser welding, in: Proc. of the 4th International Conference on Advances in Welding Processes, vol. 1, Harrogate, U.K., 1978, pp. 257–265.

Steen, William M., Laser material processing, 3rd edition, London, New York, Springer, 2003.

Teixidor, Dani & Ferrer, Inés & Criales, Luis & Özel, Tuğrul. (2019). Laser Machining. 10.1002/9781119120384.ch18.

CHAPTER IV

Boriding technology and its effects on tribological performance

Hasan onur TAN[1]
Faruk GÜNER[2]

Introduction

Boriding, a surface-hardening process, is employed to produce surfaces with exceptional wear resistance, attributed to its ability to achieve high hardness and a low coefficient of friction. This thermochemical diffusion-based surface modification technique is applied to a wide range of materials, including ferrous, nonferrous, and cermet materials, to enhance the durability of metal components, particularly in high-temperature applications. As

[1] Assist. Prof. Dr., Giresun University, Faculty of Engineering, Department of Mechanical Engineering, Giresun/Türkiye, Orcid: 0000-0003-3796-9889, hasan.tan@giresun.edu.tr
[2] Assoc. Prof. Dr., Giresun University, Faculty of Engineering, Department of Mechanical Engineering, Giresun/Türkiye, Orcid: 0000-0002-3438-0553, faruk.guner@giresun.edu.tr

described by (Sinha, 1991) the process is compatible with most ferrous materials as well as nonferrous and cermet materials. During boriding, boron atoms diffuse into the surface of the material, reacting with metals such as iron, nickel, cobalt, molybdenum, tungsten, and titanium to form metal borides. The resultant boride coatings exhibit remarkable hardness (ranging from 10 GPa to 33 GPa) combined with the thermal and chemical stability inherent to boron compounds. These characteristics render the coatings highly resistant to wear and corrosion. Notably, the hardness of boride coatings on metallic materials significantly surpasses that of conventional surface-hardening treatments and is comparable to tungsten carbide and certain hard PVD coatings(Davis, 2002; Sinha, 1991; Zimmermann, 1992).

Boriding of ferrous materials results in the formation of a single-phase or double-phase compound layer consisting of FeB and/or Fe_2B (Von Matuschka & Boronizing, 1980). Due to the minimal solubility of boron in iron, the diffusion zone beneath the compound layer is almost negligible (Brakman, Gommers, & Mittemeijer, 1989). Among these phases, FeB is significantly harder and more brittle than Fe_2B, and it also exhibits a higher coefficient of thermal expansion. Consequently, the formation of a double-phase boride layer often leads to cracking (Brakman et al., 1989). To mitigate this issue, the boriding process is typically optimized to produce a single-phase Fe_2B layer(Davis, 2002). Some properties of FeB and Fe_2B are given on Table 1. Cross-sectional views of boride coating microstructures are depicted in Figure 1, highlighting their characteristics on materials used in high-temperature applications

Table 1. Iron boride properties (Prince, Raj, Kumar, & Gopalakrishnan, 2022)

Property	FeB	Fe_2B
Microhardness	1900-2000 HV	1400-1500
Brittleness	Highly brittle	Less brittle than FeB
Fracture toughness	Low	Higher than FeB
Density	6,75 g/cm^3	7,43 g/cm^3
Boron content	Around 16,23 wt% B	Around 8,83 wt% B
Co-efficient of thermal expansion	23 x 10^{-6}/°C	7,85 x 10^{-6}/°C

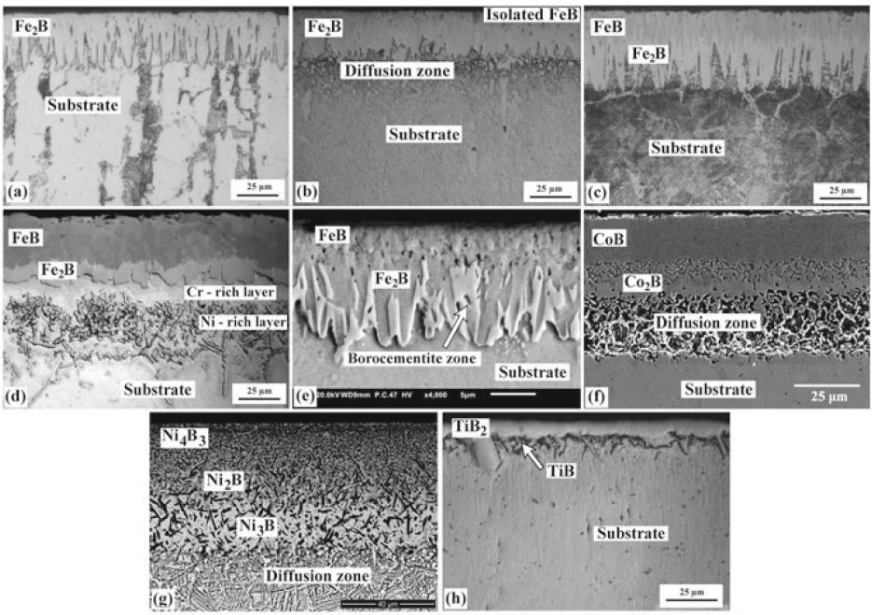

Figure 1. Cross-sectional images of some borided materials. a) Fe_2B on low-carbon steel, b) Fe_2B coating with isolated FeB on high-alloy steel, c) FeB–Fe_2B on low-alloy steel, d) FeB–Fe_2B on stainless steel, e) FeB–Fe_2B combined with borocementite, f) cobalt boride coating on Co-base alloy, g) nickel boride coating on Ni-base alloy, h) titanium boride coating on Ti-base alloy (Campos Silva, Günen, Serdar Karakaş, & Delgado Brito, 2023)

The presence of alloying elements can influence the growth of the compound layer, primarily by decelerating its propagation. Elements such as carbon, silicon, and aluminum, being insoluble in the compound layer, are displaced into the substrate during the process (Sinha, 1991). Given its capacity to endure high temperatures, the boride layer not only enhances wear resistance but also facilitates additional hardening of the material.

The boride layer on steel achieves surface hardness values in the range of 1400–2100 HV (Davis, 2002; Eyre, 1975), which is significantly higher than the hardness ranges of other conventional surface-hardening treatments. For comparison, carburizing results in hardness values of 650–950 HV (Selçuk, Ipek, & Karamış, 2003), nitriding achieves 650–1100 HV (Ashrafizadeh, 2003), carbonitriding produces 940–1000 HV (Selçuk et al., 2003), and chromium plating yields hardness values of 800–1100 HV (El-Amoush, Abu-Rob, Edwan, Atrash, & Igab, 2011). The hardness of the boride layer on carbon steels surpasses that of hardened tool steel and is comparable to tungsten carbide (Davis, 2001). Furthermore, the boride layer retains its hardness at elevated temperatures more effectively than the nitride layer (Davis, 2002; Zhang, Zhang, Yan, Wang, & Qian, 2011). Table 2 presents the typical surface hardness values of borided steels in comparison with those achieved through other treatments and hard materials.

Table 2. Comparison of Surface Hardness Achieved through Boriding, Nitriding, and Carburizing on Various Steels and Hard Materials (Prince et al., 2022)

Material	Surface Microhardness (HV)
Borided AISI 1020 steel	1240-2000
Borided AISI 1045 steel	1320-2120
Borided AISI 304 stainless steel	1000-1100
Borided AISI 316 stainles steel	1050-1200
Carburized 1020 steel	850-910
SiC	4000
B_4C	5000
Diamond	>10000

Boriding significantly enhances the chemical stability of plain carbon steels, particularly against acids such as HCl (Biddulph, 1977; Petrova & Suwattananont, 2005). The boride layer on steels demonstrates exceptional corrosion resistance to various acids, including HCl, H_2SO_4, HNO_3, and H_3PO_4 (Kartal, Kahvecioglu, & Timur, 2006). Additionally, medium carbon steels with a boride layer exhibit excellent chemical stability against copper chloride in acetic acid (Gopalakrishnan, Ramakrishnan, Shankar, & Palaniappa, 2002). The boride layer also offers moderate oxidation resistance at temperatures up to 850°C, owing to the high melting points of borides, and it is highly resistant to attack by molten metals(Davis, 2001). Moreover, borided steel components exhibit enhanced fatigue life and improved service performance in oxidizing and corrosive environments (Sinha, 1991).

The boride layer exhibits exceptional sliding wear resistance against counter bodies such as AISI 52100 steel balls and borided austenitic stainless steel discs (Martini, Palombarini, Poli, & Prandstraller, 2004; Takeuchi, Fujii, & Katagiri, 1979). It also demonstrates outstanding abrasive wear resistance against hard ceramic abrasives like Al_2O_3 and SiO_2 (Bejar & Moreno, 2006; Eyre, 1975; Martini et al., 2004). Due to its remarkable wear resistance, the boride layer is utilized as a protective coating in nuclear energy applications. The service life of the boride layer on steel is inversely proportional to the applied load (Eyre, 1975). Notably, boriding can extend the lifespan of dies by up to tenfold (Biddulph, 1977). In some instances, borided steels have replaced hard chromium plating while providing comparable improvements in service life. The wear resistance of boride layers on steels rivals that of sintered carbides (Sinha, 1991).

The superior performance of the boride layer can be attributed to its combination of high surface hardness and low coefficient of friction, which effectively mitigates primary wear mechanisms such as adhesion, tribo-oxidation, abrasion, and surface fatigue (Davis, 2001; Habig & Chatterjee-Fischer, 1981). Furthermore, various methods are available for the boride surface modification of steels, enabling the tailoring of surface properties for specific applications.

2. Boriding Methods

2.1 Pack boriding

Powder pack boriding involves embedding cleaned components into a boriding powder mixture contained within a heat-

resistant steel or similar container. The sealed container is then heated to the required temperature for 1 to 12 hours, depending on the desired thickness of the boride layer (Abdellah & Keddam, 2014; Flores-Rentería et al., 2015; Joshi & Hosmani, 2014). The resulting thickness and microstructure of the boride coating depend on key process parameters, such as temperature, holding time, and the composition of the boriding mixture. After the treatment, the container is cooled to room temperature. Pack boriding offers several advantages, including safe handling, low-cost requirements, simplicity of equipment, and the flexibility to modify the composition of the powder mixture. However, this technique is limited to small-sized components and involves high labor costs for packing and removing the powder after the boriding process (Kulka, 2019; Tsipas, 2016). Schematic wiev of the pack boriding process is given in Figure 2.

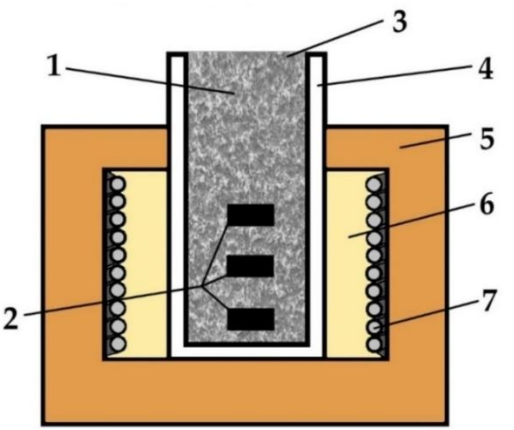

Figure 2. General wiev of pack boriding process. 1) powder mixture, 2) treated sample, 3) open upper part of the retort, 4) tube-shaped retort with a closed bottom, 5) electric resistance furnace, 6) furnace chamber, 7) heating elements (Makuch, 2022)

2.2 Gas Boriding

Gas boriding employs boron-containing gases, such as diborane (B_2H_6) and boron trichloride (BCl_3), often mixed with hydrogen (H_2), nitrogen (N_2), or dissociated ammonia (Pertek, 1994). The material is placed in a chamber or cylindrical retort under a protective atmosphere. Once the desired boriding temperature is reached, the gas mixture is activated for the required exposure time. The treated material is then cooled under the protective atmosphere to room temperature. Gas boriding provides advantages over pack boriding, including more uniform boron distribution due to gas circulation, improved temperature stability, and the elimination of post-treatment cleaning. However, the technique faces challenges related to the scarcity, toxicity, and explosiveness of boron-containing gases, such as B_2H_6, BCl_3, and BF_3. These gases are highly toxic, carcinogenic, and corrosive, which limits their industrial applicability (Kulka et al., 2019; Küper, Qiao, Stock, & Mayr, 2000; Lyakhovich, Dolmanov, & Isakov, 1982; Tsipas & Tsipas, 2016). A general wiev of the gas boriding unit is given in Figure 3.

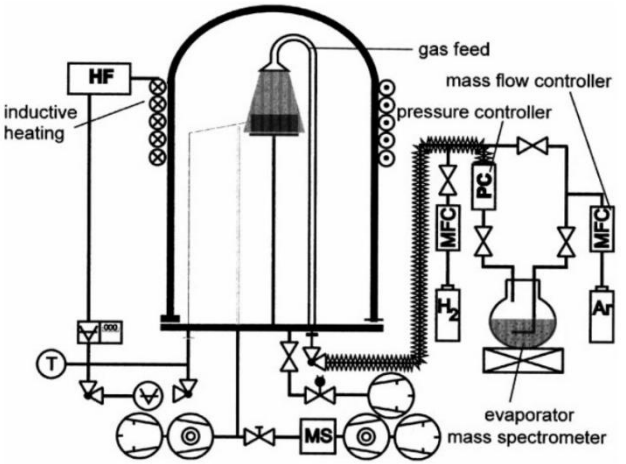

Figure 3. An overwiev of the gas boriding unit (Küper, 2000).

2.3 Plasma Boriding

Plasma boriding, a modified version of gas boriding, is conducted at relatively low temperatures (500°C–650°C) in a vacuum chamber using boron hydride and boron trichloride (Bartsch & Leonhardt, 1999; Filep & Farkas, 2005). The high-energy plasma ensures better energy efficiency (Yoon, Jee, & Lee, 1999). It was reported that high-temperature gas boriding may lead to the segregation of alloying elements in alloy steels and phase transformations in the core (Miyashita & Yokota, 1996). Plasma boriding addresses these issues, as it minimizes such undesired effects (Nam, Lee, Lee, & Kwon, 1998; Rodrı, Laudien, Biemer, Rie, & Hoppe, 1999). Despite these benefits, plasma boriding has limited industrial application due to the toxicity and hazardous nature of gaseous donor media, including diborane (B_2H_6), boron trichloride (BCl_3), and boron trifluoride (BF_3). An industial plant used for plasma boriding is shown in Figure4.

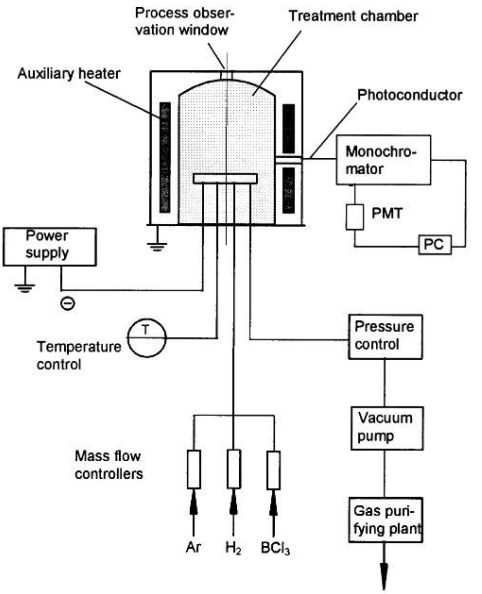

Figure 4. Schematic diagram of the plant used for plasma boriding process (Rodrı, 1999)

2.4 Molten Salt boriding

Molten salt boriding can be carried out via electroless or electrolytic processes (Bonomi, Giess, & Gentaz, 1973; Kahvecioglu, Sista, Eryilmaz, Erdemir, & Timur, 2011; Kusmanov, Silkin, & Belkin, 2020). In the electroless method, the bath typically consists of 70% $Na_2B_4O_7$ and 30% B_4C by weight, although up to 20 wt.% of B_4C can be substituted with ferroaluminum to increase the availability of boron atoms. Another common mixture includes 55% $Na_2B_4O_7$, 45% ferroboron, and 5% ferroaluminum (Chattopadhyay, 2004; Dearnley & Bell, 1985; Kulka et al., 2019; Lyakhovich et al., 1982; Tsipas & Tsipas, 2016). This method is straightforward and cost-effective to operate. However, excess salt must be removed post-treatment, which adds to the operational cost and time.

Additionally, the process requires frequent bath recharging due to increased viscosity, leading to high maintenance costs. Despite these drawbacks, molten salt boriding remains a viable method for producing uniform boride layers. A schematic diagram of the typical electric salt bath oven is given in Figure 5.

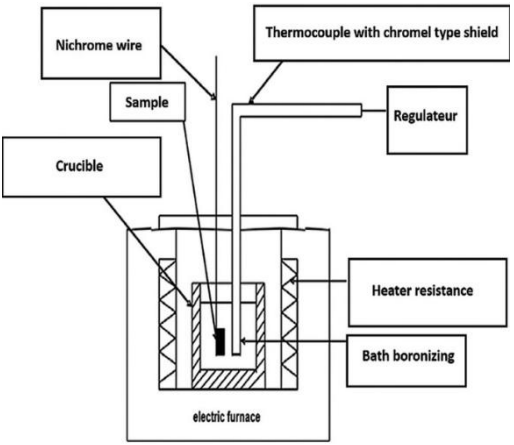

Figure 5. An illustration of the molten salt boriding system (Bouaziz, 2009)

3. Friction and Wear Characteristics

Boride coatings on various classes of steels are widely utilized to reduce the intensity of abrasive wear and thermal degradation in machine parts and equipment. Boriding is an efficient surface treatment for enhancing the wear resistance of heavily loaded friction units (Singhal, 1977; Tarasov, Trusova, Kolubaev, & Sizova, 1995). Numerous studies have investigated the tribological behavior of borided steels under different conditions. (Eyre, 1975) examined the wear resistance of borided plain carbon steels (with carbon contents of 0.1% and 0.4%) using a pin-on-disc tribometer. The borided steel pins were tested against a hardened EN 24 steel

disc at a sliding speed of 0.3 m/s, with nominal stresses ranging from 1 MPa to 8 MPa. It was observed that while unborided steel experienced a transition to severe wear beyond 2.5–3 MPa, no such transition occurred in borided steels, even at 8 MPa. Additionally, beyond 3 MPa, wear rates of borided steels were three times lower than those of unborided steels.

Krelling, Da Costa, Milan, & Almeida, (2017) and Krelling, Milan, and Da Costa (2015) studied the micro-abrasive wear mechanisms of borided AISI 1020 steel against SiO_2 abrasive particles, noting that rolling abrasion dominated the wear mechanism. Fracture of the FeB boride layer was attributed to its brittleness, although initial surface roughness did not significantly impact micro-scale abrasive wear performance. Similarly, Gutierrez-Noda et al., (2019) found that borided AISI M2 steel exhibited lower wear rates compared to untreated steel due to the effective tribological performance of surface iron borides. Erdogan, (2019) and Erdogan et al., (2020) investigated the micro-abrasion performance of borided H13 tool steel processed with nanoboron powder under various loads. Increasing loads resulted in higher volume losses across all samples, with micro-rolling and micro-scratching identified as dominant wear mechanisms. Nora et al., (2019) observed that boriding AISI 4340 steel led to lower friction coefficients and wear rates compared to nitro-carburized and duplex boro-nitro-carburized steels.

Gunes and Yıldız, (2016) reported that borided AISI 310 stainless steel exhibited a wear rate seven times lower than its unborided counterpart when tested against a WC-Co ball. Similarly, Kara, Çolak, and Kayali, (2016) showed that borided AISI P20 and

AISI D2 steels offered superior wear resistance compared to unborided steels. Habig and Chatterjee-Fischer (1981) and Keddam, et al. (2017) confirmed lower wear rates for borided steels compared to carburized and nitrided steels during pin-on-disc tribometer tests. Subrahmanyam and Gopinath (1984) noted that single-phase Fe_2B layers exhibited better wear resistance than dual-phase FeB–Fe_2B layers, as the latter's inhomogeneous microstructure led to higher wear. Takeuchi et al., (1979) also observed superior wear resistance in single-phase Fe_2B specimens compared to dual-phase ones under sliding conditions.

Venkataraman and Sundararajan (1995) studied the sliding wear of borided steel at high sliding speeds (1–8 m/s). At speeds below 2 m/s, borided and unborided steels had comparable coefficients of friction; however, at higher speeds, borided steel exhibited greater friction. Selçuk et al., (2003) showed that boriding significantly improved wear resistance under light loads during sliding tests, with friction coefficients varying from 0.36 to 0.62. Wang and Hutchings (1988) examined the two-body abrasive wear of borided steel against alumina and silicon carbide abrasive papers. The boride layer showed higher wear resistance to alumina abrasives, with wear mechanisms dominated by fatigue-induced fracture and pitting. Silicon carbide abrasives, however, induced wear mechanisms dependent on particle size, including fracture and particle pull-out.

Alloying elements in steel significantly influenced the wear behavior of boride layers. Chromium and molybdenum improved adhesive wear resistance, while vanadium and vanadium carbide enhanced abrasive wear resistance. Molybdenum and vanadium also

improved resistance to surface fatigue. Dybkov, Lengauer and Gas (2006) reported that the abrasive wear resistance of boride layers on Fe-25% Cr alloy steel was 150–300 times higher than that of the base material due to microstructural enhancements. Melendez et al., (1997) compared the wear behavior of borided AISI 1018 and AISI 9840 steels with carburized and quenched-tempered AISI 1018 steel, finding that borided steels exhibited superior wear resistance. Selçuk et al., (2000) showed that boriding AISI 1020 steel reduced adhesive and abrasive wear, outperforming carburized AISI 5115 steel under dry sliding conditions.

Martini et al., (2004) found that wear rates in borided coatings varied with the crystallographic order of iron borides. Compact, highly ordered Fe_2B crystals provided maximum resistance to sliding wear, outperforming alternative treatments such as gas nitriding but falling slightly short of WC-Co hard-metal coatings. Campos et al., (2008) evaluated borided AISI M2 cutting tools and observed that boriding increased the nominal cutting speed by 10–25% while maintaining constant feed and depth of cut. Borided tools showed flank wear due to abrasive particles but extended tool life compared to untreated tools. Tabur et al. (2009) demonstrated that wear resistance of borided AISI 8620 steel improved with exposure time at the same boriding temperature, while increasing temperature reduced wear resistance for the same exposure time. Abrasive wear resistance improved up to 500%, with wear rates increasing under higher loads.

In conclusion, boriding significantly enhances wear resistance in steels, with single-phase Fe_2B layers offering superior performance compared to dual-phase FeB–Fe_2B layers. Wear

mechanisms in borided layers vary depending on testing conditions, abrasive type, and alloy composition. These findings underline the suitability of boriding for applications requiring high wear resistance under demanding conditions.

References

Abdellah, Z. N., & Keddam, M. (2014). Estimation of the boron diffusion coefficients in FeB and Fe2B layers during the pack-boriding of a high-alloy steel. *Mater. Technol, 48*(2), 237-242.

Ashrafizadeh, F. (2003). Influence of plasma and gas nitriding on fatigue resistance of plain carbon (Ck45) steel. *Surface and Coatings Technology, 174*, 1196-1200.

Bartsch, K., & Leonhardt, A. (1999). Formation of iron boride layers on steel by dc-plasma boriding and deposition processes. *Surface and Coatings Technology, 116*, 386-390.

Bejar, M., & Moreno, E. (2006). Abrasive wear resistance of boronized carbon and low-alloy steels. *Journal of Materials Processing Technology, 173*(3), 352-358.

Biddulph, R. H. (1977). Boronizing for erosion resistance. *Thin Solid Films, 45*, 341-347.

Bonomi, A., Giess, H., & Gentaz, C. (1973). Electrochemical boriding of molybdenum in molten salts. *Electrodeposition and Surface Treatment, 1*(5), 419-427.

Brakman, C., Gommers, A., & Mittemeijer, E. (1989). Boriding of Fe and Fe–C, Fe–Cr, and Fe–Ni alloys; boride-layer growth kinetics. *Journal of Materials Research, 4*(6), 1354-1370.

Campos, I., Farah, M., López, N., Bermúdez, G., Rodríguez, G., & VillaVelázquez, C. (2008). Evaluation of the tool life and fracture toughness of cutting tools boronized by the paste boriding process. *Applied Surface Science, 254*(10), 2967-2974.

Campos Silva, I., Günen, A., Serdar Karakaş, M., & Delgado Brito, A. (2023). The Boriding Process for Enhancing the Surface Properties of High-Temperature Metallic Materials. *Coatings for High-Temperature Environments: Anti-Corrosion and Anti-Wear Applications*, 221-259.

Chattopadhyay, R. (2004). *Advanced thermally assisted surface engineering processes*: Springer Science & Business Media.

Davis, J. R. (2001). *Surface engineering for corrosion and wear resistance*: ASM international.

Davis, J. R. (2002). *Surface hardening of steels: understanding the basics*: ASM international.

Dearnley, P., & Bell, T. (1985). Engineering the surface with boron based materials. *Surface Engineering, 1*(3), 203-217.

Dybkov, V., Lengauer, W., & Gas, P. (2006). Formation of boride layers at the Fe–25% Cr alloy–boron interface. *Journal of Materials Science, 41*, 4948-4960.

El-Amoush, A. S., Abu-Rob, A., Edwan, H., Atrash, K., & Igab, M. (2011). Tribological properties of hard chromium coated 1010 mild steel under different sliding distances. *Solid State Sciences, 13*(3), 529-533.

Erdogan, A. (2019). Boriding temperature effect on micro-abrasion wear resistance of borided tool steel. *Journal of Tribology, 141*(12), 121702.

Erdogan, A., Kursuncu, B., Günen, A., Kalkandelen, M., & Gok, M. S. (2020). A new approach to sintering and boriding of

steels “Boro-sintering”: Formation, microstructure and wear behaviors. *Surface and Coatings Technology, 386*, 125482.

Eyre, T. (1975). Effect of boronising on friction and wear of ferrous metals. *Wear, 34*(3), 383-397.

Filep, E., & Farkas, S. (2005). Kinetics of plasma-assisted boriding. *Surface and Coatings Technology, 199*(1), 1-6.

Flores-Rentería, M., Ortiz-Domínguez, M., Keddam, M., Damián-Mejía, O., Elias-Espinosa, M., Flores-González, M., . . . Villanueva-Ibañez, M. (2015). A simple kinetic model for the growth of Fe2B layers on AISI 1026 steel during the powder-pack boriding. *High Temperature Materials and Processes, 34*(1), 1-11.

Gopalakrishnan, P., Ramakrishnan, S., Shankar, P., & Palaniappa, M. (2002). Interrupted boriding of medium-carbon steels. *Metallurgical and Materials Transactions A, 33*, 1475-1485.

Gunes, I., & Yıldız, I. (2016). Investigation of adhesion and tribological behavior of borided AISI 310 stainless steel. *Matéria (Rio de Janeiro), 21*(1), 61-71.

Gutierrez-Noda, L., Cuao-Moreu, C., Perez-Acosta, O., Lorenzo-Bonet, E., Zambrano-Robledo, P., & Hernandez-Rodriguez, M. (2019). The effect of a boride diffusion layer on the tribological properties of AISI M2 steel. *Wear, 426*, 1667-1671.

Habig, K.-H., & Chatterjee-Fischer, R. (1981). Wear behaviour of boride layers on alloyed steels. *Tribology International, 14*(4), 209-215.

Joshi, A. A., & Hosmani, S. S. (2014). Pack-boronizing of AISI 4140 steel: boronizing mechanism and the role of container design. *Materials and Manufacturing Processes, 29*(9), 1062-1072.

Kahvecioglu, O., Sista, V., Eryilmaz, O., Erdemir, A., & Timur, S. (2011). Ultra-fast boriding of nickel aluminide. *Thin Solid Films, 520*(5), 1575-1581.

Kara, R., Çolak, F., & Kayali, Y. (2016). Investigation of wear and adhesion behaviors of borided steels. *Transactions of the Indian Institute of Metals, 69*, 1169-1177.

Kartal, G., Kahvecioglu, O., & Timur, S. (2006). Investigating the morphology and corrosion behavior of electrochemically borided steel. *Surface and Coatings Technology, 200*(11), 3590-3593.

Keddam, M., Elias-Espinosa, M., Ortiz-Domínguez, M., Simón-Marmolejo, I., & Zuno-Silva, J. (2017). Pack-boriding of AISI P20 steel: Estimation of boron diffusion coefficients in the Fe2B layers and tribological behaviour. *International Journal of Surface Science and Engineering, 11*(6), 563-585.

Krelling, A., Da Costa, C., Milan, J., & Almeida, E. (2017). Micro-abrasive wear mechanisms of borided AISI 1020 steel. *Tribology International, 111*, 234-242.

Krelling, A., Milan, J., & Da Costa, C. (2015). Tribological behaviour of borided H13 steel with different boriding agents. *Surface Engineering, 31*(8), 581-587.

Kulka, M., Kulka, M., & Castro. (2019). *Current trends in boriding*: Springer.

Kusmanov, S., Silkin, S., & Belkin, P. (2020). Effect of plasma-electrolytic polishing on the corrosion resistance of structural steels after their anodic saturation with nitrogen, boron, and carbon. *Russian Journal of Electrochemistry, 56*, 356-364.

Küper, A., Qiao, X., Stock, H., & Mayr, P. (2000). A novel approach to gas boronizing. *Surface and Coatings Technology, 130*(1), 87-94.

Lyakhovich, L., Dolmanov, F., & Isakov, S. (1982). Boriding of steels in gaseous media. *Metal Science and Heat Treatment, 24*, 260-263.

Martini, C., Palombarini, G., Poli, G., & Prandstraller, D. (2004). Sliding and abrasive wear behaviour of boride coatings. *Wear, 256*(6), 608-613.

Melendez, E., Campos, I., & Rocha, E. (1997). Structural and Strength Characterization Boriding Thermochemical of Steels Subjected to Process. *Mater. Sci. Eng. A, 236*, 900-903.

Miyashita, F., & Yokota, K. (1996). Plasma-assisted low temperature boridation of pure iron and steels. *Surface and Coatings Technology, 84*(1-3), 334-337.

Nam, K., Lee, K., Lee, S., & Kwon, S. (1998). A study on plasma-assisted bonding of steels. *Surface and Coatings Technology, 98*(1-3), 886-890.

Nora, R., Zine, T. M., Abdelkader, K., Youcef, K., Ali, O., & Jiang, X. (2019). Boriding and boronitrocarburising effects on hardness, wear and corrosion behavior of AISI 4130 steel. *Matéria (Rio de Janeiro), 24*, e-12327.

Pertek, A. (1994). *Gas boriding conditions for the iron borides layers formation.* Paper presented at the Materials Science Forum.

Petrova, R. S., & Suwattananont, N. (2005). Surface modification of ferrous alloys with boron. *Journal of electronic materials, 34*, 575-582.

Prince, M., Raj, G. S., Kumar, D. Y., & Gopalakrishnan, P. (2022). Boriding of Steels: Improvement of Mechanical Properties - a Review. *High Temperature Material Processes, 26*(2), 43-89. Retrieved from <Go to ISI>://WOS:000809652600004

Rodrı, E., Laudien, G., Biemer, S., Rie, K.-T., & Hoppe, S. (1999). Plasma-assisted boriding of industrial components in a pulsed dc glow discharge. *Surface and Coatings Technology, 116*, 229-233.

Selçuk, B., Ipek, R., & Karamış, M. (2003). A study on friction and wear behaviour of carburized, carbonitrided and borided AISI 1020 and 5115 steels. *Journal of Materials Processing Technology, 141*(2), 189-196.

Selçuk, B., Ipek, R., Karamiş, M., & Kuzucu, V. (2000). An investigation on surface properties of treated low carbon and alloyed steels (boriding and carburizing). *Journal of Materials Processing Technology, 103*(2), 310-317.

Singhal, S. (1977). A hard diffusion boride coating for ferrous materials. *Thin Solid Films, 45*(2), 321-329.

Sinha, A. K. (1991). Boriding(boronizing). *ASM International, ASM Handbook., 4*, 437-447.

Subrahmanyam, J., & Gopinath, K. (1984). Wear studies on boronized mild steel. *Wear, 95*(3), 287-292.

Tabur, M., Izciler, M., Gul, F., & Karacan, I. (2009). Abrasive wear behavior of boronized AISI 8620 steel. *Wear, 266*(11-12), 1106-1112.

Takeuchi, E., Fujii, K., & Katagiri, T. (1979). Sliding Wear Characteristics. *Wear, 55*, 21-30.

Tarasov, S. Y., Trusova, G., Kolubaev, A., & Sizova, O. (1995). Structural properties of boride coatings for triboengineering. *Metal Science and Heat Treatment, 37*(6), 257-260.

Tsipas, D., & Tsipas, S. (2016). Boronizing of iron-based alloys. In *Encyclopedia of Iron, Steel, and Their Alloys (Online Version)* (pp. 376-400): CRC Press.

Venkataraman, B., & Sundararajan, G. (1995). The high speed sliding wear behaviour of boronized medium carbon steel. *Surface and Coatings Technology, 73*(3), 177-184.

Von Matuschka, A., & Boronizing, H. (1980). Son Inc. *Philadelphia, USA.*

Wang, A., & Hutchings, I. (1988). Mechanisms of abrasive wear in a boronized alloy steel. *Wear, 124*(2), 149-163.

Yoon, J., Jee, Y., & Lee, S. (1999). Plasma paste boronizing treatment of the stainless steel AISI 304. *Surface and Coatings Technology, 112*(1-3), 71-75.

Zhang, P., Zhang, F., Yan, Z., Wang, T., & Qian, L. (2011). Wear property of low-temperature bainite in the surface layer of a carburized low carbon steel. *Wear*, *271*(5-6), 697-704.

Zimmermann, D. (1992). Neues Schnellaufkohlungsverfahren und Anwendung in einer flexiblen Anlage. *HTM Journal of Heat Treatment and Materials*, *47*(1), 37-42.

CHAPTER V

Effect of Isentropic Efficiency On Exergetic Performance and Power Generation İn S-CO_2 Power Cycles

Mehmet ALTINKAYNAK[1]
MURAT ÖZTÜRK[2]

Introduction

In industry or in most heavy industry, there are process gases at high temperatures. These temperatures are generally used for drying needs of the industry or for preheating or annealing of raw materials. It is already known that these high temperatures are used in electricity generation with waste heat recovery systems.

In this study, it is aimed to transfer these high temperature process gases to supercritical carbon dioxide fluidity by passing

[1] Doç. Dr., Isparta University of Applied Sciences, Faculty of Technology, Department of Mechanical Engineering, Isparta/Turkey, Orcid: 0000-0003-2434-576X, mehmetaltinkaynak@isparta.edu.tr
[2] Prof. Dr., Isparta University of Applied Sciences, Faculty of Technology, Department of Mechatronics Engineering, Isparta/Turkey, Orcid: 0000-0003-1585-0449, muratozturk@isparta.edu.tr

them through a heat exchanger. The aim here is to examine the fluid efficiency at high temperatures. In addition, the energy and exergy changes of the fluid and power production will be investigated. The effects of the isentropic efficiencies of the turbine providing power generation and the compressor that presses the fluid into the heat exchanger on the exergetic efficiency and power generation will also be shown.

System Description

The flow chart of the s-CO_2 power cycle is given in Figure 1. Here, the fluid is first pressed into the recuperator with the help of a compressor. In the recuperator, the heated fluid enters the heat exchanger at a high temperature. Here, the fluid exposed to the process gas is heated further and sent to the turbine. After power generation is achieved in the turbine, the fluid that enters the recuperator again, after receiving some more heat energy from the refrigerant, enters the compressor again and the cycle is completed.

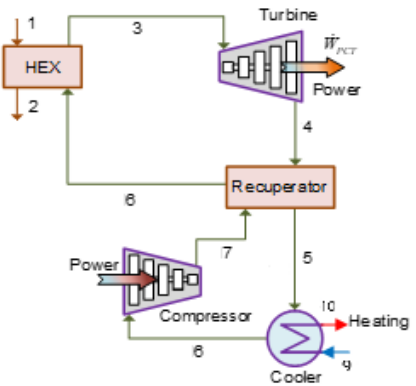

Figure 1. *Schematic diagram of s-CO_2 power cycle and power production from s-CO_2 turbine.*

Thermodynamic analysis

In this study, the comprehensive effectiveness analysis of the combined system for power, heating and cooling products is conducted by considering the energy and exergy analysis from the thermodynamic viewpoint. In general, it is necessary to provide several assumptions for the thermodynamic analysis and evaluation. Hence, the several assumptions have been defined for the thermodynamically analysis of combined plant components as written below:

- The kinetic and potential energy and exergy changes are negligible.
- The steady-state working conditions exist.
- The thermal energy losses and pressure drops in the pipe connections are neglected.
- Calculations were made using the Engineering equation Server program (EES,2011).

The balance equations of the mass, energy, entropy and exergy can be given as (Dincer, 2020):

$$\sum_{in} \dot{m} = \sum_{out} \dot{m} \quad (1)$$

$$\sum_{in} \dot{m}h + \sum_{in} \dot{Q} + \sum_{in} \dot{W} = \sum_{out} \dot{m}h + \sum_{out} \dot{Q} + \sum_{out} \dot{W} \quad (2)$$

$$\sum_{in} \dot{m}s + \sum_{in} \frac{\dot{Q}}{T} + \dot{S}_{gen} = \sum_{out} \dot{m}s + \sum_{out} \frac{\dot{Q}}{T} \quad (3)$$

$$\sum_{in} \dot{m}ex + \sum_{in} \dot{E}x^{Q} + \sum_{in} \dot{E}x^{W} = \sum_{out} \dot{m}ex + \sum_{out} \dot{E}x^{Q} + \sum_{out} \dot{E}x^{W} + \dot{E}x_{D} = 0 \quad (4)$$

Here, the exergetic quantities can be defined with:

$$\dot{E}x^{Q} = \left(1 - \frac{T_o}{T}\right)\dot{Q} \quad (5)$$

$$\dot{E}x^{W} = \dot{W} \quad (6)$$

$$\dot{E}x_{D} = T_0\dot{S}_{gen} \quad (7)$$

and,

$$ex = ex_{ph} + ex_{ch} \quad (8)$$

Here, ex_{ph} and ex_{ch} denote physical and chemical exergies, and can be defined as given below:.

$$ex_{ph} = (h - h_o) - T_o(s - s_o) \quad (9)$$

$$ex_{ch} = \sum n_i(u_i^0 - u_i^{00}) \quad (10)$$

where u_i^0 and u_i^{00} show chemical potential of i^{th} part of the thermo-mechanical and chemical equilibrium (Dincer & Rosen, 2020). The balance equations of combined system parts are tabulated in Table 1.

Table 1. Thermodynamical balance equations of system parts.

System parts	Balance equations
HEX	MB: $\dot{m}_1 = \dot{m}_2; \dot{m}_3 = \dot{m}_8$ EB: $\dot{m}_1 h_1 + \dot{m}_8 h_8 = \dot{m}_2 h_2 + \dot{m}_3 h_3$ EnB: $\dot{m}_1 s_1 + \dot{m}_8 s_8 + \dot{S}_{g,HEX} = \dot{m}_2 s_2 + \dot{m}_3 s_3$ ExB: $\dot{m}_1 ex_1 + \dot{m}_8 ex_8 = \dot{m}_2 ex_2 + \dot{m}_3 ex_3 + \dot{E}x^D_{HEX}$
s-CO_2 turbine	MB: $\dot{m}_3 = \dot{m}_4$ EB: $\dot{m}_3 h_3 = \dot{m}_4 h_4 + \dot{W}_{Tur}$ EnB: $\dot{m}_3 s_3 + \dot{S}_{g,Tur} = \dot{m}_4 s_4$ ExB: $\dot{m}_3 ex_3 = \dot{m}_4 ex_4 + \dot{E}x^W_{Tur} + \dot{E}x^D_{Tur}$
Recuperator	MB: $\dot{m}_4 = \dot{m}_8; \dot{m}_5 = \dot{m}_7$ EB: $\dot{m}_4 h_4 + \dot{m}_7 h_7 = \dot{m}_8 h_8 + \dot{m}_5 h_5$ EnB: $\dot{m}_4 s_4 + \dot{m}_7 s_7 + \dot{S}_{g,Rec} = \dot{m}_8 s_8 + \dot{m}_5 s_5$ ExB: $\dot{m}_4 ex_4 + \dot{m}_7 ex_7 = \dot{m}_8 ex_8 + \dot{m}_5 ex_5 + \dot{E}x^D_{Rec}$
Cooler	MB: $\dot{m}_5 = \dot{m}_6; \dot{m}_9 = \dot{m}_{10}$ EB: $\dot{m}_5 h_5 + \dot{m}_9 h_9 = \dot{m}_6 h_6 + \dot{m}_{10} h_{10}$ EnB: $\dot{m}_5 s_5 + \dot{m}_9 s_9 + \dot{S}_{g,Col} = \dot{m}_6 s_6 + \dot{m}_{10} s_{10}$ ExB: $\dot{m}_5 ex_5 + \dot{m}_9 ex_9 = \dot{m}_6 ex_6 + \dot{m}_{10} ex_{10} + \dot{E}x^D_{Col}$
Compressor	MB: $\dot{m}_6 = \dot{m}_7$ EB: $\dot{m}_6 h_6 + \dot{W}_{Cmp} = \dot{m}_7 h_7$ EnB: $\dot{m}_6 s_6 + \dot{S}_{g,Cmp} = \dot{m}_7 s_7$ ExB: $\dot{m}_6 ex_6 + \dot{E}x^W_{Cmp} = \dot{m}_7 ex_7 + \dot{E}x^D_{Cmp}$
MB: Mass balance *EB: Energy balance* *EnB: Entropy balance* *ExB: Exergy balance*	

Efficiencies

The energetic and exergetic efficiency viewpoints are utilized to investigate the performance of the solar energy-based combined plants. Hence, the energetic and exergetic effectiveness can described as undermentioned:

$$\eta = \frac{Useful\ energy\ output\ in\ product}{Energy\ input} \quad (11)$$

$$\psi = \frac{Exergy\ output\ in\ product}{Exergy\ input} \quad (12)$$

According to the Eqs. (11) and (12), the energetic and exergetic efficiency equations are tabulated in Table 2. Also, to perform a detailed thermodynamically analysis of multigeneration plant, the energetic and exergetic efficiency equations of the combined system and its subsystems are defined based on the following equations:

Table 2. Energetic and exergetic efficiency equations of system parts

System parts	Energetic and exergetic efficiency equations
HEX	$\eta_{HEX} = \frac{\dot{m}_3 h_3 - \dot{m}_8 h_8}{\dot{m}_1 h_1 - \dot{m}_2 h_2}$ $\psi_{HEX1} = \frac{\dot{m}_3 ex_3 - \dot{m}_8 ex_8}{\dot{m}_1 ex_1 - \dot{m}_2 ex_2}$
s-CO_2 turbine	$\eta_{Tur} = \frac{\dot{W}_{Tur}}{\dot{m}_3 h_3 - \dot{m}_4 h_4}$ $\psi_{Tur} = \frac{\dot{E}x^W_{Tur}}{\dot{m}_3 ex_3 - \dot{m}_4 ex_4}$
Recuperator	$\eta_{Rec} = \frac{\dot{m}_8 h_8 - \dot{m}_7 h_7}{\dot{m}_4 h_4 - \dot{m}_5 h_5}$ $\psi_{Rec} = \frac{\dot{m}_8 ex_8 - \dot{m}_7 ex_7}{\dot{m}_4 ex_4 - \dot{m}_5 ex_5}$
Cooler	$\eta_{Col} = \frac{\dot{m}_{10} h_{10} - \dot{m}_9 h_9}{\dot{m}_5 h_5 - \dot{m}_6 h_6}$ $\psi_{Col} = \frac{\dot{m}_{10} ex_{10} - \dot{m}_9 ex_9}{\dot{m}_5 ex_5 - \dot{m}_6 ex_6}$
Compressor	$\eta_{Cmp} = \frac{\dot{m}_7 h_7 - \dot{m}_6 h_6}{\dot{W}_{Cmp}}$ $\psi_{Cmp} = \frac{\dot{m}_7 ex_7 - \dot{m}_6 ex_6}{\dot{E}x^W_{Cmp}}$

Result and Discussion

The effect of isentropic efficiency on power generation and energy efficiency in power cycles is of great importance. As seen in Figure 2, increasing isentropic efficiency increases energy efficiency. This is due to the increase in enthalpy. As seen in the figure, increasing isentropic efficiency from 80% to 95% increased energy efficiency from 20.18% to 23.07%.

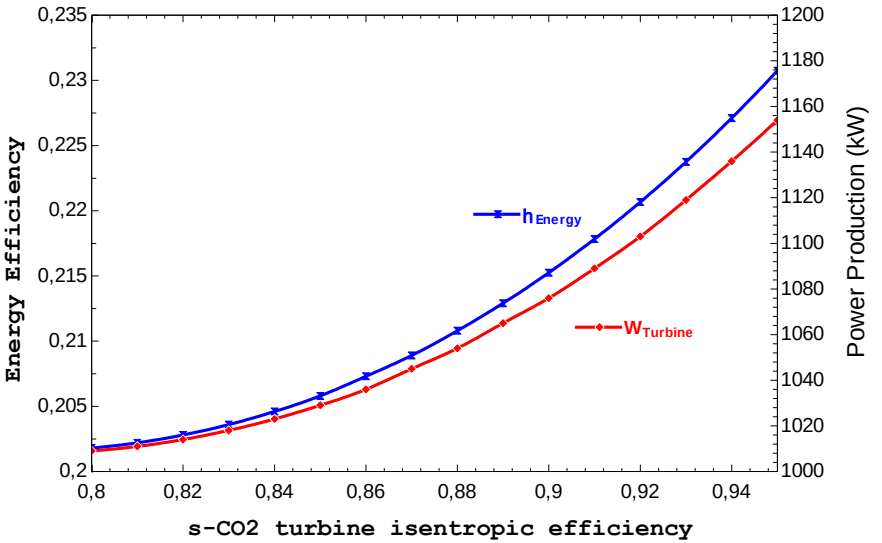

Figure 2. *Effect of s-CO_2 turbine isentropic efficiency on energy efficiencies of s-CO_2 power cycle and power production from s-CO_2 turbine.*

As seen in Figure 3, increasing isentropic efficiency increases exergy efficiency. As seen in the figure, increasing isentropic efficiency from 80% to 94% increased exergy efficiency from 17.23% to 21.21%. When the effect of increasing the isotopic efficiency on power production is examined, it is seen that the power produced in the turbine increases from 1009 kW to 1154 kW.

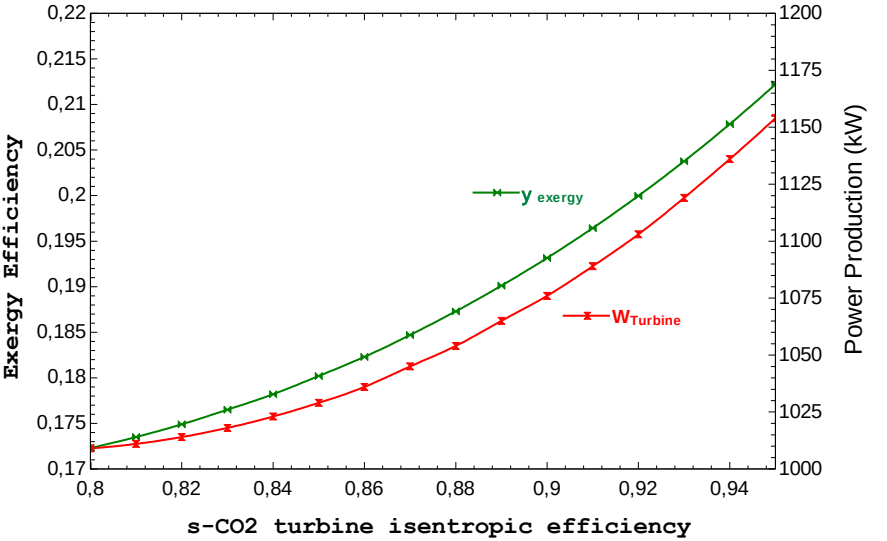

Figure 3. *Effect of s-CO_2 turbine isentropic efficiency on exergy efficiencies of s-CO_2 power cycle and power production from s-CO_2 turbine.*

Another important parameter in compressor power cycles is the isentropic unit of the compressor. Figure 4 shows the effect of the change in the isentropic efficiency of the compressor from 74% to 90% on energy efficiency and power production. As seen in the figure, while the energy efficiency is 20.36% at the 74% isentropic efficiency level, it increases to 21.78% at 90% isentropic efficiency. When we look at the power production depending on this, it is seen that the power production in the tribune has increased from 1018 kW to 1.089 kW.

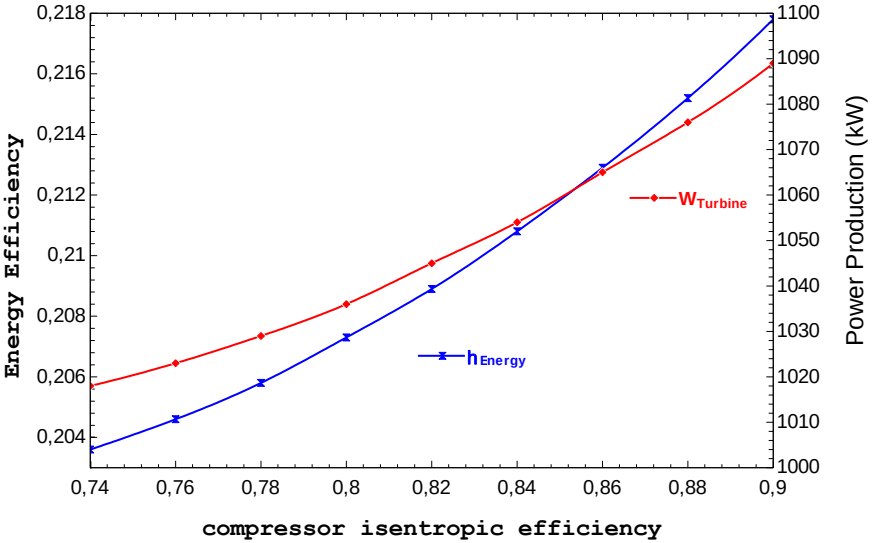

Figure 4. *Effect of Compressor isentropic efficiency on exergy efficiencies of s-CO_2 power cycle and power production from s-CO_2 turbine.*

Figure 5 shows the effect of the change in the isentropic efficiency of the compressor from 74% to 90% on exergy efficiency and power production. As seen in the figure, while the energy efficiency is 17.65% at the 74% isentropic efficiency level, it increases to 19.64% at 90% isentropic efficiency.

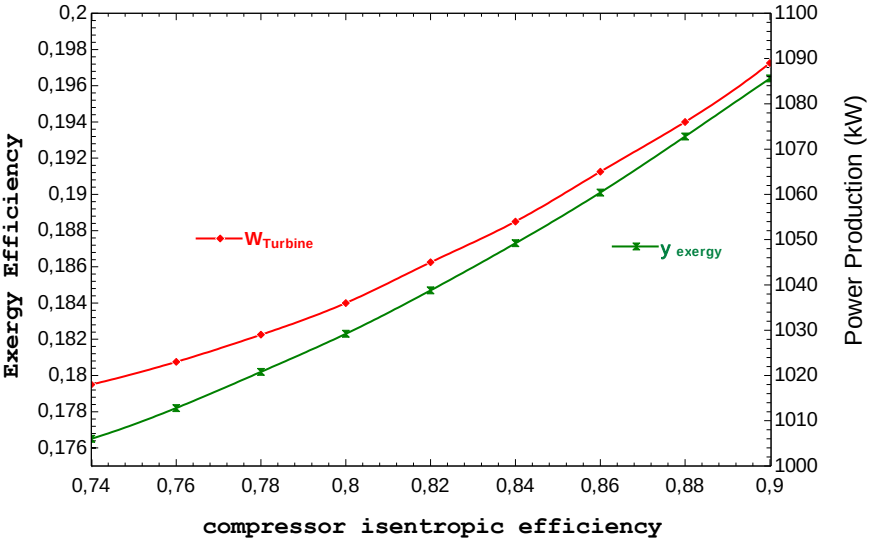

Figure 5. *Effect of Compressor isentropic efficiency on exergy efficiencies of s-CO_2 power cycle and power production from s-CO_2 turbine.*

Conclusion

Process heat can be used in heating, drying, cooking and power generation. In this study, the exergetic efficiency and performance of a high temperature process heat in power generation was investigated by applying the s-CO2 cycle. As a result of the investigation, the isentropic efficiency of the turbine was considered for the first case in the parametric studies, and the isentropic condition of the compressor was considered for the second case. When looking at the turbine accordingly; for the 86% isentropic efficiency of the compressor, the energy efficiency is calculated as 21.29%, the exergy efficiency is 19.01% and the power production is 1065 kW. The same situation is calculated for the 86% isentropic efficiency of the turbine, the energy efficiency is 20.73%, the exergy efficiency is 18.13% and the power production is 1036 kW.

It can be seen from here that increasing the isentropic efficiency for the turbine and compressor increases the energy efficiency of the system as well as the exergy efficiency. Naturally, these two increases increase the power production of the system.

Referances

Klein, S. A. (2011). *Engineering Equation Solver*. version 9.022-3D, F-Chart Software.

Dincer, I., Rosen, MA. (2020). *Exergy: Energy, Environment and Sustainable Development 3rd*. Oxford: Elsevier

Dincer, I. (2020). *Thermodynamics: A Smart Approach*, John Wiley & Sons Ltd.

CHAPTER VI

Investigation On Lean Mixture Combustion In A Port Injection Gasoline Fuelled Spark-Ignition Engine by air heating strategy

Melih YILDIZ[1]

INTRODUCTION

The strategies for fuel consumption and emission reduction in ICEs have drawn great attention due to strict emission legislation conditionally put into effect and reaching fossil fuel-based energy source limits. In this regard, research and development studies have focused on alternative fuels (Bae&Kim, 2017), advanced combustion technologies (Puskar&Kopas, 2024; Krishnamoorthi, Malayalamurthi& Kandasamy, 2019) powertrain technologies such as hybrid and electrical vehicles (Jeong& et al., 2025; Ceper&Yıldız, 2017; DeLuchi, Wang& Sperling, 1989), and exhaust gas treatment systems (Tripathi, Dhar&Sadiki, 2018). These attempts have significantly provided the development of ICEs and the advent of new

[1] Dr.Öğr.Üyesi., Iğdır Üniversitesi, Mühendislik Fakültesi, Makine Mühendisliği Bölümü, Iğdır/Türkiye, Orcid: 0000-0002-6904-9131, melih.yildiz@igdir.edu.tr

technologies to meet the legislation requirements. In particular, the development of after-treatment systems has remarkably contributed to emission reduction for several decades. Nowadays, although vehicles with hybrid and electrified power trains have been increasingly introduced to the market the research on internal combustion engines has still maintained their significance due to their high level share in the market and their use in stationary systems and high-capacity systems. Therefore, improving combustion in an internal combustion engine is essential for fuel and emission reduction.

Spark ignition (SI) and compression ignition (CI) combustion engines constitute the basic technology of internal combustion engines. The difference between these two engine technologies stems from their combustion process. The combustion process in SI engines is characterized by premixed flame propagation, while by a diffusion flame in CI engines (Stone, 1999). In SI engines where premixed combustion takes place, the fuel-air mixture in the combustion process is at stoichiometric ratios to benefit from the catalysts used in exhaust emission control. Unlike SI engines, the fuel-air mixture is close to stoichiometric only in the flame front regions in CI engines. This allows lower fuel consumption in CI engines than those in SI engines. In addition, the limited compression ratios of SI engines to 8-12 due to knocking prevents the increase in engine efficiency (Zheng &et al., 2009). In contrast, CI engines have higher compression ratios, allowing for higher efficiencies. However, CI engines suffer from soot and particulate emissions, along with unburned hydrocarbon, carbon monoxide, and nitrogen oxide emissions. The use of advanced after-treatment systems such as selective catalytic reduction, nitrogen oxide storage reduction, urea-selective reduction, etc. are required to meet the official legislation requirements for these emissions. These catalysts are costly due to their highly advanced technology (Zhao, 2007). Consequently, in addition to the development of catalyst technologies, advanced strategies have been introduced in the combustion process.

Low temperature combustion technique is one of these strategies, which are named HCCI (homogeneous charged compression ignition) (Verma& et al.,2022), CAI (controlled auto ignition) (Fu&et al., 2019), RCCI (reactivity controlled compression ignition) (Kokjohn&et al., 2011), and PCCI (premixed charge compression ignition)(Sing, Kumar&Agarwal, 2020). Theoretically, CAI/HCCI combustion occurs when a well-mixed fuel-air mixture reaches its auto-ignition temperature nearly at the end of the compression stroke. Combustion develops with simultaneous reactions at multiple points within the cylinder volume (Risberg, 2006; Cao&et al., 2010). Therefore, in the CAI/HCCI, ignition and combustion development are different in SI and CI engines and depend entirely on the chemical kinetic process. The combustion process in CAI/HCCI allows using different fuels (Yang&et al., 2011; Maurya&Agarwal, 2011; Li, Neil&Chippior, 2012), and the mixture in a cylinder can be ultra-lean, which gives rise to decreasing combustion temperature and fuel consumption. However, the CAI/HCCI combustion process has drawbacks resulting in limited operating conditions, cold-start problems, and high levels of CO, and UHC (Agarwal, Singh&Maurya, 2017). Many strategies have been brought about to overcome these challenges, which caused emerging spark-assisted CAI/HCCI (Wang&et al., 2006; Xie&et al.,2013; Middleton, Olesky& Lavoie, 2015), RCCI, PCCI combustion process (Pachiannan&et al., 2019; Zheng&et al., 2018; Li, Yang&Zhou, 2017), etc. These combustion processes have enabled extending operating limits and lowering fuel consumption and emissions. Wu and Reitz (2015) carried out the study on the RCCI engine with gasoline–diesel fuel. They showed that an indicated mean effective pressure of 18 bar can be achieved in the RCCI engine. Splitter et al. (2011) reported that the indicated thermal efficiency is 59% in ethanol-diesel fuelled RCCI combustion and 56% in RCCI with gasoline-diesel fuel. In comparison to HCCI and PCCI combustion principles, the RCCI combustion has a comparatively wider operational range. Nevertheless, optimization is still necessary to achieve a full operational range.

Lean mixture combustion in SI engines can also be considered low-temperature combustion due to the dilution effect of the excess air in a cylinder. Thus, it has the potential for a reduction in emissions and an increase in thermal efficiency. Figure 1 implies why research has focused on low-temperature and/or lean-mix combustion. As can be understood from Figure 1, in the lean mixture zones (ϕ <1.0) and temperature values between 1400-2200 K, nitrogen-oxides (NOx) and soot emission can not form. On the other hand, when local temperatures are lower than about 1400 K incomplete combustion products, like CO and HC, increase. In addition, the rich mixture zones 1.0 (ϕ > 1.0) causes an increase in fuel consumption.

Gasoline direct injection (GDI) SI engines were, therefore, introduced to be capable of achieving lean mixture combustion. Although GDI engines provide remarkable fuel savings compared to conventional port injection engines, they can result in deteriorating combustion performance at high operating speeds due to the short time for the fuel-air mixing process. Another disadvantage is the increase in particulate matter (PM) (Qian&et al., 2020). Therefore, the research on GDI has focused on overcoming the challenges by injection strategies to prepare mixture formation (Duan&et al., 2020; Yan&et al., 2022). Generally, the GDI engine switches between modes, which can be defined, as stoichiometric, stratified, and lean modes, by controlling injection timing and duration. The transitions are adjusted depending on the engine speed and load. An example map for mode regions is shown in Figure 2 (Salber&et al., 2002). However, lean mixture combustion in a GDI engine is limited, leading to higher PM emissions that do not meet the emission standard (Kalwar&Agarwal, 2021).

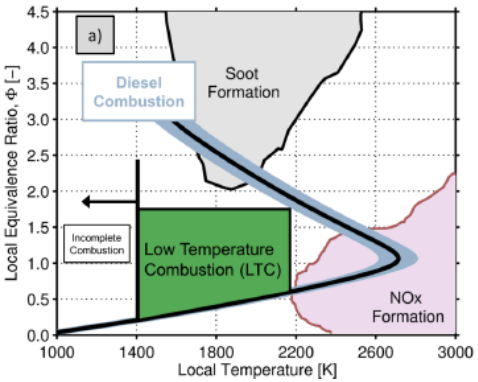

Figure 1. NOx, soot formation regions depending on both equivalence ratio and temperature value for n-heptan, from (Damsey, Curran&Wagner, 2011)

To achieve lean mixture combustion, fuel blends are also considered to increase laminar flame speed. In this regard, the gasoline hydrogen fuel blend is prominent due to the flammability properties of hydrogen (Saravanan&Nagarajan, 2008). Niu et al. (2016) performed experiments to determine the stratified lean mixture combustion characteristics in an H_2/gasoline-fuelled engine by directly injecting H_2 at different excess air ratios (λ) up to 1.8. They stated that the combustion duration decreased and combustion development increased after adding H_2. Thus, pressure development increased, and thermal efficiency elevated. Yu et al. (2019) investigated lean-mixture gasoline SI engine by adding H_2 from 5% to 25%, and introducing exhaust gas recirculation (EGR) at λ values of 1.0, 1.2, and 1.4. They stated that H_2 addition and the use of EGR can elevate the brake mean effective pressure (BMEP). The increases in the BMEP values were found higher than those without EGR at λ=1.2. However, the use of EGR contributed considerable decrease in NOx emissions.

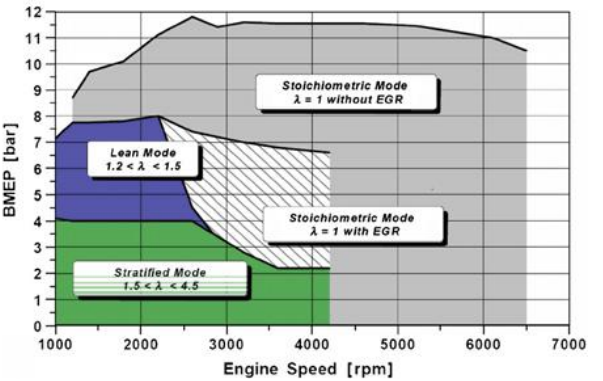

*Figure 2. Operational mode map for a GDI engine (*Salber&et al., 2002*)*

Apart from hydrogen addition, alcohol-based fuels have received much attention due to higher laminar flame speed and octane number than gasoline. Wu et al. (2016) conducted experimental studies to compare lean mixture combustion characteristics of methanol and gasoline in an SI engine at idle conditions. They concluded that methanol fuel showed better lean burn performance than gasoline in terms of indicated mean effective pressure (imep), cyclic variation and emissions, HC, CO, and NOx. Zhang&Cao (2024) investigated the effect of lean burn characteristics in a GDI engine with methanol/gasoline blends. They found that homogeneous lean burn less than λ=1.3 enhanced the power performance of the engine.

The literature survey has shown that the lean mixture combustion process in SI engines has great potential to improve fuel saving and reduce emissions. However, although many methods such as injection strategies, fuel blends, compression ratio, and EGR strategies were implemented, there are still encountered problems to be handled, which can be stated as limited operating range, cyclic variations due to misfire and partial burn, cold start problems, and high CO, HC, and particulate emissions. This study carried out an experimental study on lean-mixture gasoline-fueled SI engines for

different intake air temperatures at three different equivalence ratios. The reason for the use of the air heating strategy is to increase internal energy density for combustion development. Thus, the results give an insight into the required conditions in the cylinder for a lean mixture gasoline engine by analyzing combustion development, engine performance, cyclic variation, and emissions.

MATERIAL and METHODS

Experimental setup

The study was experimentally conducted on a two-cylinder and four-stroke SI engine at Erciyes University Engine Research Laboratory. The engine, whose specification is given in Table 1, is connected to a 40 kW hydraulic dynamometer for controlling engine speed. To heat intake air temperature, air heaters were installed on the intake line, and temperature values were controlled by a thermostat getting signals on the K-type thermocouple placed into the intake manifold. The fuel amount injected into the intake port at 4 bar was adjusted by an injector driver depending on excess ratios measured by a Bosch-BEA60 type gas analyzer.

Table 1. The main specifications of the engine

Bore	72 mm
Stoke	62 mm
Compression ratio	10.7:1
Displacement	505 cc
Injection	Port injection-4bar
Fuel	Gasoline 95 RON
Spark advance	-20 ^{o}CA
Cooling	Water cooling
Intake pressure	Natural aspirated

In-cylinder pressure signals were obtained by a Kistler 6053CC60 pressure transducer and these incoming signals were conditioned into a Kistler-5018A amplifier. Thus, the signals were, then,

displayed on a Picoscope-4425 oscilloscope, and stored with 0.1 ^{o}CA interval for 300 consecutive cycles. The emissions, CO, UHC, and NO were measured Bosch-BEA60 type gas analyzer. The experimental setup and its schematic layout are shown in Figure 3.

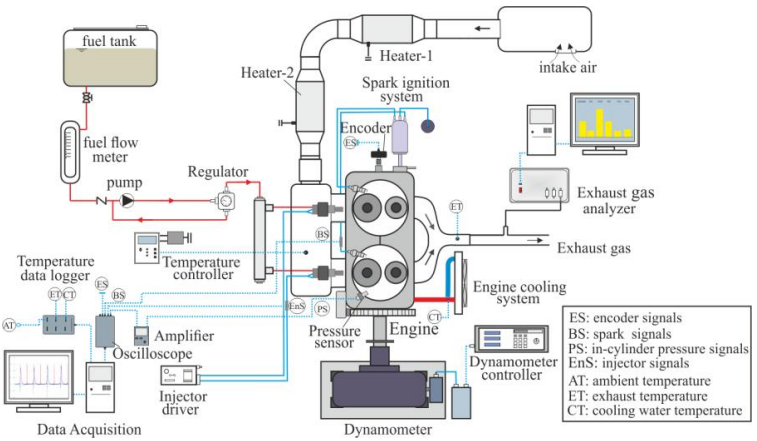

Figure 3. Schematic experimental setup

Experimental process

The experiments were carried out at a constant rotational speed of 2000 rpm with a wide-open throttle position. Initially, the engine started at a stochiometric air-fuel ratio, and then the heater was turned on to increase intake temperature up to the set values. To adjust equivalence ratios, the injected fuel was controlled by an injector driver by considering the excess air ratio value displayed on the gas analyzer. After the engine warmed up to its cooling temperature of 85 ± 2 ^{o}C, the required data was recorded on the experimental system. The experiments were performed for equivalence ratios (ϕ) of 0.710, 0.670, and 0.625 at intake temperatures in the range from 100 ^{o}C to 175 ^{o}C with a 25 ^{o}C increment.

After recording data for 300 consecutive cycles with 0.1 ^{o}CA at each case, combustion developments were investigated by calculating instantaneous net heat release rates and mass burnt fraction curves based on the first law of thermodynamics and Rassweiler-Withrow methods as expressed below (Yıldız&Albayrak Ceper, 2021)

The net heat release rates(HRR):

$$HRR_{\theta i} = \frac{\gamma}{\gamma - 1} P_{\theta i} \frac{V_{\theta i+1} - V_{\theta i}}{\Delta\theta} + \frac{1}{\gamma - 1} V_{\theta i} \frac{P_{\theta i+1} - P_{\theta i}}{\Delta\theta} \quad (1)$$

In Equation 1, *P*, and *V* are instantaneous pressure and volume as a function of the crank angle of θ. γ is the ratio of specific heat capacity. The subscript, θi represents i *th* the crank angle position.

Mass fraction burnt (MFB):

$$MFB_{\theta i} = \frac{\sum_s^i \Delta P_c}{\sum_s^e \Delta P_c} \quad (2)$$

In Equation 2, ΔP_c is the pressure difference resulting from combustion, and *s* and *e* represent the crank angle positions of the starting and ending of combustion phases. The pressure difference due to combustion is calculated as follows [8].

$$\Delta P_{c,\theta i} = \left[P_{\theta i+1} - P_{\theta i} \left(\frac{V_{\theta i}}{V_{\theta i+1}} \right)^k \right] \frac{V_{\theta i}}{V_c} \quad (3)$$

In Equation 3, V_c is the clearance volume, and *k* is a polytropic index.

Lean mixture combustion suffers from cyclic variation due to misfires and partial burns occurring in cycles, resulting in relatively lower engine performance and unstable engine operating (Kalwar&Agarwal, 2021; Böhm&Kempf, 2023). Therefore, the present study investigates the cyclic variation considering the parameter the coefficient of variations (CoV) of indicated mean

effective pressure(imep). The indicated mean effective pressure for each cycle was calculated by the following equation,

$$imep = \frac{1}{V_d}\sum_{i=1}^{j}\left(\frac{P_{\theta i+1} + P_{\theta i}}{2}\right)(V_{\theta i+1} - V_{\theta i}) \quad (4)$$

where, V_d is the displacement volume. j denotes the data number in a cycle corresponding to 720 ^oCA with 0.1 ^oCA resolution. Thus, the coefficient of variance of imep denoted by CoV_{imep} was determined as follows.

$$CoV_{imep} = \frac{\sigma_{imep}}{\overline{imep}} \quad (5)$$

In Equation 5, $\overline{imep}$ is the arithmetic average of imep values for 300 consecutive cycles. σ_{imep} is the standard deviation, and it is calculated by the following equation,

$$\sigma_{imep} = \left(\frac{1}{c-1}\sum_{i=1}^{c}(imep_i - \overline{imep})^2\right)^{1/2} \quad (6)$$

where, c represents the cycle number.

RESULTS and DISCUSSIONS

Combustion development

Figure 4 shows the pressure development and net heat releases for different intake air temperature values at various equivalence ratios. At ϕ= 0.71, the pressure developments first increased and then decreased with an increasing temperature. However, these pressure developments were obtained at higher values compared to those in the case of the inlet air temperature of 100 ^oC. A similar trend is shown at ϕ=0.625, but the pressure developments at 175 ^oC are slightly lower than those at 100 ^oC. The

reasons can be attributed to the increase in intake temperature reduces the amount of air-fuel mixture due to decreasing air density, which results in lower energy density in the cylinder (Jo, Kim&Park, 2020). Moreover, considering heat release rates, their heat releases relatively developed late, which causes lower pressure development. At ϕ=0.670, pressure developments are prone to increase with elevating intake air temperature.

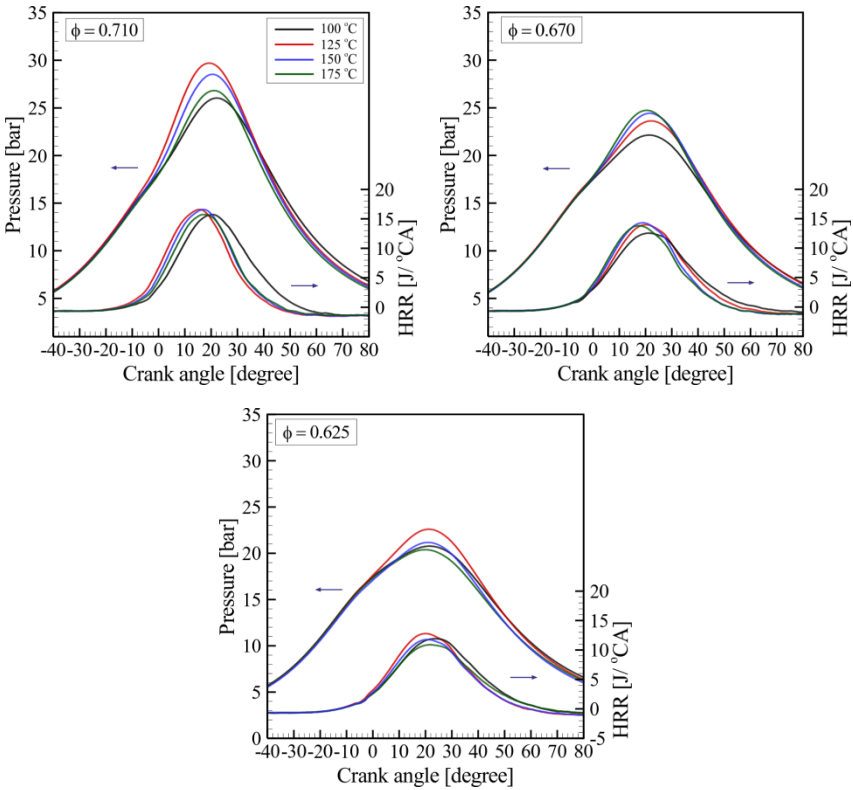

Figure 4. Average in-cylinder pressure traces and heat release rates (HRR) for different intake temperatures and equivalence ratios.

When increasing the equivalence ratio, the pressure development and heat release rate at the same intake air temperature

has a decreasing trend since the mixture becomes leaner (Yu& et al., 2011). Table 2 presents the pressure development characteristics, maximum pressures, and maximum pressure rise rates(PRR_{max}).

Table 2. The obtained maximum pressures and pressure rise rates

ϕ	0.710				0.670				0.625			
T_{int} [^{o}C]	100	125	150	175	100	125	150	175	100	125	150	175
P_{max} [bar]	26.03	29.71	28.52	26.82	22.12	23.63	24.54	24.78	20.77	22.59	21.16	20.38
P_{max} location [^{o}CA-ATDC]	22.2	19.2	20.6	21.1	21.4	22.1	21.5	20.5	21.5	21.2	21.0	19.9
PRR_{max} [bar/^{o}CA]	0.47	0.75	0.66	0.56	0.37	0.38	0.41	0.46	0.37	0.37	0.37	0.37

MFB curves provide an understanding of the combustion phases, CA10, CA50, and CA90 which are ^{o}CA positions corresponding to 10%, 50 %, and 90% of the fuel consumed, respectively. These phases, CA10 and CA90 are generally characterized by the start and end of the main combustion location. CA50 corresponds to nearly occurring maximum heat release rates crank angle position. Besides, combustion duration is usually regarded as the crank angle interval between C10 and CA90 (Cinar& et al., 2015). Figure 5 shows the MFB curves calculated by the average cycles. Considering the CA10 position over 0.1 MFB, the onset of the main combustion is the tendency to move to an earlier ^{o}CA position with an increasing intake air temperature. The CA10 position varies between -3.5 ^{o}CA and -1.2 ^{o}CA at ϕ=0.710, -4.1 ^{o}CA and -2.8 ^{o}CA at ϕ=0.670, and -5.3 ^{o}CA and -4.7 ^{o}CA at ϕ=0.710.

CA50 locations over 0.5 MFB don't show a correlation with the increasing intake air temperature as in the pressure development curves. But, as expected, the increasing equivalence ratio retarded the combustion phases. The maximum combustion durations were found to be about 35 ^{o}CA at ϕ=0.625.

Cyclic variations

As mentioned before, lean mixture combustion has drawback cyclic variation due to deteriorating combustion development

resulting in highly unstable engine operation. Therefore, the CoVimep is a useful indicator to evaluate cyclic variation. Table 3 presents the calculated mean imep and CoV of imep values for different each intake air temperature at different equivalence ratios. As shown in Table 3, an increase in intake air temperature reduces the imep values. On the other hand, CoV_{imep} values are prone to decrease with increasing temperature except for in the case of ϕ=0.625 and Tint = 175 ^{o}C. With increasing the equivelance ratio, the instability of combustion increases under all cases. The highest COVimep values were found at ϕ = 0.625 compared to those at the same intake air temperature. In addition, some CoV_{imep} values obtained higher than 10 %, which can be considered unacceptable levels.

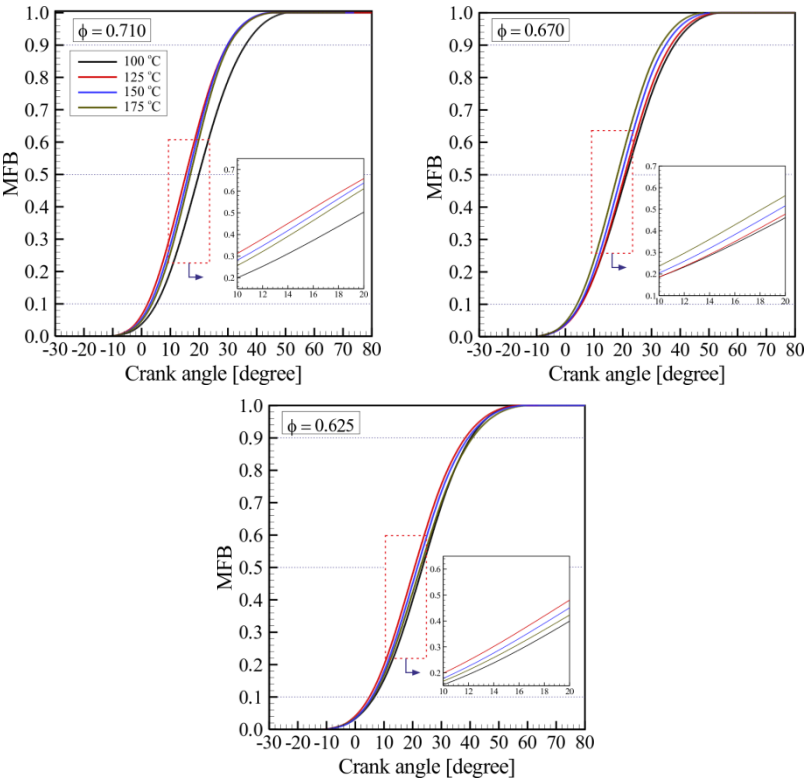

Figure 5. The variation of mass fraction burnt (MFB) for different air temperatures and equivalence ratios

Tablo 3. Mean imep and CoV_{imep} values

ϕ	0.710				0.670				0.625			
T_{int} [°C]	100	125	150	175	100	125	150	175	100	125	150	175
imep [bar]	6.49	6.39	6.22	5.89	5.65	5.92	5.8	5.59	5.48	5.54	5.10	5.04
CoV_{imep} [%]	5.47	3.51	3.31	3.83	10.89	6.34	5.31	6.1	12.42	8.77	8.99	10.98

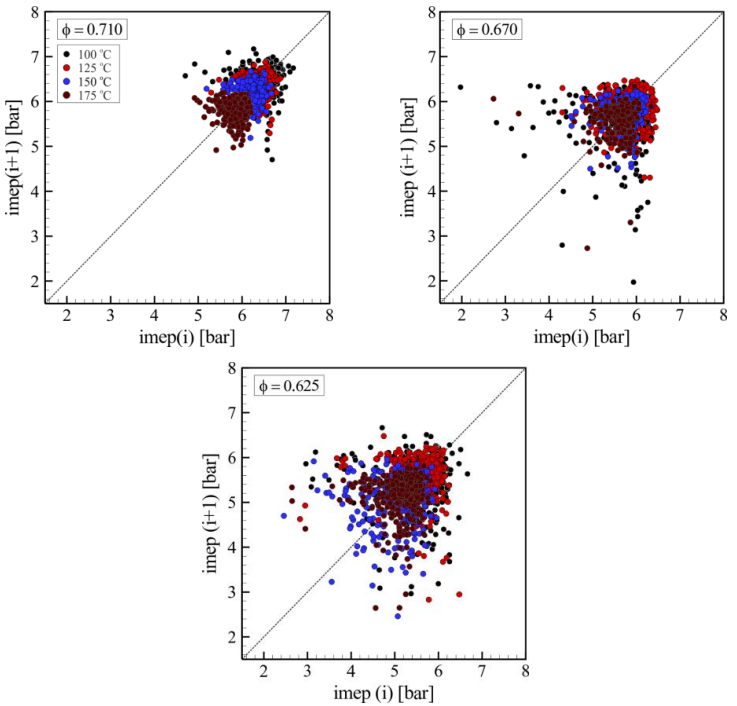

Figure 6. Return maps of imep values

Figure 6 illustrates the return map of the imep values to clearly understand the cycle-to-cycle dynamics (Xu&et al., 2014). A desired appearance is a nearly circular distribution with a narrow range to lower cyclic variation. As shown in Figure 6, when the mixture gets leaner, some imep values scatter quite away from their mean values. It can be stated that these cycles resulted in partial combustion or misfire.

Performance and emissions

CO and HC emissions are related to temperature values and mixture properties. CO emission formation occurs in the zone lower than 1500 K. On the other hand, the zone lower than about 1000 K

contributes to HC formation due to not having adequate thermal conditions to oxidate the fuel (Bhave&et al., 2006). Moreover, although there are adequate thermal conditions in a cylinder, high CO and HC formation may occur due to insufficient O_2 in local zones in the cylinder.

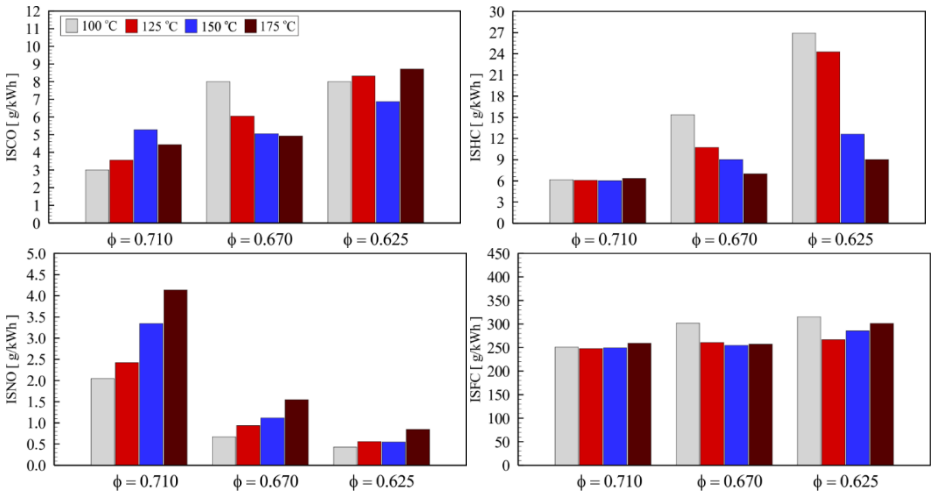

Figure 7. Variation of indicated specific emissions (ISCO, ISHC, ISNO) and specific fuel consumptions (ISFC) with intake air temperature at different equivalence ratios.

Figure 7 shows the indicated specific CO and HC emissions (ISCO, ISHC) at different intake air temperatures at various equivalence ratios. The increasing air temperature shows the different effects on CO emissions. At ϕ=0.710, the ISCO emissions have an increasing trend with an increase in intake air temperature while having a decreasing trend at ϕ=0.670. ISHC emissions values decreased with the increasing air temperature intake. It should be noted that although there can be an improvement in the ISCO and ISHC emissions, they are still high value.

NO formation depends on combustion temperature over 1800 K and prompt reaction at high temperatures

(Maurya&Agarwal, 2011). Therefore, lean mixture combustion reduces NO emissions due to low temperature combustion. As shown in Figure 7, ISNO emissions increase with the increasing air temperature. This is because increasing intake air temperature raises the temperature value during the onset of the combustion reaction, which increases combustion temperature. Additionally, increasing the excess air ratio reduced ISNO since a higher diluted mixture with air reduced the combustion temperature, resulting in lower ISNO emissions as in the study performed by Zhang and Cao (2024, pp:1169-1180).

The increasing intake air temperature has different effects on ISFC values depending on ϕ values. At ϕ=0.710, ISFC first slightly decreases from 250.85 to 247.67 g/kWh, and then it has an increasing trend. Thus, it reached 259 g/kWh at 175 ^{o}C. At ϕ=0.670, ISFC is prone to decreasing with increasing intake air temperature. The values varied from 301.72 to 257.12 g/kWh. Finally, the change in ISFC values at ϕ=0.625 has the same trend at ϕ=0.710. The ISFC is 315.21 g/kWh at ϕ=0.625 and 100 ^{o}C while 301.39 g/kWh at ϕ=0.625 and 175 ^{o}C.

CONCLUSIONS

This study focused on lean mixture combustion in a port injection gasoline engine. The research was experimentally conducted to determine the effect of intake air temperature values on combustion, cyclic variation, emissions, and performance. The following conclusions can be stated.

-Increasing air temperature affected combustion developments differently depending on the equivalence ratios. At ϕ = 0.710 and 0.625, pressure values first increased, and then decreased while they increased at ϕ = 0.670.

- The lowest pressure rise rates were found at ϕ = 0.625 and increasing intake air temperature has no discernible effect on the pressure rise rates at ϕ = 0.625.

- Some of the cycles at ϕ = 0.670 and 0.625 resulted in misfires and partial combustion even if the intake air temperature increased. Hence, this caused high cyclic variability values over 10% CoV at ϕ = 0.670 with 100 ^{o}C intake temperature, and ϕ = 0.625 with both 100 ^{o}C and 175 ^{o}C intake temperatures.

- Generally, the increase in the air temperature decreased ISCO and ISHC emissions. In contrast, ISNO emissions increased by elevating the intake air temperature. However, it can also be stated that the equivalence ratio has more effect than the intake air temperature on ISNO emission reduction. These results stem from lower-temperature combustion when the mixture becomes leaner.

- Increasing intake temperature has different effects on ISFC values depending on the equivalence ratio. First, ISFC decreased and then decreased with the increasing intake air temperature at both ϕ = 0.710 and 0.625. ISFC is likely to decrease as intake air temperature rises, with a value of ϕ=0.670. It should be noted that the high ISFC values correspond to high CoV_{imep} values.

Acknowledgements: The author would like to Erciyes University for providing opportunities at the Engine Research Laboratory.

REFERENCES

Agarwal, A.K., Singh, A.P., Maurya, R.K.(2017). Evolution, challenges and path forward for low temperature combustion engines. *Progress in Energy and Combustion Science*, 61:1 – 56. Doi: 10.1016/j.pecs.2017.02.001.

Bae, C., Kim, J. (2017). Alternative fuels for internal combustion engines. *Proceedings of the Combustion Institute*, 36(3): 3389-3413. Doi:10.1016/j.proci.2016.09.009

Bhave, A., Kraft, M., Montorsi, L., Mauss, F. (2006). Sources of CO emissions in an HCCI engine: A numerical analysis. *Combustion and Flame*, 144(3):634 – 637. Doi: 10.1016/j.combustflame.2005.10.015.

Böhm, B., Kempf, A. (2023). Cyclic variations in internal combustion engines. *Flow Turbulence Combust* **110**, 1–2 .Doi:10.1007/s10494-022-00380-4.

Ceper, B.A., Yıldız, M. (2017). Experimental investigation of performance and emissions of the SICAI-hybrid engine systems. *International Journal of Hydrogen Energy*, 42(40): 25791-25800. Doi: 10.1016/j.ijhydene.2017.05.025

Cho, G., Jeong, D., Moon, G., Bae, C. (2010). Controlled auto-ignition characteristics of methane–air mixture in a rapid intake compression and expansion machine. *Energy*, 35(10):4184 – 4191.Doi: 10.1016/j.apenergy.2020.115644

Cinar, C., Uyumaz, A., Solmaz, H., Sahin, F., Polat, S., Yilmaz. E. (2015). Effects of intake air temperature on combustion, performance and emission characteristics of a HCCI engine fueled with the blends of 20% n-heptane and 80% isooctane fuels. *Fuel Processing Technology*, 130: 275-281. Doi: 10.1016/j.fuproc.2014.10.026.

DeLuchi, M., Wang, Q., Sperling, D. (1989). Electric vehicles: Performance, life-cycle cost, emissions, and recharging requirements. *Transportation Research Part A: General*, Vol:3, No:3, pp:255-278. Doi: 10.1016/0191-2607(89)90007-1

Dempsey, A.B., Curran, S.J., Wagner, R.M. (2016). A perspective on the range of gasoline compression ignition combustion strategies for

high engine efficiency and low NOx and soot emissions: Effects of in-cylinder fuel stratification. *International Journal of Engine Research*, 17(8):897–917. Doi: 10.1177/1468087415621805.

Duan, X., Li, Y., Liu, Y., Liu, J., Wang, S., Guo, G. (2020). Quantative investigation the influences of the injection timing under single and double injection strategies on performance, combustion and emissions characteristics of a GDI SI engine fueled with gasoline/ethanol blend. *Fuel*, 260:116363. Doi: 10.1016/j.fuel.2019.116363.

Fu, X-Q., He, B-Q., Zhao, H., Zhang, Y., Li, Y., Bai, H.(2019). The Application of Controlled Auto-Ignition Gasoline Engines -The Challenges and Solutions. *SAE Technical Paper*, 2019-01-0949. Doi:10.4271/2019-01-0949.

Jeong, J.W., Woo, S., Koo, B., Lee, K. (2025) Analysis of hybrid electric vehicle performance and emission applied to LPG fuel system. *Fuel*, 380: 133225.Doi: 10.1016/j.fuel.2024.133225

Jo, S., Kim, H.J., Park, S. (2020). Effect of high-air temperature on emissions characteristics under constant charging effeciency. *Fuel*, 273117733. Doi: 10.1016/j.fuel.2020.117733.

Kalwar, A., Agarwal, A.K. (2021). Lean-Burn Combustion in Direct-Injection Spark-Ignition Engines. In: Singh, A.P., Kumar, D., Agarwal, A.K. (eds) Alternative Fuels and Advanced Combustion Techniques as Sustainable Solutions for Internal Combustion Engines. Energy, Environment, and Sustainability. Springer, Singapore. Doi:10.1007/978-981-16-1513-9_12.

Kokjohn S.L., Hanson R.M., Splitter D.A., Reitz R.D.(2011). Fuel reactivity controlled compression ignition (RCCI): a pathway to controlled high-efficiency clean combustion. *International Journal of Engine Research*, 12(3): 209-226. Doi: 10.1177/14680874114015

Krishnamoorthi, M., Malayalamurthi, R., He,Z., Kandasamy S.(2019). A review on low temperature combustion engines: Performance, combustion and emission characteristics. *Renewable and Sustainable Energy Reviews*, 116 :109404.Doi : 10.1016/j.rser.2019.109404

Li J., Yang W., Zhou D.(2017). Review on the management of RCCI engines. *Renew Sustain Energy Rev*, 69 , pp. 65-79. Doi: 10.1016/j.rser.2016.11.159.

Li, H., Neill, W., Chippior, W.L. (2012). An experimental investigation of HCCI combustion stability using n-Heptane. *Journal of Energy Resources Technology*, 134(2):022204–1–022204–8. Doi: 10.1115/1.4005700.

Maurya, R.K. Agarwal, A.K. (2011). Experimental investigation on the effect of intake air temperature and air–fuel ratio on cycle-to-cycle variations of HCCI combustion and performance parameters. *Applied Energy*, 88(4):1153–1163. Doi: 10.1016/j.apenergy.2010.09.027.

Maurya, R.K., Agarwal, A.K. (2011). Experimental study of combustion and emission characteristics of ethanol fuelled port injected homogeneous charge compression ignition (HCCI) combustion engine. *Applied Energy*, 88 (4):1169-1180. Doi: 10.1016/j.apenergy.2010.09.015.

Middleton, R.J., Olesky, L.K.M., Lavoie, G.A.(2015). Wooldridge, M.S., Assanis, D.N., Martz, J.B. The effect of spark timing and negative valve overlap on spark assisted compression ignition combustion heat release rate. *Proc Combust Inst* ; 35(3): 3117–3124. Doi: 10.1016/j.proci.2014.08.021.

Niu, R., Yu, X., Du, Y., Xie, H., Wu, H., Sun, Y. (2016). Effect of hydrogen proportion on lean burn performance of a dual fuel SI engine using hydrogen direct-injection. *Fuel*, 186 :792-799. Doi: 10.1016/j.fuel.2016.09.021.

Pachiannan, T., Zhong, W., Rajkumar, S., He, Z., Leng, X., Wang, Q.(2019). A literature review of fuel effects on performance and emission characteristics of low-temperature combustion strategies. *Applied Energy*, 251:113380. Doi: 10.1016/j.apenergy.2019.113380.

Puskar, M., Kopas, M. (2024) Advanced hybrid combustion systems as a part of efforts to achieve carbon neutrality of the vehicles. *MRS Energy&Sustainability*, 11, 123-135. Doi: 10.1557/s43581-023-00079-7. Doi: 10.1557/s43581-023-00079-7

Qian, Y., Wang, J., Li, Z., Jiang, C., He, Z., Yu, L., Lu, X. (2020). Improvement of combustion performance and emissions in a gasoline

direct injection (GDI) engine by modulation of fuel volatility. *Fuel*, 268:117369. Doi: 10.1016/j.fuel.2020.117369.

Risberg, P. (2006). Describing the auto-ignition quality of fuels in HCCI engines, Ph.D. thesis, School of Industrial Engineering and Management Royal Institute of Technology-Stockholm.

Salber, W., Wolters, P., Esch, T., Geiger, J., Dilthey, J. (2002). Synergies of variable valve actuation and direct injection. SAE Tecnical Paper. 2002-01-0706. Doi: 10.4271/2002-01-0706.

Saravanan, N., Nagarajan, G.(2008). An experimental investigation of hydrogen-enriched air induction in a diesel engine system. *International Journal of Hydrogen Energy*, 33(6):1769-1975. Doi: 10.1016/j.ijhydene.2007.12.065.

Singh A.P., Kumar V., Agarwal A.K. (2020). Evaluation of comparative engine combustion, performance and emission characteristics of low temperature combustion (PCCI and RCCI) modes. Applied Energy, 278 :115644. Doi: 10.1016/j.apenergy.2020.115644

Splitter D., Hanson R., Kokjohn S., Reitz R.D.(2011). Reactivity controlled compression ignition (RCCI) heavy-duty engine operation at mid-and high-loads with conventional and alternative fuels. *SAE technical paper*, 2011-01-0363. Doi:10.4271/2011-01-0363.

Stone, R. (1999). Introduction to internal combustion engines. (4*th* Edition). SAE International and Macmillan Press

Tripathi, G., Dhar, A., Sadiki, A. (2018). Recent Advancements in After-Treatment Technology for Internal Combustion Engines—An Overview. In: Srivastava, D., Agarwal, A., Datta, A., Maurya, R. (eds) Advances in Internal Combustion Engine Research. Energy, Environment, and Sustainability. Springer, Singapore. Doi:10.1007/978-981-10-7575-9_8.

Verma, .K., Gaur, S., Akram, T., Gautam, S., Kumar, A.(2022). Emissions from homogeneous charge compression ignition (HCCI) engine using different fuels: A review. *Environ Sci Pollut Res*, 29, 50960–50969 (2022). Doi:10.1007/s11356-021-15602-x.

Wang Z, Wang JX, Shuai SJ, Tian GH, An X, Ma QJ. (2006). Study of the effect of spark ignition on gasoline HCCI combustion. *Proc IMechE, Part D: J Automobile Engineering* , 220(6): 817–825. Doi: 10.1243/09544070JAUTO15.

Wu Y., Reitz R.D.(2015). Effects of exhaust gas recirculation and boost pressure on reactivity controlled compression ignition engine at high load operating conditions. *J Energy Resour Technol*, 137 (3) (2015). Doi: 10.1115/1.4029866.

Wu, B., Wang, L., Shen, X., Yan, R., Dong, P. (2016). Comparison of lean burn characteristics of an SI engine fueled with methanol and gasoline under idle condition. *Applied Thermal Engineering*, 95:264-270. Doi: 10.1016/j.applthermaleng.2015.11.029.

Xie, H., Li, L., Chen, T., Yu, W., Wang, X., Zhao, H. (2013). Study on spark assisted compression ignition (SACI) combustion with positive valve overlap at medium–high load. *Appl Energ*, 101: 622–633. Doi: 10.1016/j.apenergy.2012.07.015.

Xu, K., Xie, H., Chen, T., Wan, M., Zhao, H.(2014). Effect of flame propagation on the auto-ignition timing in SI-CAI hybrid combustion (SCHC). *SAE technical paper*, 2014-01-2672. Doi: 10.4271/2014-01-2672.

Yan, Y., Yang, R., Sun, X., Li, R., Liu, Z. (2022). Numerical investigations of injection timing effects on a gasoline direct injection engine performance: Part A, In-cylinder combustion process. *Front. Energy Res*., 10:828167. Doi: 10.3389/fenrg.2022.828167.

Yang, Y., Dec, J.E., Dronniou, N., Sjöberg, M. (2011). Tailoring HCCI heat-release rates with partial fuel stratification: Comparison of two-stage and single-stage-ignition fuels. *Proceedings of the Combustion Institute*, 33(2):3047 – 3055. Doi: 10.1016/j.proci.2010.06.114.

Yıldız, M., Albayrak Çeper, B. (2021). Combustion development in a gasoline-fueled spark ignition-controlled auto-ignition engine operated at different spark timing and intake air temperatures. *International Journal of Engine Research*, 22(2):351-363. Doi: 10.1177/1468087419894165.

Yu, X., Guo, Z., He, L., Dong, W., Sun, P., Du, Y., Li, Z., Yang, H., Wang, S., Wu, H. (2019). Experimental study on lean-burn characteristics

of an SI engine with hydrogen/gasoline combined injection and EGR. *International Journal of Hydrogen Energy*, 44:13988-13998. Doi: 10.1016/j.ijhydene.2019.03.236.

Yu, X.-c., Liu, Z.-c. Wang, Z.-s., Dou, H.-l. (2011) Effects of EGR rate and excess air ratio on the combustion characteristics of compressed natural gas engine. *Proceedings 2011 International Conference on Transportation, Mechanical, and Electrical Engineering (TMEE)*, 2011, Changchun, China, (pp. 1177-1180). Doi: 10.1109/TMEE.2011.6199415.

Zhang, M., Cao, J. (2024). Effects of lean burn on combustion and emissions of a DISI engine fueled with Methanol–Gasoline Blends. *Energies*, *17*(16), 4023. Doi: 10.3390/en17164023.

Zhao, H. (2007). Motivation, definition and history of HCCI/CAI engines, H. Zhao, (edt), HCCI and CAI Engines for the Automotive Industry, 3 – 19, Woodhead Publishing.

Zheng, J-J., Wang, J-H., Wang, B., Huang, Z-H. (2009). Effect of the compression ratio on the performance and combustion of a natural-gas direct-injection engine.*Proceeding of the Institution of Mechanical Engineers, Part D: Journal of Automobile Engineering*, 223(1): 85-98. Doi: 10.1243/09544070JAUTO

Zheng, Z., Xia, M., Liu, H., Shang, R., Ma, G., Yao, M. (2018). Experimental study on combustion and emissions of n-butanol/biodiesel under both blended fuel mode and dual fuel RCCI mode. *Fuel*, 226, pp. 240-251. Doi: 10.1016/j.fuel.2018.03.151.

CHAPTER VII

Polymer, Metal, and Ceramic Matrix Composites in the Aerospace and Defense Industry

Sakine KIRATLI[1]

1. Introduction

Countries face internal and external threat elements due to various factors. These elements jeopardize national security and independence, highlighting the importance of the defense industry. For this reason, governments around the world make significant investments in research for the defense industry. Special designs are being made for many vehicles such as warships, helicopters, unmanned aerial vehicles, combat tanks, reconnaissance aircraft, and fighter jets.

The defense industry refers to all industrial facilities that produce the weapons, ammunition, equipment inputs, and spare

[1] Çankırı Karatekin University, Faculty of Engineering, Department of Mechanical Engineering, Çankırı, Turkey

parts needed by a country's armed forces. This sector encompasses services provided by various businesses for the use of the armed forces, research and development activities for defense systems, technological innovations, and the production of military weapons, weapon subsystems, and spare parts [1].

The aviation sector is of great importance to a country's economy due to reasons such as transportation (cargo and passenger), trade, and tourism. This sector generally operates in two main areas: civil aviation and military aviation. Due to the intense workflow of air vehicles, special attention is given to the development of these vehicles.

The defense industry and aerospace sector are continuously evolving and developing with the advancement of technology. Many components and systems, such as spacecraft, military vehicles, ammunition, weapons, missiles, and explosives, are designed and manufactured in this field. These sectors constantly turn to advanced materials to meet critical requirements such as security, durability, lightness, and efficiency. One of the most notable materials among these is composite materials.

Composite materials are structural materials formed by combining various components. They are typically created by combining a reinforcing fiber, such as glass, carbon, or aramid, with a polymer, metal, or ceramic matrix [2]. The materials used in industry must be resistant to harsh conditions such as corrosive environments and high temperatures, while also being lightweight for fuel efficiency. This is where composite materials stand out, demonstrating their properties of lightness, strength, and

machinability. Due to these properties, they are widely used in many vehicles within the aerospace and defense industries.

Fiber-reinforced composites can be combined with either thermoset or thermoplastic-based polymer matrices. While recycling is not possible with thermoset-based polymers, it is achievable with thermoplastic-based polymers. For example, carbon fiber-reinforced epoxy (thermosets) composites are used to produce structural frames in aircraft [3]. Additionally, in applications such as military aircraft, unmanned aerial vehicles, marine vessels, and weapons, properties such as high stiffness, high strength, low density, corrosion resistance, and vibration resistance are emphasized [4]. Carbon or aramid fiber-reinforced polyethylene (thermoplastic) composites are used in high-maneuverability military aircraft for their impact resistance, flexibility, and lightness [5]. Glass fiber-reinforced polylactic acid composites are used in aerospace for achieving maximum bending strength [6].

2. Areas of Use of Composite Materials in Aerospace and Defense Industry

In the defense industry and aerospace sector, composite materials play a crucial role due to their properties such as lightness, high strength, corrosion resistance, impact resistance, stiffness, and flexibility. From the perspective of the defense industry, many aircraft, missiles, and rockets occupy a significant place in these fields. Below are some examples of the use of composite materials in these sectors.

- Aircraft Fuselages and Wings: Composites commonly used in structural components such as aircraft fuselages and wings

are lighter than aluminum, reducing the overall weight of the aircraft and providing fuel savings [7].

- Interior Components: Parts used in the interiors of aircraft and helicopters are typically made from composite materials. It is important for these parts to be lightweight while also being fire-resistant [7].

- Rotor Blades: Helicopter rotor blades are components that require high strength and lightness. Carbon fiber composites meet these requirements, enhancing the performance of helicopters [7].

- Missiles and Rockets: In the defense industry, composite materials used in the construction of missiles and rockets offer high-temperature resistance and low weight, improving the performance of the missiles and extending their range [7].

- Military Vehicles: Armored vehicles and transports must be resistant to bullets and shockwaves. Composite armor materials provide high strength while being lighter than traditional metal armor [8].

- Defense Equipment: Military equipment needs to be easy to transport and durable for field use. Composite materials are used in the design of such equipment, ensuring both lightness and durability [8].

In Figure 1, the use of composite materials in an Airbus A380 aircraft and its components is shown.

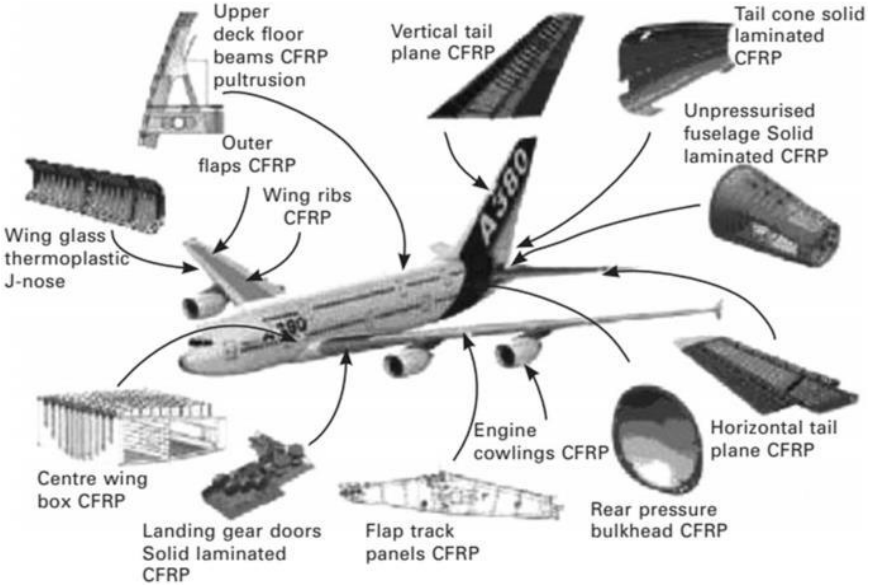

Figure 1. Composites in aircraft and components [9]

Figures 2 and 3 show, respectively, composite aircraft wings and composite interior lining systems.

Figure 2. Composites in various aircraft wing designs [10]

Figure 3. Composites in interior lining systems [11]

3. Composite Materials in the Aerospace and Defense Industry

Composites can be classified based on the fiber and matrix elements. The fiber element can be continuous, discontinuous, or short in form, while the matrix element can be polymer-based, metal-based, or ceramic-based. Commonly used fiber elements include glass, carbon, and aramid synthetic fibers. Despite recent studies on the use of natural fibers, they have found limited applications in the industry. However, as research progresses, their usage area will expand. In the aerospace and defense industries, synthetic-based continuous fibers are primarily used due to their high mechanical, chemical, electrical, and thermal properties, such as chemical and corrosion resistance, impact resistance, and vibration damping.

Composite materials are preferred in military air vehicles such as aircraft and helicopters for components like wings and tail sections, as well as in runways, armored vehicles like tanks and armored personnel carriers, bulletproof vests, weapon bodies, liquid

armor, unmanned aerial vehicles, military vehicle seat upholstery, and fire-resistant military tents [12].

Table 1 examines the characteristics of an aircraft structure.

Table 1. Aircraft structure and characteristics [13]

REQUIREMENT	APPLICABILITY	EFFECT
Light-weight	All Aerospace Programs	➢ Semi-monocoque construction *Thin-walled-box or stiffened structures ➢ Use of low density materials : *Wood, Al-alloys, Composites ➢ High strength/weight, High stiffness weight
High reliability	All Space Programs	➢ Strict quality control ➢ Extensive testing for reliable data ➢ Certification : Proof of design
Passenger safety	Passenger vehicles	➢ Use of fire retardant material ➢ Extensive testing : Crashworthiness
Durability-Fatigue and corrosion Degradation : Vacuum Radiation Thermal	Aircraft Spacecraft	➢ Extensive fatigue analysis/testing *Al-alloys do not have a fatigue limit ➢ Corrosion prevention schemes ➢ Issues of damage and self-life, life extension ➢ Extensive testing for required environment ➢ Thin materials with high integrity
Aerodynamic performance	Aircraft Reusable spacecraft	➢ Highly complex loading ➢ Thin flexible wings and control surfaces *Deformed shape-Aero elasticity Dynamics ➢ Complex contoured shapes *Manufacturability NC Machining ; Molding
Multi-role or functionality	All Aerospace Programs	➢ Efficient design ➢ Use : Composites with functional properties
Fly-by-wire	Aircrafts, mostly for fighters but also some in passenger a/c	➢ Structure-control interactions *Aero-servo-elasticity ➢ Extensive use of computers and electronics *EMI shielding
Stealth	Specific military aerospace applications	➢ Specific surface and shape of aircraft *Stealth coatings
All-Weather operation	Aircraft	➢ Lightning protection erosion resistance

3.1 Polymer Matrix Composites

The matrix material of polymer composites is reinforced with high-strength fibers like aramid, glass, or carbon. The reinforcing fibers serve as load-bearing elements to boost stiffness and strength, and the polymer matrix serves as a binder to give the composite cohesiveness and structural integrity. Superior mechanical qualities, including rigidity, resistance to corrosion and fatigue, and a high strength-to-weight ratio, are imparted to the composite by this combination. For aerospace structures, where lightweight design and outstanding performance are essential, these qualities make polymer composites perfect [14]. Aeronautics frequently uses polymer composites to reinforce structural integrity, lower weight, and increase fuel efficiency in parts including fuselages, wings, and tail assemblies. Furthermore, numerous aerospace applications, including as propulsion systems, interior structures, and thermal protection systems, greatly appreciate their versatility and adaptability [14].

Certain natural or artificial conditions are used to cure thermoset polymers, which maintain their solid state when heated. Because thermoset-based composites have favorable mechanical and chemical qualities, they are frequently utilized in airplane structures. They have extremely low fracture toughness and fracture stresses. At high temperatures, they are rather unstable, albeit [15].

Thermoplastics, as opposed to thermosets, melt when heated after manufacture. Because they are easily molded after manufacture, have a long shelf life, and can be recycled, thermoplastics are sought as raw materials. In this situation, alternative polymers are preferred over thermosets due to the recent

growth of high-performance engineering polymers [16]. Polyphenylene sulfide (PPS), polyether ether ketone (PEEK), polyether ketone ketone (PEKK), polyphenylene ether, polysulfone, polyoxadiazole, polyimide, polyether amide, polyether amide imide, polynaphthalene, and polyamide imide are an example of high-performance engineering thermoplastics. These polymers have promise for use in the energy, medical, automotive, marine, aerospace, and defense sectors. They have high service temperatures, superior mechanical and physical qualities, favored chemical resistance, and the ability to process quickly and without the need for an autoclave under trying circumstances such high pressure, temperature, and abrasive environments [16]. Figure 4 shows the historical development of thermoplastic use in aircraft.

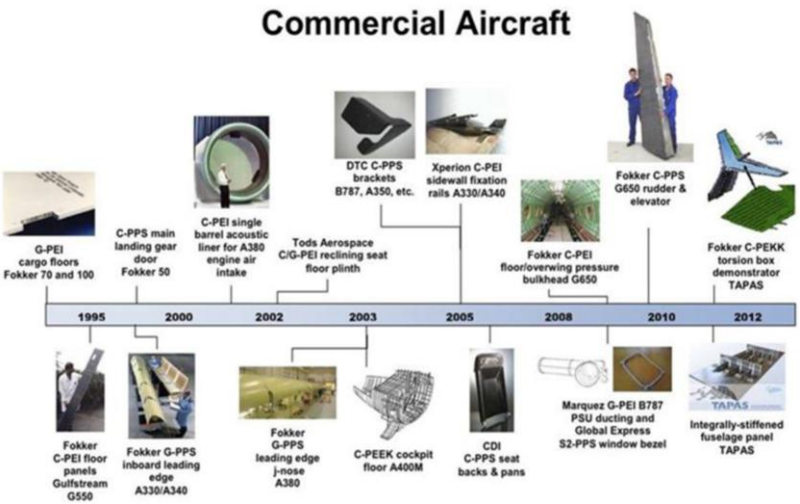

Figure 4. The evolution of thermoplastic usage in commercial aircraft [17]

Glass fibers with a polymer matrix, such as vinyl ester resin, epoxy, or polyester, are mixed to create glass fiber-reinforced polymers, or GFRP. Glass fibers are more cost-effective than carbon fibers and provide better strength and stiffness. Usually, they are composed of silica and other oxides. Although glass fibers are not as strong or lightweight as carbon fibers, they are less expensive than other fiber types and offer good mechanical performance and corrosion resistance. Many industries use GFRPs when cost-effectiveness and modest mechanical performance are required. They are especially utilized in aircraft for non-structural parts like interior panels and fuselage coverings [14].

In composite polymers, reinforcing fibers play a major role in mechanical performance. Because carbon fibers are so lightweight, rigid, and strong, they are perfect for high-performance applications where weight reduction is essential. Carbon precursor materials like pitch or polyacrylonitrile (PAN) are used to make carbon fibers [18].

Carbon fiber-reinforced polymers are composite materials formed by embedding fine carbon filaments, known as carbon fibers, into a polymer matrix. These materials combine the high strength and lightness of carbon fiber with the flexibility and moldability of the polymer matrix. The polymer matrix holds the reinforcing fibers together like an adhesive and deforms when a load is applied, transferring the stress to the solid and stiff fibers. Additionally, polymer matrices have energy-absorbing properties that reduce stress concentration. The main matrices used include polymers such as epoxy, phenolic, or polyurethane [19].

Carbon fiber-reinforced polymers are actively used in aircraft fuselage parts, wings and wing tips, interior components, and engine components. In the defense industry, they are used in armored vehicles, marine vessels, missile and rocket structures, and military equipment [20]. Figure 5 shows the carbon fiber-reinforced composites used in practice.

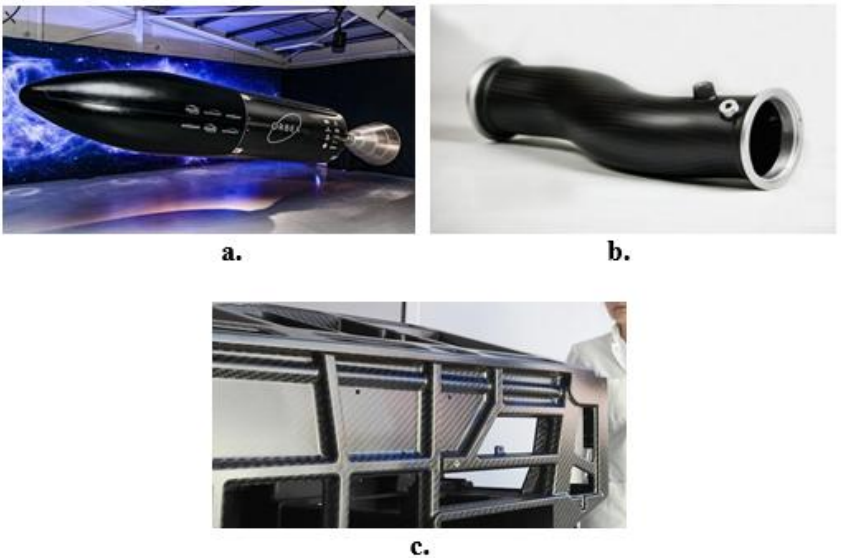

Figure 5. Examples of carbon fiber reinforced composites [21, 22]

Aramid fiber-reinforced composites are composite materials formed by embedding aramid fibers, made from polyester or nylon, into an aramid polymer matrix. These composites combine the high strength and impact absorption properties of aramid fibers with the flexibility and durability of the polymer matrix. Typically, matrices such as epoxy, phenolic, or polyurethane are used [23]. However, these fibers are sensitive to UV radiation when exposed for extended

periods. Additionally, they perform at lower levels compared to carbon fibers at high temperatures [24].

They are commonly used in military equipment, armored vehicles, ballistic protection gear, sports equipment, and other applications that require impact resistance. These materials are preferred for their high strength-to-reinforcement ratio and impact absorption properties. Due to their excellent impact absorption, they are particularly favored in ballistic protection applications [25]. Figure 6 shows the aramid fiber-reinforced composites used in practice.

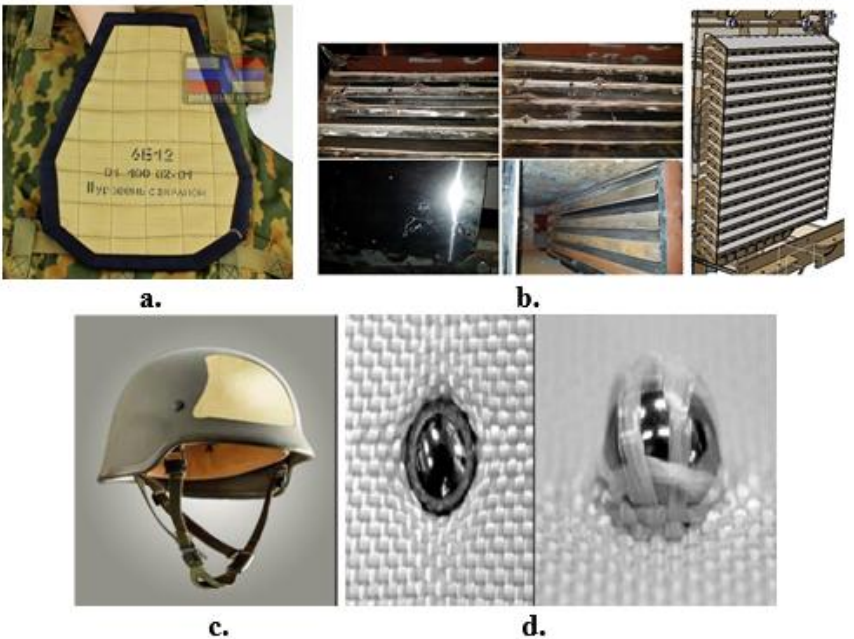

Figure 6. Examples of aramid fiber reinforced composites [11, 26]

3.2 Metal Matrix Composites

Composite materials known as metal matrix composites (MMCs) have reinforcement components like carbon, ceramics, or organic fibers scattered throughout a metal matrix. These reinforcing elements lower the composite's overall density while improving the metal matrix's mechanical qualities [27]. High strength, high electrical and thermal conductivity, low weight, resistance to wear, and thermal stability are among the qualities of MMCs. Usually, the matrices in these composites are metal alloys like nickel, titanium, magnesium, or aluminum. These matrices offer excellent thermal stability and strength. Engine parts, propulsion systems, structural elements, and other defense systems are among the many components in the aerospace and defense industries that use metal matrix composites [28]. Figure 7 shows the metal matrix composites used in practice.

Figure 7. Examples of metal matrix composites [29, 30]

3.3 Ceramic Matrix Composites

A ceramic matrix is typically a matrix formed by the combination of ceramic fibers or particles. This matrix provides high temperature resistance and chemical durability. Reinforcement materials are evenly distributed within the matrix and are often fixed to the matrix with a special binder. Ceramic matrix composites are used in many industries such as aerospace, the space industry, energy production, and defense due to their properties like high temperature resistance, wear resistance, lightness, and chemical resistance [31]. These materials are especially preferred in high-temperature applications and environments that require wear resistance. A

disadvantage is their low fracture toughness. Aluminum oxide ceramic matrix composites are used in high-temperature applications in the aerospace and defense industries, such as exhaust nozzles, propulsion systems, ignition, and combustion chambers. Silicon carbide ceramic matrix composites are used in applications requiring high temperature and wear resistance, such as certain engine parts and thermal insulation panels. Silicon nitride ceramic matrix composites are used in applications like gas turbines and ballistic protection systems due to their properties such as wear resistance and low density [32]. Figure 8 shows the ceramic matrix composites used in practice.

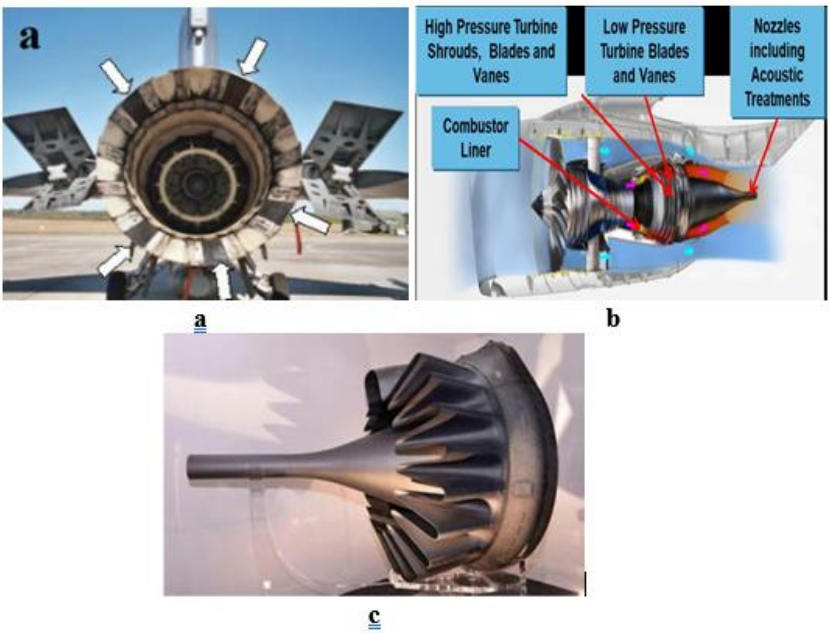

Figure 8. Ceramic matrix composites examples [33, 34]

4. Conclusions

Many industrial sectors conduct research and development activities to continuously improve and innovate materials. In these sectors, while there is a distribution of materials across different areas, composite materials occupy a significant place. Composite materials, which belong to the advanced materials class, are increasing in popularity every day. Advanced composite materials are rapidly replacing traditional metal materials such as aluminum, steel, and titanium. The wide range of applications of composite materials in the aerospace and defense industries will continue to increase due to many factors. Innovations in manufacturing methods and developments in nanotechnology are among these factors.

Composite materials are produced using classical methods such as hand lay-up, vacuum infusion, and hot pressing. However, in recent years, methods like additive manufacturing and automated fiber placement have gained attention due to the advantages they provide. Additive manufacturing enables easier production of products. It is intensively used for both the manufacturing and repair of parts for vehicles, ships, and aircraft in the defense industry. Especially in cases where spare parts are needed, the ability to produce them on-site reduces the time required and decreases the need for access. Additionally, it reduces production costs by using less material compared to other manufacturing methods. Moreover, it facilitates the creation of new material combinations for armor, military clothing, ammunition, etc. The ease it offers compared to traditional manufacturing methods allows this technology to be used more and more in the coming years. Automated fiber placement, like additive manufacturing, is an ongoing area of research and will shape

future applications in the aerospace and defense industries. These methods have improved manufacturing processes for the use of polymer composites in aerospace, making it possible to produce complex composite structures with exceptional efficiency and precision.

Intensive research has been conducted in recent years for many applications of nanocomposites. However, as the gap in the use of suitable nanocomposites in the aerospace industry and defense sector is filled, it will expand the scope of future applications.

Polymer, metal, and ceramic matrix composites, thanks to the design flexibility they provide, can maximize component performance in the aerospace and defense industries. Improvements in these composites' resilience to damage, impact durability, resilience at high and low operating temperatures, and chemical resistance are the focus of future study. Because of this continuous innovation, it looks potential that next-generation aerospace vehicles will be developed that can satisfy the changing demands of space exploration and transportation.

References

[1] Yılmaztürk, A. (2023). Türkiye'de savunma sanayi sektörü ve ekonomi üzerindeki etkisinin değerlendirilmesi. *Enderun*, *7*(2), 139-165.

[2] Gay, D. (2022). *Composite materials: Design and applications*. CRC press.

[3] Soutis, C. (2005). Carbon fiber reinforced plastics in aircraft construction. *Materials Science and Engineering: A*, *412*(1-2), 171-176.

[4] Siengchin, S. (2023). A review on lightweight materials for defence applications: Present and future developments. *Defence Technology*, *24*, 1-17.

[5] Shubham, & Ray, B.C. (2024). Polymer Matrix Materials for Ballistic Armors. *In fiber reinforced polymer (FRP) composites in ballistic protection: Microstructural and Micromechanical Perspectives* (pp. 21-34). Singapore: Springer Nature Singapore.

[6] Wang, G., Zhang, D., Wan, G., Li, B., & Zhao, G. (2019). Glass fiber reinforced PLA composite with enhanced mechanical properties, thermal behavior, and foaming ability. *Polymer*, *181*, 121803.

[7] Mangalgiri, P.D. (1999). Composite materials for aerospace applications. *Bulletin of Materials Science*, *22*, 657-664.

[8] National Research Council, Division on Engineering, Physical Sciences, National Materials, Manufacturing Board, Committee on Benchmarking the Technology, & Application of

Lightweighting. (2012). *Application of lightweighting technology to military aircraft, vessels, and vehicles*. National Academies Press.

[9] N Ramli, N., Norkhairunnisa, M., Ando, Y., Abdan, K., & Leman, Z. (2022). Advanced polymer composite for aerospace engineering applications. *In Advanced Composites in Aerospace Engineering Applications* (pp. 1-21). Cham: Springer International Publishing.

[10] Brocklehurst, A., & Barakos, G.N. (2013). A review of helicopter rotor blade tip shapes. *Progress in Aerospace Sciences*, *56*, 35-74.

[11] GMKA A.Ş. (2024) Kompozit balistik ve zırh. (18/12/2024 tarihinde https://gmkas.com/kompozit-balistik-ve-zirh/ adresinden ulaşılmıştır).

[12] Eryıldız, E., & Eker, A.A. (2015). Savunma sanayinde kullanılan ileri kompozit malzemeler ve uygulama alanları. *International Journal of Engineering Research and Development*, *7*(4), 8-12.

[13] Shivi, K. (2017). Polymer composites in aviation sector. A brief review article. *International Journal of Engineering Research & Technology (IJERT)*, 6(6), 518.

[14] Samir, S., Gewali, J.P., Singh, T., Debbarma, K., Mazumdar, S., Lone, F., & Daniella, U.E. Introduction to polymer composites in aerospace. *CNS&E Journal*, *1*(4), 329-339.

[15] Sehgal, A.K., Juneja, C., Singh, J., & Kalsi, S. (2022). Comparative analysis and review of materials properties used in

aerospace Industries: An overview. *Materials Today: Proceedings*, *48*, 1609-1613.

[16] Guney Yilmaz, S., Ferik, E., Birak, S.B., Ozkutlu Demirel, M., Oz, Y., & Kaboglu, C. (2024). High-performance thermoplastic nanocomposites for aerospace applications: A review of synthesis, production, and analysis. *Journal of Reinforced Plastics and Composites*, 07316844241272035.

[17] Ozturk, F., Cobanoglu, M., & Ece, R.E. (2024). Recent advancements in thermoplastic composite materials in aerospace industry. *Journal of Thermoplastic Composite Materials*, *37*(9), 3084-3116.

[18] Parveez, B., Kittur, M.I., Badruddin, I.A., Kamangar, S., Hussien, M., & Umarfarooq, M.A. (2022). Scientific advancements in composite materials for aircraft applications: A review. *Polymers*, *14*(22), 5007.

[19] Das, T.K., Ghosh, P., & Das, N.C. (2019). Preparation, development, outcomes, and application versatility of carbon fiber-based polymer composites: A review. *Advanced Composites and Hybrid Materials*, *2*, 214-233.

[20] Harussani, M.M., Sapuan, S.M., Nadeem, G., Rafin, T., & Kirubaanand, W. (2022). Recent applications of carbon-based composites in defence industry: A review. *Defence Technology*, *18*(8), 1281-1300.

[21] Scalia, T., Bonventre, L., & Terranova, M.L. (2023). From protosolar space to space exploration: the role of graphene in space technology and economy. *Nanomaterials*, *13*(4), 680.

[22] Hintsteiner Group (2024). Askeri araçlar için karbondan yapılmış patlamaya dayanıklı hava kanalları (15/12/2024 tarihinde https://esut.de/en/2020/10/sponsored-content/23570/carbon-kein-fortschritt-ohne-verbundwerkstoffe-moeglich/ adresinden ulaşılmıştır).

[23] Gore, P.M., & Kandasubramanian, B. (2018). Functionalized aramid fibers and composites for protective applications: A review. *Industrial & Engineering Chemistry Research*, *57*(49), 16537-16563.

[24] He, A., Xing, T., Liang, Z., Luo, Y., Zhang, Y., Wang, M., ... & Xu, W. (2024). Advanced aramid fibrous materials: Fundamentals, advances, and beyond. *Advanced Fiber Materials*, *6*(1), 3-35.

[25] Kukreja, K., & Panda, P.K. (2024). Aramid fiber, its composites and applications. *In synthetic and mineral fibers, their composites and applications* (pp. 61-99). Woodhead Publishing.

[26] Kushan, M.C., Gurgen, S. & Sofuoglu, M.A. (2021). Aramid fabrics used as ballistic plate for army. *8. Internatıonal Fiber And Polymer Research Symposium*, Eskisehir, Turkey.

[27] Miracle, D.B. (2005). Metal matrix composites–from science to technological significance. *Composites Science and Technology*, *65*(15-16), 2526-2540.

[28] Koczak, M.J., Khatri, S.C., Allison, J.E., & Bader, M.G. (1993). *Metal-matrix composites for ground vehicle, aerospace, and industrial applications* (pp. 297-326). Stoneham, MA: Butterworth-Heinemann.

[29] Karaoğlu, S.Y., Karaoğlu, S., & Ünal, İ. (2021). Aerospace industry and aluminum metal matrix composites. *International Journal of Aviation Science and Technology*, 2(02), 73-81.

[30] Srinivasan, V., Kunjiappan, S., & Palanisamy, P. (2021). A brief review of carbon nanotube reinforced metal matrix composites for aerospace and defense applications. *International Nano Letters*, *11*(4), 321-345.

[31] Dhanasekar, S., Ganesan, A.T., Rani, T.L., Vinjamuri, V.K., Nageswara Rao, M., Shankar, E., ... & Misganaw Golie, W. (2022). A comprehensive study of ceramic matrix composites for space applications. *Advances in Materials Science and Engineering*, *2022*(1), 6160591.

[32] Binner, J., Porter, M., Baker, B., Zou, J., Venkatachalam, V., Diaz, V.R., ... & Murthy, T.S.R. C. (2020). Selection, processing, properties and applications of ultra-high temperature ceramic matrix composites, UHTCMCs–a review. *International Materials Reviews*, *65*(7), 389-444.

[33] Gomez, P. (2015). Standardisation of ceramic matrix composites. *In MATEC Web of Conferences* (Vol. 29, p. 00003). EDP Sciences.

[34] Bouillon, E. (2021). Ceramic matrix composite behavior enhancement for gas turbines hot sections. *In Conference of NATO Science and Technology Organization, AVT-356 Research Symposium on Physics of Failure for Military Platform Critical Subsystems* (pp. 15-19).

CHAPTER VIII

An Overview of EMI Shielding Studies for Polymer Matrix Composites

Tuba ÖZDEMİR ÖGE[1]
Mecit ÖGE[2]

1. Introduction

Electromagnetic interference (EMI) refers to transmission of disruptive interfering electromagnetic energy between electromagnetic devices or between devices and environment through radiation or conduction, hence, propagation of EMI might be governed through one of these ways depending on the type of interaction between devices or environments (Hassan et al., 2024; C. Wang et al., 2018). The harmful effects of EMI shielding also

[1] Bartın University, Faculty of Forestry, Department of Forestry Industry Engineering, Bartin, Turkey (ORCID ID, 0000-0001-6690-7199) e-mail: tozdemir@bartin.edu.tr
[2] Bartın University, Faculty of Engineering, Architecture and Design, Department of Mechanical Engineering, Bartın, Türkiye (ORCID: 0000-0001-5243-0828) email: mecitoge@bartin.edu.tr

involve its adverse impacts on human health, such as increased risk of health-related issues, cancer, migraine, asthma, miscarriage, etc. (Kondawar & Modak, 2020). The term “EMI shielding” relates to the efforts to absorb and/or reflect this electromagnetic radiation through utilization of magnetic and conducting materials acting as a shield against such types of conducting or radiating transmission of electromagnetic energy, or by utilization of manufacturing techniques against EMI (*What Is EMI Shielding and Why Is It Important for Your Design?*, n.d.). EMI shielding can also be defined as prevention of microwave and radio wave radiation from penetrating the intended region of area, thus serving as a radiation shield, and it differs from magnetic shielding which is basically shielding from magnetic fields typically with low frequencies (Chung, 2020). Electromagnetic radiation as a relatively new type of environmental pollution has become an important issue against human health as well as efficient operation of electronic devices by increasing use of electric-electronic devices in parallel with rapid technological developments. The reduced weights and higher speeds of electronic devices attained through the advent of technology brought about the issue of undesired transmission of electromagnetic radiation emitted by these gadgets, which is harmful for both human health and operation of other devices. Such that, the mutual and reciprocal interference arising among these devices such as TVs, computers, etc., particularly those emitting high frequency radiation

such as mobile phones also impair the operational efficiency of the same devices (Kondawar & Modak, 2020). Thus, minimization of EM transmission through EMI shielding has become an important research area for several key industries that involve intensive use of electronics such as aerospace, military, communication, etc. (Abedin et al., 2024). Numerous materials and methods have been employed to enable electromagnetic interference shielding. The main types of materials serving as shielding structures or agents are shown in Fig. 1.

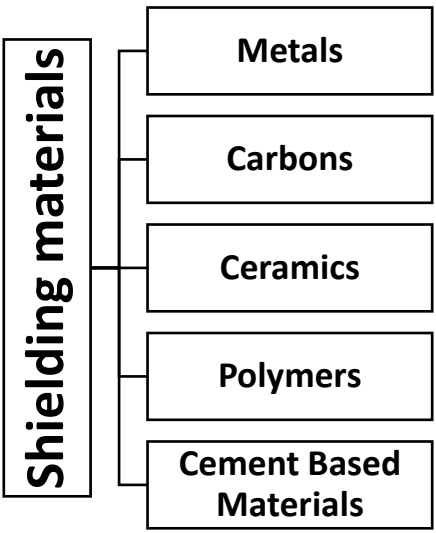

Fig. 1. *Main shielding material types*

2. The Basic Theory of Electromagnetic Interference Shielding

As an electromagnetic wave passes through an EMI shield, reflection and absorption of the wave occurs. The effectiveness of EMI shielding is basically measured as the ratio between the

impinging energy and the residual energy, which is the part of the energy that is not reflected or absorbed (Geetha et al., 2009). As inferred from the term (electromagnetic wave), an electromagnetic wave comprises of two distinct fields, namely magnetic field (B) and electric field (E) (*Plane Electromagnetic Waves - Physics LibreTexts*, n.d.). The magnitude of the wave is correlated with waveform and source of the waveform, its propagation direction is at the right-angle side of the plane involving the magnetic and electric field constituents and E/B ratio gives the impedance of the wave (Geetha et al., 2009). EMI shielding can be roughly categorized as near-field and far-field shielding. Near field shielding relates to the attenuation of EM fields that are close to the radiation source (the distance is smaller than $\lambda/2\pi$, λ being the source wavelength), whereas far-field shielding relates to attenuation of the waves that are away from the EM radiation source (the distance is larger than $\lambda/2\pi$) (*EMI Shielding: Protecting Electronic Devices in a Noisy World*, n.d.; Geetha et al., 2009; X. Y. Wang et al., 2022). The effectiveness of shielding is measured via shielding effectiveness (SE) evaluation and is the ratio between the incident and transmitted radiation or the intensity of field (Mikinka & Siwak, 2021), is quantified in frequency and can be defined by below Equations 1 and 2.

$$SE = 20 \log (E_t/E_i) \quad (1)$$

$$SE = 20 \log (B_t/B_i) \quad (2)$$

where E and B are electric field and magnetic field, respectively, t and i referring to the transmitted and incident waves. Electromagnetic wave attenuation takes place via three mechanisms, namely absorption (A), reflection (R) and multiple reflections (B), so SE can be quantified as the sum of these three terms (SE = A + R + B) (Geetha et al., 2009). SE measurement methods can be chosen based on the intended shielding application and can be categorized as the free space or open field test, coaxial transmission line test, shielded box test and shielded room test.

3. Polymer Matrix Composites

As a pioneering field of material technology, polymer matrix composites (PMC) have been attracting a great deal of interest from various industries and academic fields. Polymers as structural materials have various advantages over their metal-based counterparts in terms of strength-to-weight ratio, ease of manufacturing, design flexibility, functionality etc. Addition of various types of fillers such as organic, inorganic, in fiber or particle form, and in various other types of classifications has been a very popular means to enhance the various properties and functionalities of polymer matrices. The vast number of manufacturing methodologies, structural and reinforcing material have resulted in the introduction of vast number of studies by researchers in the literature of polymer matrix composites. PMCs generally comprise of a matrix constituent which is generally either a thermosetting or

thermoplastic material, reinforced with various type of fillers such as carbon-based fillers, glass, fibers, Kevlar, etc. (Rajak et al., 2019). These materials have been widely preferred for structural and functional purposes in the fields of automotive, aerospace, marine, energy generation, military, communication, oil industry, etc. (Abdulrahman et al., 2024; Dhir et al., 2017; Harussani et al., 2022; Khan et al., 2024). Structural use of polymer matrix composites generally involves the use of fiber reinforcements due to significant enhancements achieved by these fillers in modulus and strength values (Deb, 2010) whereas the functional use of polymer matrix composites is rather related with the use of micro-and nanofillers which are generally of carbon-based materials due to the enhanced thermal, electrical, opto-electric, optical, EMI shielding and other enhanced properties achieved through use of these materials as reinforcements (Omana et al., 2022; Rahimi-Ahar & Rahimi Ahar, 2024). In the present study the recent research attempts for improvement of the EMI shielding capabilities of polymer matrix composites have been compiled and introduced along with brief information related to the materials and methodologies for shielding applications.

4. Recent Studies on EMI Shielding Properties of Polymer Matrix Composites

The studies on enhancement of EMI shielding capabilities of polymer-based composites can be categorized in various ways. In

the current work, we classify and introduce these studies as those on fiber-reinforced composites and polymer nanocomposites.

4.1 Recent Studies on EMI Shielding Properties of Fiber-Reinforced Polymers

To bring an environment-friendly approach for EMI shielding carbon-fiber reinforced composites, Wang et al. (2024) evaluated the EMI shielding and flame-retardancy capabilities of carbon fiber-reinforced composites comprising of CF recycled via pyrolysis recycling (K. Wang et al., 2024). Reportedly, pyrolysis recycling process has been utilized as an effective way to extract fiber via decomposition of the polymer matrix, however the compromised physicochemical and structural properties of the resulting fibers have been an issue which have been addressed by researchers. In their work, the authors propose a surface modification route for the recycled carbon fiber felts, which is reported to lead to significant electromagnetic shielding interference effectiveness (SE) reaching 70.5 dB in the X band after reconstruction of the recycled fiber felt-reinforced resin matrix composites (K. Wang et al., 2024). Munalli et al. (2019) evaluated the shielding effectiveness of carbon fiber-reinforced epoxy laminated composites utilizing a coaxial transmission line test chamber and reported that, slabs with four reinforced prepreg layers attenuated more than 99.9% of electromagnetic radiation. In this work the authors underline the consequences of undesired

electromagnetic fields arising from the densely packed electronic components operating at low voltage within various electronic devices. The authors also highlighted that, the main parameters contributing to the achievement of an improved absorption mechanism were the volume ratio of the reinforcing carbon fibers as well as the number of prepreg layers (Munalli et al., 2019).

In some instances, various nanofillers are introduced into the intended polymer matrices reinforced with carbon fibers, resulting in highly functional composites with hybrid reinforcements. In such a work presented recently, Anu et al. (2024) attempted to introduce an EMI shielding lightweight epoxy-matrix carbon fiber reinforced composites filled with CuO-activated carbon (Anu et al., 2024). The authors reported that, the synergistic effect of carbon fiber reinforced epoxy composites filled with 10 wt.% CuO-activated carbon demonstrated an excellent electromagnetic interference shielding effectiveness of 52.02 dB at 11.48 GHz frequency level which is attributed to the improved ohmic and dielectric losses achieved with this specific samples. Aside from the improved thermal and mechanical properties achieved at this design parameters, the authors postulate that this material is highly applicable for aerospace applications (Anu et al., 2024). In a similar work on hybrid reinforcements, Eken et al. (2023) introduced hematite (Fe_2O_3) and goethite (FeO(OH)) particles with two different particle sizes into carbon fiber reinforced (CFRP) composites comprising of two-

layers and evaluated the resulting hybrid composites' drop impact strength and EMI shielding effectiveness (in the frequency range of 700-6000 MHz) (Yasin Eken et al., 2024). Reportedly, they achieved a maximum EMI SE parameter of 57.85 dB (at 5800 MHz) with hematite reinforcement, and 60.19 d (at 5900 MHz) with goethite reinforcements. Reportedly, the produced CRFP composites offered improved shielding and mechanical properties for demanding applications (Yasin Eken et al., 2024). Durmaz et al. (2023) evaluated the electromagnetic interference shielding improvements of carbon-fiber-reinforced bio-based polyamid 11/poly(lactic acid) (PA11/PLA) samples within X-Band frequencies and utilized conventional extrusion and molding techniques to produce the composite samples. In this comprehensive evaluation of the morphological, thermal, dielectric, electrical conductivity and EMI shielding properties of the samples, they concluded that, inclusion of CF in PA11/PLA blends led to a progressive increase in the EMI SE parameter which were reported to be higher than the CR-reinforced polymer composites in similar works (Ucpinar Durmaz et al., 2023). Küçükelyas et al. (2024) recently performed a study on assessment of the shielding performance of carbon-fiber reinforced polymers filled with CoCuFeNi high entropy alloy (HEA) particles (Küçükelyas et al., 2024). They synthesized the HEA particles via mechanical alloying and reported significant improvements in the EMI SE parameter reaching 73.09 dB at 4.72 GHz (Küçükelyas et

al., 2024). Chen et al. (2024) investigated the effect of silane coupling agent KH570 modified Nano-ZnO particles to enhance the EMI SE of two-dimensional carbon fiber cloths (CFC), and they reportedly achieved an average shielding efficiency of 52.72 dB in the X-band, along with significant improvements in mechanical properties (Chen et al., 2024).

4.2 Recent Studies on EMI Shielding Properties of Polymer Nanocomposites

Along with other research fields on improvement of various functional and structural characteristics of polymer nanocomposites, studies on improvement of EMI shielding efficiencies of polymer-based materials through nanofiller addition also involves a vast number recent and ongoing research studies. In one of these works, Yazdi et al. (2020) conducted a research study on enhancement of EMI shielding capabilities of inherently conducting polymers (ICPs) via addition of conductive non-metallic fillers. To produce conductive nanocomposites, they used polyaniline (PANI) as the ICP, and multi-walled carbon nanotubes (MWCNT) and graphene as the carbon-based nanofillers. They reported high EMI SE acquisition at high filler fractions (Khodadadi Yazdi et al., 2020). In an earlier study, Li et al. (2006) studied the electromagnetic interference shielding of single-walled carbon nanotube (SWCNT) reinforced epoxy-based polymer nanocomposites to attain lightweight materials with high EMI shielding efficiency. The

experimental setup was arranged for 10 MHZ-1.5 GHz frequency range and they accordingly reported up to 49 dB at 10 MHz (Li et al., 2006). Sriseubsai et al. (2020) investigated the EMI shielding effectiveness of polycarbonate (PC) and acrylonitrile–butadiene–styrene (ABS) based nanocomposites with carbon black powder (CBp) nanofiller addition produced via injection molding. Their multi-response optimization studies demonstrated that, employment of higher amounts of PC and CB resulted with higher performance enhancement and that increased filler amount particularly improved the EMI SE parameter (Sriseubsai et al., 2020). Filak et al. (2024) carried out research on evaluation of the EMI shielding performance of fluorinated ethylene propylene (FEP) based nanocomposites filled with graphene nanoplatelets (GNPs) and they reportedly attained significant enhancements in thermal properties in addition to improved EMI SE parameters. They reportedly achieved a homogeneous dispersion of fillers by utilizing a powdered masterbatch pressing technique, thus reaching an outstanding EMI SE of 50 dB at 5 GHz in addition to enhanced thermal conductivity attributes (Filak et al., 2024). Pavlou et al. assessed the shielding capabilities of thin graphene/poly(methyl methacrylate) (PMMA) nanolaminates and they used graphene in discontinuous flake form for this purpose. They reportedly achieved an absolute EMI SE of 60 dB at 33-micron thickness in the terahertz range (Filak et al., 2024).

5. Conclusion

As indicated by the brief survey of the literature works, the subject of EMI shielding improvements for polymer matrix composites evolved mainly around composite types, fiber reinforced polymers, and polymer nanocomposites. The studies related to the shielding improvements for fiber reinforced composites are suitable for applications that demand high EMI shielding efficiency in addition to meeting structural requirements, whereas the performance criteria expected from polymer nanocomposites are rather related to functional requirements such as enhanced thermal and electrical properties in addition to improved EMI SE parameters. As demonstrated by the abovementioned research findings, researchers aim to achieve higher EMI SE parameters as the electronic devices become increasingly more densely packed in smaller dimensions, thus leading to higher extents of interference-related functional impairments in devices. The attenuation of electromagnetic radiation also holds critical importance in terms of protection of human health. The future work on this subject is likely to evolve around additively manufactured fiber and nano-filler reinforced polymers as most of these studies shift to enhancement of these types of materials due to the various advantages of 3D printing technologies in various areas.

References

Abdulrahman, J., Ebhota, W. S., & Tabakov, P. Y. (2024). Biopolymer Composite Materials in Oil and Gas Sector. *International Journal of Polymer Science, 2024*. https://doi.org/10.1155/2024/8584879

Abedin, M. J., Rahman, M. Z., Rahman, S., Sarker, M., Saha, B., Sazal, Y. I., & Salsabil, Z. (2024). Recent advances in applications of hybrid composites. *Comprehensive Materials Processing*, 41–57. https://doi.org/10.1016/B978-0-323-96020-5.00134-5

Anu, K. S., Vishnumurthy, K. A., Mahesh, A., & Natarajan, K. (2024). Carbon fiber-reinforced, activated carbon-embedded copper oxide nanoparticles/epoxy hybrid composites for EMI shielding in aircraft applications. *Polymer Bulletin*, *81*(10), 8723–8750. https://doi.org/10.1007/S00289-023-05112-W/METRICS

Chen, Z. C., Wang, X., An, T., Zhang, F. Z., Peng, Y. Q., Li, A. J., & Liu, L. Q. (2024). Structure-function integrated design of electromagnetic interference shielding and mechanical properties of 2D carbon fiber reinforced polymer composites based on absorption loss regulation. *Polymer Composites*. https://doi.org/10.1002/PC.29097

Chung, D. D. L. (2020). Materials for electromagnetic interference shielding. *Materials Chemistry and Physics*, *255*, 123587. https://doi.org/10.1016/J.MATCHEMPHYS.2020.123587

Deb, A. (2010). Crashworthiness design issues for lightweight vehicles. In *Materials, Design and Manufacturing for*

Lightweight Vehicles. Elsevier Ltd. https://doi.org/10.1533/9781845697822.2.332

Dhir, R. K., Brito, J. de, Mangabhai, R., & Lye, C. Q. (2017). Production and Properties of Copper Slag. *Sustainable Construction Materials: Copper Slag*, 27–86. https://doi.org/10.1016/B978-0-08-100986-4.00003-1

EMI Shielding: Protecting Electronic Devices in a Noisy World. (n.d.). Retrieved December 22, 2024, from https://www.wevolver.com/article/emi-shielding-protecting-electronic-devices-in-a-noisy-world

Filak, K., Sitek, J., Michalski, P., Gołofit, T., Szymański, K. R., Zaleski, P. A., & Łapińska, A. (2024). Fluorinated ethylene propylene (FEP)/graphene nanoplatelet (GNP) nanocomposites as outstanding EMI shielding and heat dissipation material. *Journal of Materials Science*, *59*(7), 2924–2939. https://doi.org/10.1007/S10853-024-09365-2/METRICS

Geetha, S., Kumar, K. K. S., Rao, C. R. K., Vijayan, M., & Trivedi, D. C. (2009). EMI shielding: Methods and materials - A review. *Journal of Applied Polymer Science*, *112*(4), 2073–2086. https://doi.org/10.1002/APP.29812

Harussani, M. M., Sapuan, S. M., Nadeem, G., Rafin, T., & Kirubaanand, W. (2022). Recent applications of carbon-based composites in defence industry: A review. *Defence Technology*, *18*(8), 1281–1300. https://doi.org/10.1016/J.DT.2022.03.006

Hassan, M. W., Elshazly, T. M., & Ponnamma, D. (2024). Cellulose-inspired approaches to sustainable EMI shielding

materials: A comprehensive review. *International Journal of Biological Macromolecules*, *273*, 132920. https://doi.org/10.1016/J.IJBIOMAC.2024.132920

Khan, F., Hossain, N., Mim, J. J., Rahman, S. M., Iqbal, M. J., Billah, M., & Chowdhury, M. A. (2024). Advances of composite materials in automobile applications – A review. *Journal of Engineering Research*. https://doi.org/10.1016/J.JER.2024.02.017

Khodadadi Yazdi, M., Noorbakhsh, B., Nazari, B., & Ranjbar, Z. (2020). Preparation and EMI shielding performance of epoxy/non-metallic conductive fillers nano-composites. *Progress in Organic Coatings*, *145*, 105674. https://doi.org/10.1016/J.PORGCOAT.2020.105674

Kondawar, S. B., & Modak, P. R. (2020). Theory of EMI shielding. *Materials for Potential EMI Shielding Applications: Processing, Properties and Current Trends*, 9–25. https://doi.org/10.1016/B978-0-12-817590-3.00002-6

Küçükelyas, B., Kaykılarlı, C., Eken, T. Y., Erbaş, U., & Tabakcıoğlu, M. B. (2024). High entropy alloy reinforcement for superior electromagnetic interference shielding performance in carbon fiber-reinforced polymer composites. *Polymer Composites*. https://doi.org/10.1002/PC.29260

Li, N., Huang, Y., Du, F., He, X., Lin, X., Gao, H., Ma, Y., Li, F., Chen, Y., & Eklund, P. C. (2006). Electromagnetic Interference (EMI) shielding of single-walled carbon nanotube epoxy composites. *Nano Letters*, *6*(6), 1141–1145. https://doi.org/10.1021/NL0602589/ASSET/IMAGES/MEDIUM/NL0602589N00001.GIF

Mikinka, E., & Siwak, M. (2021). Recent advances in electromagnetic interference shielding properties of carbon-fibre-reinforced polymer composites—a topical review. *Journal of Materials Science: Materials in Electronics 2021 32:20*, *32*(20), 24585–24643. https://doi.org/10.1007/S10854-021-06900-8

Munalli, D., Dimitrakis, G., Chronopoulos, D., Greedy, S., & Long, A. (2019). Electromagnetic shielding effectiveness of carbon fibre reinforced composites. *Composites Part B: Engineering*, *173*, 106906. https://doi.org/10.1016/J.COMPOSITESB.2019.106906

Omana, L., Chandran, A., John, R. E., Wilson, R., George, K. C., Unnikrishnan, N. V., Varghese, S. S., George, G., Simon, S. M., & Paul, I. (2022). Recent Advances in Polymer Nanocomposites for Electromagnetic Interference Shielding: A Review. *ACS Omega*, *7*(30), 25921–25947. https://doi.org/10.1021/ACSOMEGA.2C02504/ASSET/IMAGES/LARGE/AO2C02504_0018.JPEG

Plane Electromagnetic Waves - Physics LibreTexts. (n.d.). Retrieved December 22, 2024, from https://phys.libretexts.org/Bookshelves/University_Physics/University_Physics_(OpenStax)/University_Physics_II_-_Thermodynamics_Electricity_and_Magnetism_(OpenStax)/16%3A_Electromagnetic_Waves/16.03%3A_Plane_Electromagnetic_Waves

Rahimi-Ahar, Z., & Rahimi Ahar, L. (2024). Thermal, optical, mechanical, dielectric, and electrical properties of

nanocomposites. *European Polymer Journal*, *218*, 113337. https://doi.org/10.1016/J.EURPOLYMJ.2024.113337

Rajak, D. K., Pagar, D. D., Kumar, R., & Pruncu, C. I. (2019). Recent progress of reinforcement materials: a comprehensive overview of composite materials. *Journal of Materials Research and Technology*, *8*(6), 6354–6374. https://doi.org/10.1016/J.JMRT.2019.09.068

Sriseubsai, W., Tippayakraisorn, A., & Lim, J. W. (2020). Robust Design of PC/ABS Filled with Nano Carbon Black for Electromagnetic Shielding Effectiveness and Surface Resistivity. *Processes 2020, Vol. 8, Page 616*, *8*(5), 616. https://doi.org/10.3390/PR8050616

Ucpinar Durmaz, B., Salman, A. O., & Aytac, A. (2023). Electromagnetic Interference Shielding Performances of Carbon-Fiber-Reinforced PA11/PLA Composites in the X-Band Frequency Range. *ACS Omega*, *8*(25), 22762–22773. https://doi.org/10.1021/ACSOMEGA.3C01656/ASSET/IMAGES/LARGE/AO3C01656_0008.JPEG

Wang, C., Murugadoss, V., Kong, J., He, Z., Mai, X., Shao, Q., Chen, Y., Guo, L., Liu, C., Angaiah, S., & Guo, Z. (2018). Overview of carbon nanostructures and nanocomposites for electromagnetic wave shielding. *Carbon*, *140*, 696–733. https://doi.org/10.1016/J.CARBON.2018.09.006

Wang, K., Chu, W., Chen, Y., Li, H., & Liu, H. (2024). Maintaining electromagnetic interference shielding and flame-retardant performance of recycled carbon fiber-reinforced composites under multiple pyrolysis recycles. *Composites Science*

and Technology, *248*, 110470. https://doi.org/10.1016/J.COMPSCITECH.2024.110470

Wang, X. Y., Liao, S. Y., Wan, Y. J., Huang, H. P., Li, X. M., Hu, Y. G., Zhu, P. L., Sun, R., & Wong, C. P. (2022). Near-field and far-field EMI shielding response of lightweight and flexible MXene-decorated polyester textiles. *Materials Today Physics*, *23*. https://doi.org/10.1016/J.MTPHYS.2022.100644

What is EMI Shielding and Why is it Important for Your Design? (n.d.). Retrieved December 22, 2024, from https://www.modusadvanced.com/resources/blog/what-is-emi-shielding-and-why-is-it-important-for-your-design

Yasin Eken, T., Kaykilarli, C., Kucukelyas, B., Baris Tabakcioglu, M., Eken, T. Y., Kaykilarli, C., Kucukelyas, B., & Tabakcioglu, M. B. (2024). Electromagnetic Shielding Effectiveness and Impact Test Performance of Carbon Fiber Reinforced Polymer Composites with Hematite and Goethite. *Macromolecular Materials and Engineering*, *309*(2), 2300271. https://doi.org/10.1002/MAME.202300271

CHAPTER IX

Fracture Mechanics of Failure Analysis and Applications

Ferit ARTKIN[1]

Introduction

Fracture mechanics still seems to be a secondary issue in failure analysis, even though fatigue crack propagation and fracture are responsible for a large portion of failure events in industrial practice. Following a summary of the main issues in both failure analysis and fracture mechanics, scientists determine which failure analysis problems fracture mechanics can (and cannot) resolve. Its usefulness in failure analysis is determined by the accuracy of fracture mechanics, which is much more obvious from the design stage. In failure analysis, it would be helpful to have a better grasp

[1] Lect.Dr., Kocaeli University, Hereke Asimkocabiyik Vocational School, Department of Machinery and Metal Technologies, Machinery Programme, Kocaeli/Türkiye, Orcid: 0000-0002-8543-6334, artkinf@kocaeli.edu.tr

of the application conditions as well as the limitations and requirements of fracture mechanics.

The technique of fracture mechanics is used to identify and forecast failure of a component that has a crack or other flaw. A part's existence of a fracture increases the stress in the vicinity of the crack, which might lead to failure sooner than anticipated when utilizing conventional material strength techniques. The principles of material strength are used in the conventional method of part design and analysis. The stresses brought on by the imposed loading in this instance are computed. Depending on the failure criterion, failure occurs when the applied stress is greater than the material's strength (either yield strength or ultimate strength).

A stress intensity factor is determined in fracture mechanics by taking into account the component shape, crack size, and applied stress. When the material's fracture toughness is exceeded by the stress intensity factor, a fracture occurs. The crack then grows quickly and unsteadily until it cracks.

The Importance of Fracture Mechanics

There are numerous significant reasons why fracture mechanics is a topic worth considering:

- Cracks and crack-like flaws are far more common than one might think. Cracks could be already present in a section or could appear as a result of extreme stress or exhaustion.

- In general, a material's fracture toughness reduces as its strength increases. It is possible for many engineers to make mistakes due to their innate preference for stronger materials.

- Parts may fail at lower loads than anticipated when utilizing the material strength technique if fracture mechanics are ignored.

- Brittle fractures fail quickly and catastrophically, and there is little warning.

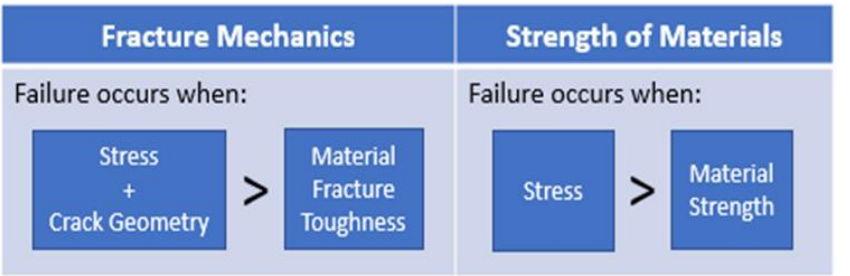

Figure 1. Fracture and Mechanics and Strength of Materials.

The tanker SS Schenectady, one of the Liberty Ships of World War II and one of its most famous wrecks, is seen in the picture below. She was moored at a handy pier at Swan Island in calm weather on January 16, 1943, just after returning from sea trials. The hull abruptly broke in two right aft of the superstructure, with a bang that was audible from at least a mile distant.

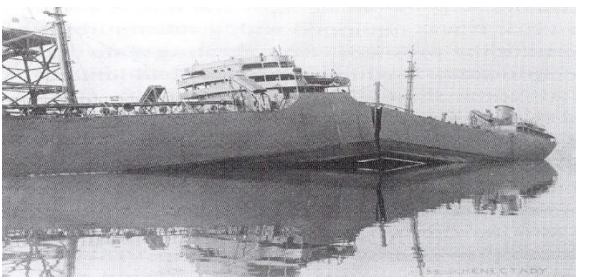

Figure 2. The SS Schenectady breaks in two while docked (Wikipedia, 2024).

Near the keel, the fissures extended from port and starboard, and the keel itself was broken, with the bow and stern curving upward out of the water and sinking to the river floor (Thompson, P., 2001).

The reason of the fracture was not entirely known at the time; the Board of Inquiry examined a number of possibilities, such as "locked" strains, abrupt climatic changes, or systemic design defects, while the Coast Guard's official report blamed the incident on a defective weld. The most frequent reason for these incidents was defective welding, particularly when subsequent investigations showed that several shipyards had used subpar working procedures. However, even in such cases, it was evident that fewer than half of all significant fractures were caused by this type of welding. Subsequent analysis revealed that a brittle fracture brought on by subpar steel was most likely the cause of failure. This would become extremely fragile in cold temperatures, aggravating pre-existing flaws and increasing the likelihood of fracture (Thompson, P., 2001) (Murray, C., 2015).

Concentrations of Stress Near Cracks

The tension in the component increases close to the crack's tip because cracks behave as stress risers. Consider the situation of an elliptical crack in the middle of an infinite plate as a straightforward example:

According to theory, the tension at the ellipse's tip is determined by:

$$\sigma_{max} = \sigma\left(1 + 2\sqrt{\frac{a}{\rho}}\right) \quad (1)$$

where σ is the nominal stress and ρ is the radius of curvature of the ellipse, $\rho = b^2/a$.

The theoretical stress becomes closer to infinity as the fracture tip's radius gets closer to zero. Physically impossible, this infinite tension is referred to as a stress singularity. Rather, the material experiences plastic deformation at a certain distance from the fracture tip as a result of the stress being dispersed across the surrounding material. The term "plastic zone" refers to this area of plastic deformation, which will be covered in more detail later. When the fracture point is blunted by plastic deformation, the radius of curvature rises and the stresses return to finite values (Figure 3.).

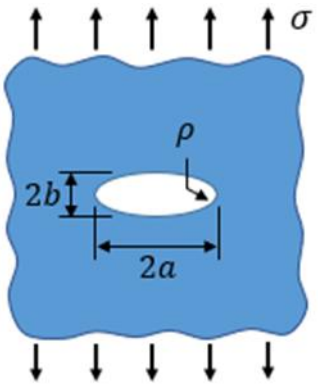

Figure 3. The concentration of tension surrounding a crack is shown schematically.

Alternative techniques have been developed to describe the stresses around the fracture tip due to the plastic zone that forms around the crack tip and the stress singularity issues that occur when the stress concentration approach is utilized. Today, the most popular approach is to compute a stress intensity factor, which is covered in more detail in a subsequent section.

Modes of Loading

The direction of a crack with regard to loading is defined by three fundamental modes. One or more modes may be used to load a crack. The three fundamental mechanisms of fracture loading are depicted in the image below. The fracture surfaces are separated by a tensile tension in mode I, also known as the opening mode. The shear mode, or mode II, is characterized by shear stress that causes the fracture surfaces to shift parallel to the principal crack size. The tearing mode, or mode III, is characterized by shear stress that causes the fracture surfaces to shift perpendicular to the size of the original crack.

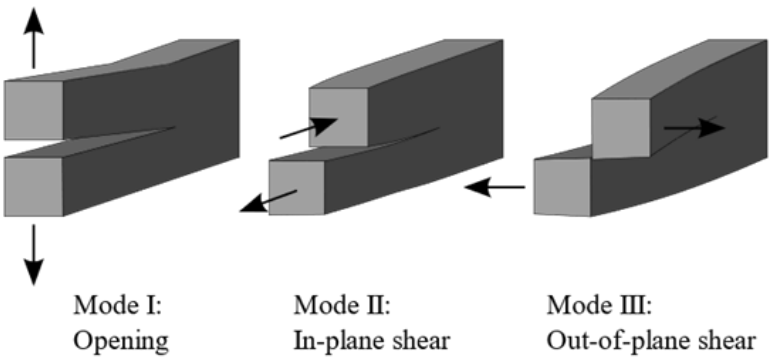

Figure 4. Schematic representation of the three basic modes of crack loading (Wikipedia).

As the worst scenario and most prevalent, Mode I is nearly often taken into account in engineering analysis. Cracks often develop in Mode I, however as the picture above illustrates, if a crack does not begin in Mode I, it will change into Mode I on its own.

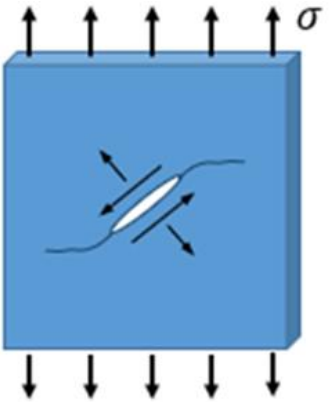

Figure 5. Tensile Forces on the Crack.

Fracture Toughness

A material may withstand applied stress intensity up to a critical value, after which it will fail and a fracture will form unsteadily. This essential stress intensity is the material's fracture toughness. The environmental composition (air, freshwater, saltwater, etc.), loading rate, material thickness, material processing, crack direction, and ambient temperature are some of the numerous variables that affect a material's fracture toughness. These considerations should be made when deciding on a fracture toughness value to use in design and analysis.

Fracture Toughness and Thickness

As material thickness grows, fracture toughness falls until the component is sufficiently thick to be in the plane-strain state. Fracture toughness is a constant number called the plane-strain fracture toughness above this plane-strain thickness. Of major relevance is plane-strain fracture toughness in Mode I loading, which is represented by the value K_{IC}.

$$K_c = K_{IC}\left[1 + B_k\, e^{-(A_k t/t_0)^2}\right] \tag{2}$$

The plane strain thickness at critical loading, denoted by t0, is determined as follows: t represents the material thickness, while Ak and Bk are material constants

$$t_0 = 2.5\left(\frac{K_{IC}}{S_{ty}}\right)^2 \tag{3}$$

where Sty is the material's tensile yield strength.

The thickness-specific fracture toughness calculation mentioned above was used to create the following graph for a sample material, 15-5PH, H1025. It is evident that this material's fracture toughness is 90 ksi*in $^{0.5}$ at lower thickness values and drops to plane strain toughness of 60 ksi*in $^{0.5}$ as thickness rises, after which it stays constant.

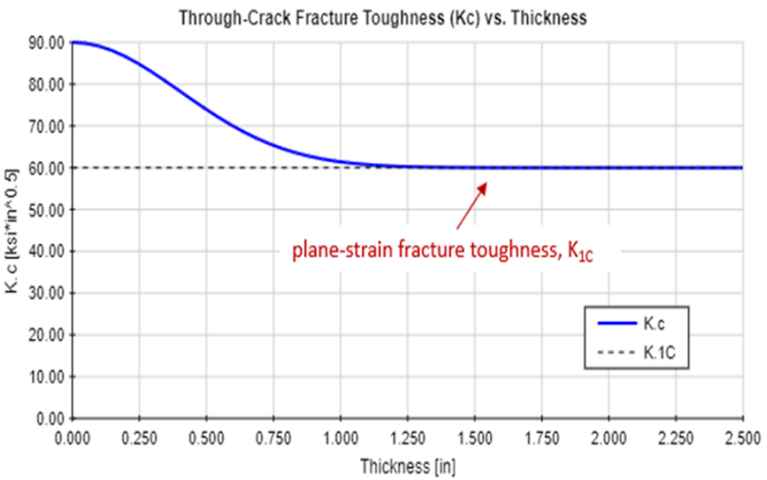

Figure 6. Fracture Toughness and Thickness Graph.

In design and analysis, it is still a good idea to utilize the plane strain fracture toughness value, even if fracture toughness may be roughly estimated as a function of component thickness.

Fracture Toughness and Strength

Fracture toughness typically reduces as strength increases for a particular class of materials. Heat treating a block of material to improve its strength characteristics will typically result in a decrease in the material's fracture toughness.

The fracture toughness and material strength for different material classes are displayed in the figure below. It is evident that the fracture toughness of many materials, particularly engineering metal alloys and engineering polymers, diminishes as strength increases.

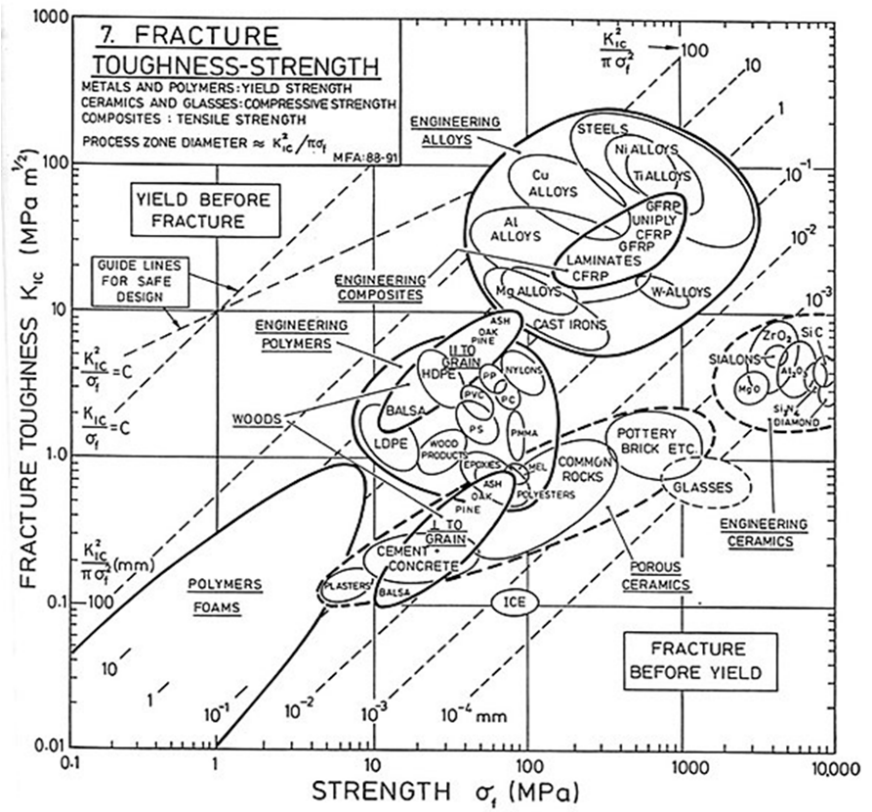

Figure 7. Fracture Toughness and Strength, (Wikipedia, 2024).

Fracture Toughness and Crack Orientation

Crack orientation in relation to grain direction usually affects a material's fracture toughness. Thus, crack orientation is usually given together with fracture toughness measurements.

The following graphic illustrates potential fracture orientation and grain orientation combinations for both rectangular and cylindrical geometries. The orientation of cracks is indicated by two-digit codes. Perpendicular to the crack face is the direction indicated

by the first digit. The direction of the fracture path is indicated by the second number.

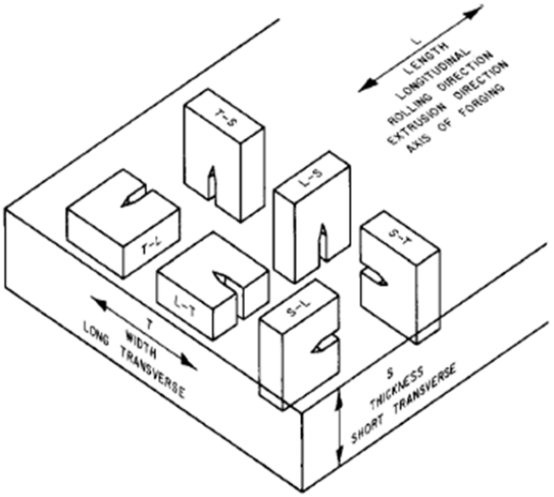

Figure 8. Fracture Toughness and Crack Direction I, (MIL-HDBK-5J).

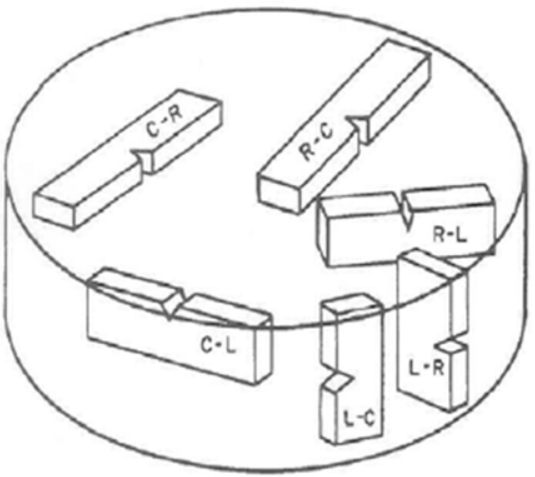

Figure 9. Fracture Toughness and Crack Direction II, (MIL-HDBK-5J).

Ductile and Brittle Fracture

The terms "brittle fracture" and "ductile fracture" are used in two different contexts. The fracture mode and fracture mechanism are these frameworks of reference.

Materials scientists typically refer to the fracture mechanism, which explains the fracture event at the microscopic level, when discussing brittle and ductile fracture. Cleavage is typically the brittle fracture mechanism, while dimpled fracture, commonly referred to as microvoid coalescence, is the ductile fracture mechanism. Brittle fracture is linked to the mechanism of cleavage. Very little plastic deformation occurs, and the fracture surface has ridges and seems smooth. Ductile fracture is linked to the microvoid coalescence process. The fracture surface appears dimpled like a golf ball due to this process, which involves the development, growth, and coalescence of tiny voids in the material that are triggered by plastic movement.

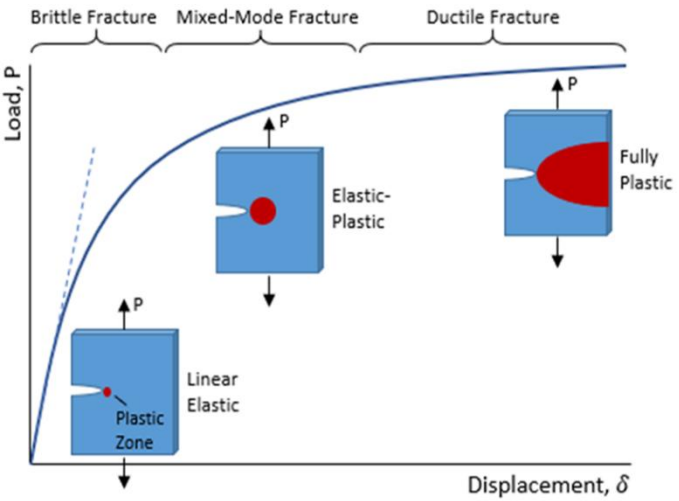

Figure 10. Fracture Toughness and Crack Direction II, (MIL-HDBK-5J).

The fracture mode, which characterizes the material's high-level behavior during the fracture event, is typically referred to by mechanical engineers when discussing brittle and ductile fracture. The fracture mode is seen in the image above.

The load-displacement curve is depicted with broken specimens at various points along it. Stresses in the component are less than the material's yield strength in the linear section of the curve with the lower applied load. If the part breaks in this location, it is referred to be a brittle fracture because it fails earlier than expected using material strength measures. Note that in this location, the plastic zone (shown in red) surrounding the fracture tip is generally tiny, thus the linear elastic assumption is true, and Linear Elastic Fracture Mechanics (LEFM) may be utilized to evaluate the component. The plastic zone size grows in proportion to the load. Ductile fracture occurs when a component fails in the upper portion of the load-displacement curve.

If the plastic zone size exceeds the application of LEFM but has not yet extended throughout the cross-section, elastic-plastic techniques such as the Failure Assessment Diagram (FAD) can be employed to examine the part. Once the plastic zone size has expanded over the whole cross-section (gross cross-section yields), fracture mechanics methods are no longer applicable, and the cross-section must be studied using the material strength approach.

Failure Assessment Diagram (FAD)

If LEFM is not applicable, elastic-plastic analysis should be employed to account for plasticity effects around the fracture. The Failure Assessment Diagram (FAD) is the most used elastic-plastic analysis approach.

Note that in the picture below, the failure locus for LEFM is shown by a dotted horizontal line, whereas the FAD failure locus is located below the LEFM. This suggests that the failure forecasts provided by LEFM are insufficient. The decreased failure locus on the FAD curve is due to plasticity around the crack tip, which increases the effective crack length and consequently the severity of the crack condition.

Also, the failure locus for plastic collapse (i.e., the failure locus anticipated using material strength techniques) is represented by a vertical dotted line. The FAD failure locus crosses across the plastic collapse locus and pushes it to the right, suggesting that the component is becoming stronger. This significant increase in strength is due to strain hardening.

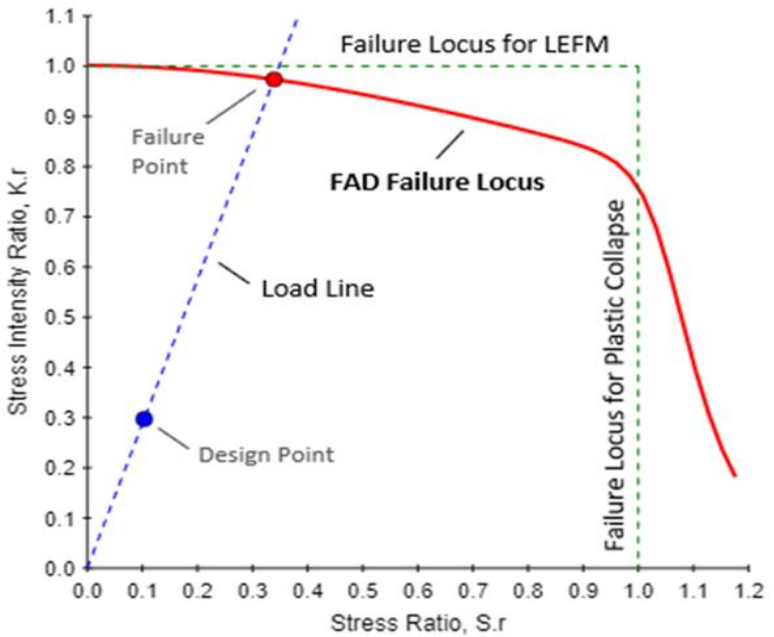

Figure 11. Fracture Toughness and Crack Direction II, (MIL-HDBK-5J).

The FAD approach's ability to account for material plasticity while employing linear elastic stress intensities is its last noteworthy feature. This offers the FAD method's simplicity and is a significant benefit over alternative elastic-plastic techniques.

Residual Strength Curve

The residual strength curve displays the part's strength in relation to the size of the crack. The part's strength and the material's yield strength are equivalent in the absence of a crack. Nevertheless, strength (i.e., the amount of stress that can be tolerated before collapse) declines as the fracture widens.

The residual strength curve is displayed in the example scenario in the following figure. The material used in this instance has a yield strength of 145 ksi and a plane strain fracture toughness of 60 ksi*in$^{0.5}$. The plate is 2 inches broad and has a crack down the middle. In red is the residual strength curve. Above this curve, failure will occur for any stress value for a given fracture size.

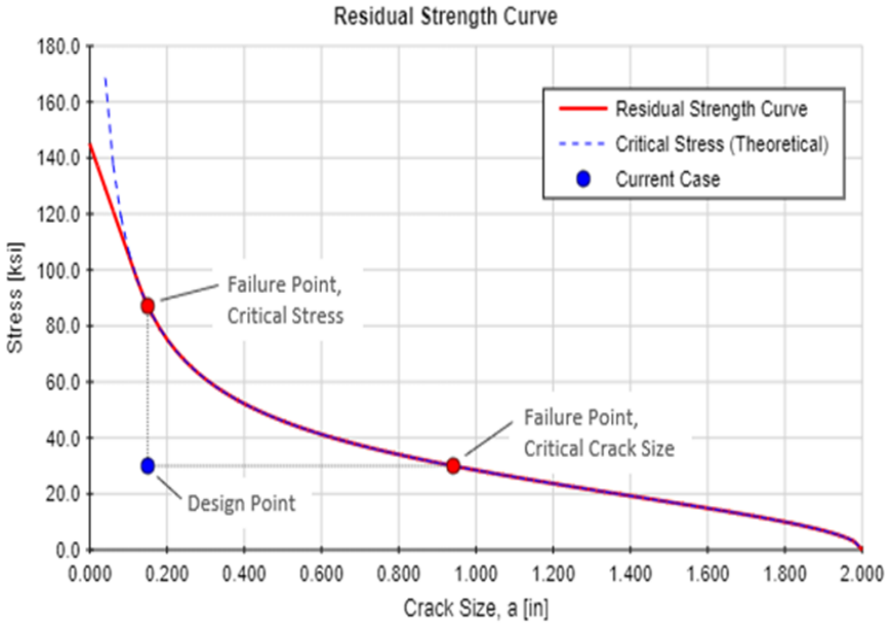

Figure 12. Residual Strength Graph.

Take note of the blue dotted line in the graph above, which represents the theoretical critical stress curve. This theoretical curve may be characterized as follows: It gives the theoretical critical stress value as a function of fracture length.

$$\sigma_{crit} = \frac{K_{IC}}{Y\sqrt{\pi a}} \tag{4}$$

The fact that the geometry factor Y depends on the fracture size is often significant. As the fracture size varies, the Y value will also fluctuate. At the part boundary, the residual strength curve falls to the critical stress value of 0, which is explained by the fact that the Y value will typically peak as the crack size rises in relation to the part dimensions.

When the fracture size becomes closer to zero, it's also crucial to remember that the theoretical critical stress gets closer to infinite. Since the material's tensile strength establishes an upper limit on the amount of stress it can tolerate, this is obviously impractical. A straight line is formed between the material's tensile yield strength and the tangent point on the theoretical critical stress curve in order to smooth out the residual strength curve in the tiny fracture area. In certain situations, determining the tangent point is impossible. In this instance, Liu advises that the point at which the theoretical critical stress equals two-thirds of the material's tensile yield strength might be interpreted as the transition point between the straight line curve and the theoretical critical stress curve.

Conclusion

For the analysis and prevention of equipment and structural component failures brought on by the formation and spread of fractures, fracture mechanics is the finest technique currently available.

The study of fractured components under static load circumstances—that is, settings with constant loads that do not fluctuate over time—has been covered in this material on fracture mechanics. The stress level at the crack tip will fluctuate in the event that the load varies over time. If the change in stress intensity is greater than the material's threshold stress intensity, a fracture will develop. Fatigue crack growth is the development of a crack under situations of fluctuating stress intensity. It is crucial to remember that the geometry factor Y generally depends on the size of the fracture. As a result, the Y value will fluctuate along with the fracture size.

The behavior of materials with defects may be understood and predicted with the help of fracture mechanics. Engineers are able to

build and operate structures and components more safely and effectively by using the concepts of fracture mechanics. Fracture mechanics should be used in conjunction with other engineering tools and approaches, but it's crucial to understand its limits.

REFERENCES

AFRL-VA-WP-TR-2003-3002, "USAF Damage Tolerant Design Handbook: Guidelines for the Analysis and Design of Damage Tolerant Aircraft Structures," 2002.

Anderson, T.L., "Fracture Mechanics: Fundamentals and Applications," 3rd Edition.

API 579-1 / ASME FFS-1, "Fitness-For-Service," The American Petroleum Institute and The American Society of Mechanical Engineers, 2007.

Budynas-Nisbett, "Shigley's Mechanical Engineering Design," 8th Ed.

Callister, William D., "Materials Science and Engineering: An Introduction," 9th Edition.

Dowling, Norman E., "Mechanical Behavior of Materials: Engineering Methods for Deformation, Fracture, and Fatigue," 3rd Edition.

https://en.wikipedia.org/wiki/SS_Schenectady Accessed 23 December 2024

Liu, Alan F., "Structural Life Assessment Methods," ASM International, 1998.

MIL-HDBK-5J, "Metallic Materials and Elements for Aerospace Vehicle Structures," Department of Defense Handbook, 2003.

Murray, Charles (5 March 2015). "Engineering Disasters: SS Schenectady, a Lesson in Brittle Fracture". Design News. Informa Markets. Retrieved 18 November 2022.

NASA-STD-5009, "Nondestructive Evaluation Requirements for Fracture-Critical Metallic Components," 2008.

Naval Sea Systems Command, "Fracture Toughness Review Process for Metals in Critical Non-Nuclear Shipboard Applications," 1998.

Sanford, R.J., "Principles of Fracture Mechanics," 1st Edition.

Thompson, Peter (2001). "How Much Did the Liberty Shipbuilders Learn? New Evidence for an Old Case Study". The Journal of Political Economy. 109 (1). The University of Chicago Press: 103–137. CiteSeerX 10.1.1.197.1438. doi:10.1086/318605

CHAPTER X

Examination of Wear Performance of Surface-Hardened Materials by Boronizing Method: A Literature Review

Taha ÖZEL [1]
Emre ALTAŞ [2]

1. Introduction

The main reasons for machine elements to be out of service in the industry are; wear, fatigue, and corrosion. Wear that occurs in machine parts that work in contact with each other causes quite serious economic losses if precautions are not taken. Therefore, knowing and preventing wear or at least taking the necessary precautions to reduce it can reduce these losses. Wear that occurs

[1] Unvan, Üniversite, Bölüm, Orcıd: Bartin University, Institute of Science, Department of Mechanical Engineering, Bartın, Turkey,
email: tahaozel@gmail.com
[2] Unvan, Üniversite, Bölüm, Orcıd: Asst. Prof. Dr., Bartın University, Mechanical Engineering Department, Engineering Faculty, Bartın, Turkey, email: emrealtas@bartin.edu.tr, ORCID: 0000-0002-9296-8881

when surfaces in contact with each other move will cause damage to both surfaces, including increasing material loss (Etsion, 2005). Wear can cause an increase in the gap between the parts, loss of sensitivity to unwanted freedom of movement, and therefore much faster wear and sometimes fatigue fracture. This problem, which was tried to be prevented only by using liquid or solid lubricants, is now being prevented by using surface treatments or coatings with tribological approaches. Today, there are many techniques used to increase wear resistance (Tabur, Izciler, Gul, & Karacan, 2009).

Boriding is a metallurgical process used to strengthen the surfaces of metals or other materials with a chemical process and increase their durability. During this process, the material is exposed to a special boron solution or gas environment. This creates a durable boron carbide coating on the surface of the material. Boriding is a common process used to increase wear resistance, improve surface hardness, protect against corrosion, and extend the life of parts used in industrial applications such as cutting tools, bearings, and gears (Wahab, Ghazali, Yusoff, & Sajuri, 2016).

Surface material loss occurs due to wear and corrosion mechanisms. In order to eliminate these negative effects, material surface treatments are the most common modification methods. In general, cementation, nitriding or boronizing processes are widely used to improve the surface properties of iron-based metals. Increasing the service life of materials with surface coating applications is a common method. Boriding process is generally the process of diffusion of boron atoms into steel in the high temperature range of 700-1000 oC. Boriding process is carried out in these temperature ranges for different periods (2-10 hours) and in different

boronizing environments (Riveiro, Maçon, del Val, Comesaña, & Pou, 2018). As a result of boron treatment, FeB, Fe2B or FeB+Fe2B boride layers appear on the surface of iron-based metals as single or double phase. In the box boronizing method, it is carried out by waiting for at least one hour in the temperature range of 800-1050 oC in boron donor powders depending on the chemical composition of the material, its thickness and the desired boron layer thickness. Depending on the chemical structure of the material, the boronizing method and conditions, the boron layer on the surface of the boronized material can have a hardness of approximately 2000 HV. Depending on the layer phase obtained, the material surface gains wear resistance . In this way, the service life of machine parts can be extended (Shivakoti, Kibria, Cep, Pradhan, & Sharma, 2021).

Wear is a significant problem for materials that work in contact with each other. It is possible to increase the life of the material by reducing wear with boronizing. For this purpose, the surface of the coated material is coated with ceramic ferro-boron. This also reduces adhesive wear. The boron atom has a high affinity for oxygen. Therefore, a protective thin oxide layer is formed on the surface during the boronizing process. This layer creates a lubricating effect, reduces the coefficient of friction and ensures that the material wears less. It is possible to obtain a structure that is both hard and has a low coefficient of friction (equivalent to the coefficient of friction) with the boronizing process (Moskal, Martan, & Honner, 2023; Vilhena et al., 2009) .

2. Boroning Method Procedures.

Today, engineering parts are processed with many boriding methods such as box or paste boriding, boriding in liquid or molten salt, electrochemical boriding, plasma-assisted boriding, etc. One of the most important disadvantages of boriding processes such as box boriding, which is widely used, is the use of expensive powder mixtures and the necessity of long processing times. On the other hand, electrochemical boriding appears as a much more cost-effective method in boriding iron-based materials, considering that the cost of the chemicals used in the system is much lower and the processing time is much shorter (Cunha et al., 2016).

It is the most common boronizing technique because it is easy to apply, requires simple equipment, is economical, safe and can be changed in the chemical composition of the powder mixture used. Box boronizing is performed by keeping the material to be boronized in the powder mixture, which is a boron donor medium, at certain temperatures and for certain periods of time. Paste boriding is a method used in cases where box boriding is difficult or expensive. In this method, 45% B4C and 55% cryolite are used or a traditional boriding powder mixture is used in a good binding agent. With this method, the boriding mixture is created by spraying or brushing on the surface of the material (Obilor, Pacella, Wilson, & Silberschmidt, 2022).

Internal stresses occurring in materials to which boronizing process is applied are of critical importance. Therefore, the ideal structure of the boron layer is a single-phase and recessed-protruding structure. If the structure is double-phase, these phases will create compressive and tensile stresses on each other, thus cracks will form

between the two phases and as a result, separation and ruptures will occur from the material surface over time due to the mechanical stress (Etsion, 2010).

3. Literature studies on wear performance of materials hardened by boronizing method

Fernández-Valdés et al. investigated the wear behavior of the iron boride layer obtained on the surface of the sample by boronizing disk-shaped AISI 316L steel samples at 900 ℃ for 2 and 6 hours using the box boronizing method. According to the experimental results, wear in boronized samples decreased approximately 10 times compared to non-boronized samples. In addition, under a normal load of 5 N, the wear surface of boronized samples exhibited elastic behavior, while the wear surface of non-boronized samples exhibited plastic behavior (Fernández-Valdés, Meneses-Amador, López-Liévano, & Ocampo-Ramírez, 2021).

Krelling et al. applied box boronizing process to AISI 1020 steel at 1000 ℃ for 4 hours. Fe2B phase was determined on the surface of the boronized sample in XRD analysis. The thickness of the boronized layer formed on the surface was 177 μm and the surface hardness was measured as 2100 HK0.01. Since the hardness of the abrasive particles was close to the hardness of the Fe2B layer in microabrasive wear experiments, it reduced the wear resistance of the boronized sample (Krelling, Da Costa, Milan, & Almeida, 2017).

Shinde and Dhokey investigated the relationship between carbide density and surface roughness and dry sliding wear of subzero treatment on AISI H13 hot work tool steels. Oil quenching at 1020°C, double tempering at 500°C and different subzero holding

times from 8 to 32 hours at -185°C were applied to AISI H13 samples. Dry sliding wear behavior of pin on disk was investigated under 40 N load, 3 m/s speed, 6000 m sliding distance. A relationship was established between carbide density and surface roughness. It was found that the subzero treatment time for AISI H13 steel was optimized and carbide density affected the surface roughness and hence the wear rate in subzero treated samples (Shinde & Dhokey, 2017).

4. Conclusions

- It has been concluded that further research is needed to optimize boronizing parameters (such as temperature, time, environment, etc.) for greater efficiency.
- It has been observed that the boron layer thickness increases with increasing time and temperature as a result of the boronizing process.
- It has been observed that the development of the boron layer is negatively affected by the increase in alloying elements.

5. References

Cunha, A., Elie, A.-M., Plawinski, L., Serro, A. P., do Rego, A. M. B., Almeida, A., . . . Vilar, R. (2016). Femtosecond laser surface texturing of titanium as a method to reduce the adhesion of Staphylococcus aureus and biofilm formation. *Applied Surface Science, 360*, 485-493.

Etsion, I. (2005). State of the art in laser surface texturing. *J. Trib., 127*(1), 248-253.

Etsion, I. (2010). Laser surface texturing and applications. *Recent developments in wear prevention, friction and lubrication*, 137-158.

Fernández-Valdés, D., Meneses-Amador, A., López-Liévano, A., & Ocampo-Ramírez, A. (2021). Sliding wear analysis in borided AISI 316L steels. *Materials Letters, 285*, 129138.

Krelling, A., Da Costa, C., Milan, J., & Almeida, E. (2017). Micro-abrasive wear mechanisms of borided AISI 1020 steel. *Tribology international, 111*, 234-242.

Moskal, D., Martan, J., & Honner, M. (2023). Scanning strategies in laser surface texturing: A review. *Micromachines, 14*(6), 1241.

Obilor, A. F., Pacella, M., Wilson, A., & Silberschmidt, V. V. (2022). Micro-texturing of polymer surfaces using lasers: A review. *The International Journal of Advanced Manufacturing Technology, 120*(1), 103-135.

Riveiro, A., Maçon, A. L., del Val, J., Comesaña, R., & Pou, J. (2018). Laser surface texturing of polymers for biomedical applications. *Frontiers in physics, 6*, 16.

Shinde, T., & Dhokey, N. (2017). Influence of carbide density on surface roughness and quasi-stable wear behaviour of H13 die steel. *Surface engineering, 33*(12), 944-952.

Shivakoti, I., Kibria, G., Cep, R., Pradhan, B. B., & Sharma, A. (2021). Laser surface texturing for biomedical applications: a review. *Coatings, 11*(2), 124.

Tabur, M., Izciler, M., Gul, F., & Karacan, I. (2009). Abrasive wear behavior of boronized AISI 8620 steel. *Wear, 266*(11-12), 1106-1112.

Vilhena, L., Sedlaček, M., Podgornik, B., Vižintin, J., Babnik, A., & Možina, J. (2009). Surface texturing by pulsed Nd: YAG laser. *Tribology international, 42*(10), 1496-1504.

Wahab, J., Ghazali, M., Yusoff, W., & Sajuri, Z. (2016). Enhancing material performance through laser surface texturing: a review. *Transactions of the IMF, 94*(4), 193-198.

CHAPTER XI

Contributions of Laser Surface Modification to Wear Resistance: A Literature Review

Turgay ÇAKIR[1]
Emre ALTAŞ[2]

1. Introduction

Advancements in industrial technology have increased the need to enhance the mechanical and surface properties of engineering materials. Specifically, the durability of surfaces subject to wear directly impacts the reliability and lifespan of components in use. Consequently, there is a growing demand for materials with high wear performance across industries such as machinery, automotive, aerospace, and defense (Ayers, Schaefer, & Robey,

[1] Unvan, Üniversite, Bölüm, Orcıd: Bartin University, Institute of Science, Department of Mechanical Engineering, Bartın, Turkey,
Email: tcakir039@gmail.com
[2] Unvan, Üniversite, Bölüm, Orcıd: Asst. Prof. Dr., Bartın University, Mechanical Engineering Department, Engineering Faculty, Bartın, Turkey, email: emrealtas@bartin.edu.tr, ORCID: 0000-0002-9296-8881

1981). Wear resistance refers to a component's ability to withstand environments involving high temperatures, high pressure, or intense friction. Strengthening this property not only reduces application costs but also enhances sustainability and energy efficiency (Tian, Chen, Li, & Huo, 2005)

Today, machine elements are expected to perform certain functions. However, while performing these functions, the surfaces of the elements are exposed to more effects such as stress and abrasion than their internal parts. If the material's resistance limit is exceeded as a result of these effects, damage begins to occur on the surface of the material. For this reason, some surface treatments are performed to increase the resistance on the surface of the material. Developments in surface engineering in recent years have led to the emergence of new and different surface modifications (Gachot, Rosenkranz, Hsu, & Costa, 2017; Kaur, Ghadirinejad, & H. Oskouei, 2019).

One of the most important causes of damage to machinery and construction elements is wear. In factories, aircraft, rocket systems and many other advanced technology systems, the parameters that form the basis of tribology such as friction, wear and lubrication are accepted as the most important design criteria (Tian, Chen, Wang, & Lei, 2005). Statistical studies conducted in industrialized countries show that a large portion of the energy used in the world is used to overcome friction resistance. Therefore, studies to be conducted on friction indicate that significant energy savings will be achieved. Because most of the energy is related to friction, and a significant portion of the material is related to wear (Chi, Gu, Yu, & Chen, 2018; De Damborenea, 1998).

2. Laser processing methods

Due to the widespread use of advanced engineering materials, complex design geometries and high surface precision due to low dimensional performances limit the use of traditional processing methods. It is understood that laser processing has many advantages over traditional methods (plasma, oxygen cutting, sawing). It has the ability to process materials without contact, and it offers the opportunity to cut brittle, soft or hard, thin materials that are difficult to cut in cutting and drilling processes quickly and with high precision (Salter & Booth, 2019). Laser processing is a thermal process and thermal effects can be kept in a very limited area in materials sensitive to thermal work. Other advantages are narrow cutting trace (kerf) that gives minimum material loss, very flat cutting edge, minimum metallurgical and surface defects, high cutting speed, easy integration into computer-aided numerical control machines for complex cuts (Duley, 2012).

Laser is a unique type of light and is much more intense than other lights in nature due to its focusability. Laser beam does not show dispersion and exhibits monochromatic properties. Laser beam, which can be focused to a point smaller than 0.001 inches in diameter, can be used in medicine, welding manufacturing, cutting high-hardness metals, processing, joining and cutting micro-sized electronic parts, and in addition, laser beam has various applications in different areas of industry (Dutta Majumdar & Manna, 2011). In surface modification with the help of laser beam, there are changes in the properties of the metallic material interacting with the beam. In particular, the crystal structure of the material in the interaction area can change, and surface hardness and wear resistance increase

with the rapid cooling effect. In addition, there are improvements in the tribological performance of the material. These changes in the properties and behavior of the material interacting with the laser beam have significant effects on changing the mechanical properties and performance of the surface. As it is known, by changing the chemical composition of a material surface, surface properties, mechanical properties of the surface and performance can be changed (Narayan, Biunno, Singh, Holland, & Auciello, 1987).

In laser processing applications, the type of laser has an impact on the processing results. In addition, critical factors such as laser output power, frequency and pulse width, which are effective in the transformations on the material, are affected by the type of laser. High-power lasers provide faster processing and enable the beams to reach deeper than the surface (Malinauskas et al., 2016).

3. Literature review of wear performance of laser surface modification

Lee et al. ın the laser surface hardening study of AISI H13 steel, studies were carried out to improve the surface hardness and wear performance properties of tool steel by using a 200 W fiber laser for solution hardening and heating of microstructures. The hardness of the laser melted region was investigated and the scanning conditions were controlled to determine the effect of heat input on the laser melting region. As a result of the tests, it was determined that the hardness of AISI H13 steel was HV 240 and the hardness after laser surface hardening was around HV 480-510 (Jae-Ho, Jeong-Hwan, Byeong-Don, Young-Myung, & Young-Hoon, 2009).

Tani, et al. conducted a study called laser surface hardening of martensitic stainless steel hollow parts. In this study, laser surface hardening process was applied to hollow cylindrical martensitic stainless steel (AISI 420) component. The process was applied by changing only the peripheral speed from the process parameters without changing the workpiece dimensions. As a result of these processes, it was possible to confirm the previously estimated results numerically (Tani, Fortunato, Ascari, & Campana, 2010).

Min Ji et al. produced micro-textures by laser ablation of zirconium ceramic surfaces and investigated the effects of these textures on tribological performance. The tests were carried out by measuring the surface at different depths and widths. The results showed that the best friction coefficient was 11 microns at the highest depth and 20 microns at the smallest width. They reported that the small groove width is important for wear performance (Ji, Xu, Chen, & El Mansori, 2020).

4. Conclusions

- As the laser power increases, surface microhardness and wear resistance increase,
- Laser pulse number and scanning speed affect the surface quality,
- Surface pattern density reduces the friction coefficient and wear rate,
- Patterns and pattern shifts have significant effects on friction,
- The results have determined that processing geometries have an effect on tribological properties.

5. References

Ayers, J., Schaefer, R., & Robey, W. (1981). A laser processing technique for improving the wear resistance of metals. *Jom, 33*, 19-23.

Chi, Y., Gu, G., Yu, H., & Chen, C. (2018). Laser surface alloying on aluminum and its alloys: A review. *Optics and lasers in engineering, 100*, 23-37.

De Damborenea, J. (1998). Surface modification of metals by high power lasers. *Surface and Coatings Technology, 100*, 377-382.

Duley, W. W. (2012). *Laser processing and analysis of materials*: Springer Science & Business Media.

Dutta Majumdar, J., & Manna, I. (2011). Laser material processing. *International Materials Reviews, 56*(5-6), 341-388.

Gachot, C., Rosenkranz, A., Hsu, S., & Costa, H. (2017). A critical assessment of surface texturing for friction and wear improvement. *Wear, 372*, 21-41.

Jae-Ho, L., Jeong-Hwan, J., Byeong-Don, J., Young-Myung, S., & Young-Hoon, M. (2009). Laser surface hardening of AISI H13 tool steel. *Transactions of Nonferrous Metals Society of China, 19*(4), 917-920.

Ji, M., Xu, J., Chen, M., & El Mansori, M. (2020). Enhanced hydrophilicity and tribological behavior of dental zirconia ceramics based on picosecond laser surface texturing. *Ceramics International, 46*(6), 7161-7169.

Kaur, S., Ghadirinejad, K., & H. Oskouei, R. (2019). An overview on the tribological performance of titanium alloys with surface modifications for biomedical applications. *Lubricants, 7*(8), 65.

Malinauskas, M., Žukauskas, A., Hasegawa, S., Hayasaki, Y., Mizeikis, V., Buividas, R., & Juodkazis, S. (2016). Ultrafast laser processing of materials: from science to industry. *Light: Science & Applications, 5*(8), e16133-e16133.

Narayan, J., Biunno, N., Singh, R., Holland, O., & Auciello, O. (1987). Formation of thin superconducting films by the laser processing method. *Applied physics letters, 51*(22), 1845-1847.

Salter, P. S., & Booth, M. J. (2019). Adaptive optics in laser processing. *Light: Science & Applications, 8*(1), 110.

Tani, G., Fortunato, A., Ascari, A., & Campana, G. (2010). Laser surface hardening of martensitic stainless steel hollow parts. *CIRP Annals, 59*(1), 207-210.

Tian, Y., Chen, C., Li, S., & Huo, Q. (2005). Research progress on laser surface modification of titanium alloys. *Applied Surface Science, 242*(1-2), 177-184.

Tian, Y., Chen, C., Wang, D., & Lei, T. (2005). Laser surface modification of titanium alloys—a review. *Surface Review and Letters, 12*(01), 123-130.

CHAPTER XII

From Ideas to Implementation: A Roadmap for Mechanical Engineering Students

Onat Halis TOTUK[1]

1. Introduction

Engineering design is a complex, iterative process that forms the core of mechanical engineering practice. As technology advances and systems become more sophisticated, there is an increasing need for structured approaches to guide engineers through the design process from initial concept to final product (Dieter & Schmidt, 2021). This chapter aims to provide mechanical engineering students with a comprehensive overview of modern design methodologies and tools to tackle complex engineering challenges systematically and effectively.

[1] Asst. Prof. Dr, Çankaya University Engineering Faculty, Mechanical Engineering Department. Ankara/TÜRKİYE, onattotuk@cankaya.edu.tr ORCID No: 0000-0002-9314-9204

The engineering design process encompasses several key phases, including problem definition, conceptual design, embodiment design, and detailed design (Pahl et al., 2007). While the specific steps may vary across different methodologies, the overall goals remain consistent to develop innovative, optimized solutions that meet customer needs and engineering requirements. By following a structured approach, engineers can better manage complexity, reduce development time and costs, and improve the quality and reliability of their designs (Ullman, 2015).

In recent years, there has been growing emphasis on integrating considerations beyond pure technical performance into the design process. Factors such as sustainability, manufacturability, and user experience are now recognized as critical elements that must be addressed from the earliest stages of design (Chakrabarti & Blessing, 2014). Modern design methodologies aim to provide frameworks for holistically considering these multifaceted requirements throughout the development cycle. Additionally, the increasing use of computer-aided design, simulation, and optimization tools has dramatically expanded the capabilities of engineers to rapidly explore design alternatives and predict performance (Chandrasegaran et al., 2013).

For mechanical engineering students, developing strong design skills is essential for future career success. The ability to apply systematic design approaches to solve open-ended problems is highly valued by employers across industries (Dym et al., 2005). By mastering foundational design methodologies, students can cultivate critical thinking, creativity, and technical skills that will serve them well as they transition into professional practice. This chapter aims

to provide students with both theoretical understanding and practical guidance for implementing engineering design processes.

As engineering challenges continue to grow in scale and complexity, the importance of robust design methodologies will only increase. From developing sustainable energy systems to advancing medical technologies, mechanical engineers play a crucial role in addressing society's most pressing issues (National Academy of Engineering, 2004). By equipping the next generation of engineers with powerful design approaches and tools, we can accelerate innovation and develop solutions to improve lives around the world. The following sections will explore key design methodologies in detail, providing students with a comprehensive toolkit to tackle diverse engineering problems.

2. Engineering Design Process Overview

The engineering design process is a systematic, iterative approach used by engineers to develop innovative solutions to complex problems. This structured methodology provides a framework for transforming abstract ideas into tangible products or systems that meet specific needs and requirements. While the exact steps may vary depending on the project scope or engineering discipline, the core principles remain consistent across different fields, emphasizing creativity, critical thinking, and problem-solving skills (Dieter & Schmidt, 2021).

The engineering design process begins with problem identification and definition, where engineers clearly articulate the issue, identify stakeholder needs, and establish project objectives and constraints. This crucial first step involves gathering information

from various sources to create a well-defined problem statement. Following this, the research and investigation phase commences, during which engineers collect relevant information about existing technologies, materials, and methods that could potentially solve the problem. This phase includes literature reviews, patent analyses, competitor product studies, and expert consultations, aiming to build a strong knowledge base for the subsequent stages of the design process.

The process then progresses through ideation and concept generation, where creativity is emphasized to develop multiple potential solutions. This is followed by evaluation and selection, where concepts are critically assessed against predetermined criteria. The chosen concept then undergoes detailed design and development, transforming it into a comprehensive, implementable design. Prototype testing and iteration allow for real-world validation and refinement of the design. The final stages involve documenting the final design, implementing production processes, conducting quality assurance, and establishing procedures for maintenance and continuous improvement. Throughout this process, engineers employ various tools and techniques to ensure the resulting product meets all specifications and performs optimally in real-world conditions.

2.1. Problem Identification and Definition:

The first crucial step in the engineering design process is problem identification and definition. This stage involves clearly articulating the issue at hand, identifying the needs of end-users or stakeholders, and establishing the project's objectives and constraints. Engineers must gather information from various

sources, including customer feedback, market research, and technical requirements, to gain a comprehensive understanding of the problem (Pahl et al., 2007). The goal of this phase is to create a well-defined problem statement that outlines the specific challenges to be addressed, the desired outcomes, and any limitations or constraints that may impact the solution. A clear and concise problem definition serves as the foundation for the entire design process, guiding all subsequent stages and ensuring that the final solution effectively addresses the core issues (Dym et al., 2005).

2.2. Research and Investigation:

Once the problem is defined, engineers embark on a thorough research and investigation phase. This step involves gathering relevant information about existing technologies, materials, and methods that could potentially be applied to the problem. Engineers conduct literature reviews, analyze patents, study competitor products, and consult with experts in the field to build a strong knowledge base that will inform and inspire subsequent stages of the design process (Chakrabarti & Blessing, 2014). During this phase, market analysis and feasibility studies may also be carried out to assess the viability of potential solutions. Engineers explore not only technical aspects but also economic, social, and environmental factors that may influence the design. This comprehensive approach ensures that the resulting solutions are not only technically sound but also commercially viable and sustainable (Ulrich & Eppinger, 2020).

2.3. Ideation and Concept Generation:

The ideation and concept generation phase is where creativity takes center stage. Engineers use various techniques such

as brainstorming, mind mapping, and morphological analysis to generate a wide range of potential solutions to the defined problem. This stage emphasizes quantity over quality, encouraging the exploration of diverse and innovative ideas that may challenge conventional thinking (Cross, 2008). During this phase, engineers may sketch concepts, create rough prototypes, or use digital tools to visualize their ideas. The goal is to develop multiple conceptual solutions that address the problem from different angles, providing a rich pool of options for further evaluation. This divergent thinking approach helps to ensure that potentially groundbreaking solutions are not overlooked and that the design team has a comprehensive view of possible approaches (Kelley & Littman, 2001).

2.4. Evaluation and Selection:

Following the generation of multiple concepts, the evaluation and selection phase involves critically assessing each potential solution against predetermined criteria. These criteria typically include factors such as feasibility, performance, cost, manufacturability, and alignment with project objectives. Engineers may use decision matrices, Pugh charts, or other analytical tools to compare and rank the concepts objectively (Ulrich & Eppinger, 2020). Through this systematic evaluation process, the most promising concept or concepts are selected for further development. This stage is crucial in ensuring that resources are focused on solutions with the highest potential for success. The evaluation process often involves input from various stakeholders, including end-users, manufacturing experts, and marketing teams, to ensure a holistic assessment of each concept's viability and potential impact (Dieter & Schmidt, 2021).

2.5. Detailed Design and Development:

Once a concept is chosen, the detailed design and development phase begins. This stage involves transforming the selected concept into a comprehensive, implementable design. Engineers create detailed specifications, develop 3D models, perform engineering calculations, and conduct simulations to refine and optimize the design. Material selection, component sizing, and manufacturing process considerations are all addressed during this phase (Pahl et al., 2007). The goal of this stage is to produce a complete set of design documentation that fully describes the product or system, including all necessary technical drawings, specifications, and manufacturing instructions. Engineers must consider not only the functionality of the design but also factors such as reliability, safety, maintainability, and cost-effectiveness. This phase often involves collaboration between various engineering disciplines to ensure all aspects of the design are thoroughly addressed (Ullman, 2015).

2.6. Prototype Testing and Iteration:

Prototyping is a critical step in the engineering design process, allowing engineers to test and validate their designs in real-world conditions. This phase involves creating physical or virtual prototypes of the product or system, which are then subjected to rigorous testing to assess performance, reliability, and user interaction. Engineers analyze the test results to identify any flaws, limitations, or areas for improvement in the design (Ulrich & Eppinger, 2020). Based on these findings, engineers iterate and refine the design, making necessary adjustments to enhance functionality, usability, or manufacturability. This iterative process

of prototyping, testing, and refinement continues until the design meets all specified requirements and performance criteria. Prototyping not only helps in validating the design but also in identifying unforeseen issues and opportunities for innovation that may not have been apparent in earlier stages of the process (Otto & Wood, 2001).

2.7. Final Design and Documentation:

After multiple iterations and refinements, the design reaches its final form. In this phase, engineers complete all remaining design details and prepare comprehensive documentation for the product or system. This documentation typically includes final engineering drawings, 3D models, material specifications, assembly instructions, and any other information necessary for manufacturing and implementation (Dieter & Schmidt, 2021). The final design documentation serves as a complete and authoritative reference for all aspects of the product, ensuring that it can be accurately produced and maintained throughout its lifecycle. This phase also often includes the creation of user manuals, maintenance guides, and other supporting documentation to ensure proper use and upkeep of the product. The thoroughness and clarity of this documentation are crucial for successful manufacturing, assembly, and long-term support of the product (Pahl et al., 2007).

2.8. Implementation and Production:

The implementation and production phase marks the transition from design to reality. Engineers work closely with manufacturing teams to translate the final design into a producible product or system. This stage involves setting up production lines,

developing manufacturing processes, and establishing quality control procedures. Engineers may need to refine the design further to optimize it for manufacturing efficiency or to address any unforeseen production challenges (Groover, 2010). During this phase, engineers must consider factors such as material sourcing, production scalability, and supply chain logistics. They may also be involved in training production staff, setting up quality assurance protocols, and establishing procedures for handling any manufacturing variations or defects. The goal is to ensure that the product can be consistently and efficiently produced at the required quality level and scale, while also considering factors such as cost-effectiveness and sustainability (Ulrich & Eppinger, 2020).

2.9. Testing and Quality Assurance:

Once production begins, rigorous testing and quality assurance processes are implemented to ensure that the manufactured product meets all design specifications and quality standards. This phase involves developing and executing comprehensive test plans that cover all aspects of the product's functionality, performance, and reliability. Engineers may conduct various types of tests, including functional tests, stress tests, and environmental tests, to verify that the product performs as intended under different conditions (Juran & De Feo, 2010). Quality control measures are put in place to monitor the production process and catch any deviations from the design specifications. This may involve statistical process control, automated inspection systems, and regular audits of the manufacturing process. The goal is to identify and address any quality issues early in the production process, ensuring that only products meeting the specified standards

reach the end-users. This phase is crucial for maintaining customer satisfaction, brand reputation, and regulatory compliance (Montgomery, 2019).

2.10. Maintenance and Continuous Improvement:

The engineering design process doesn't end with product launch. The maintenance and continuous improvement phase focuses on monitoring the product's performance in real-world use, gathering feedback from users, and identifying opportunities for enhancement. Engineers analyze data from product usage, customer feedback, and service reports to inform future design iterations or new product development (Blanchard & Fabrycky, 2011). This phase may also involve developing maintenance procedures, creating user manuals, and providing technical support. By maintaining a cycle of continuous improvement, engineers ensure that the product remains competitive, reliable, and aligned with evolving user needs and technological advancements. This ongoing process not only extends the life cycle of the product but also provides valuable insights that can drive innovation in future designs and contribute to the overall advancement of engineering knowledge and practice (Ulrich & Eppinger, 2020).

At its heart, the engineering design process is a cycle of continuous improvement and refinement. It begins with problem identification and progresses through stages of research, ideation, evaluation, detailed design, prototyping, and implementation. Each stage builds upon the previous one, with feedback loops allowing for iterative improvements based on new insights or changing requirements. This approach not only ensures that the final product meets its intended purpose but also promotes innovation and

efficiency in the development process (Ullman, 2015). General Engineering Design steps are shown in Figure 1.

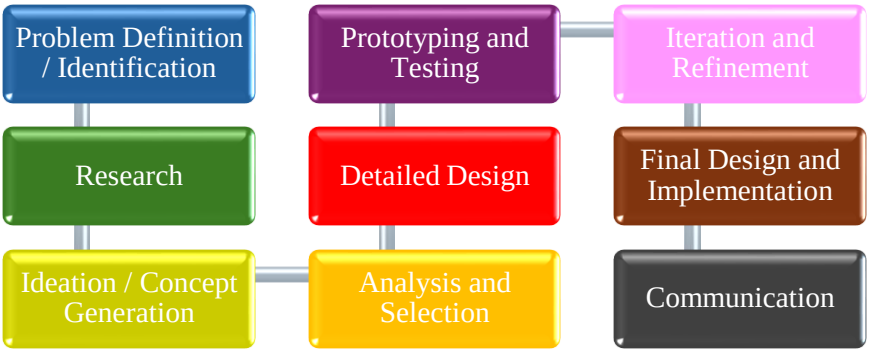

Figure 1. General Engineering Design Steps

The engineering design process provides a structured framework for developing innovative solutions to complex problems. As we transition from the overview to the specific phases of design, we delve deeper into the practical application of these principles. Phase I: Conceptual Design marks the beginning of the hands-on design work, where engineers define the problem, gather information, plan the project, generate concepts, and evaluate potential solutions. This phase lays the foundation for all subsequent design activities. Phase II: Embodiment Design builds upon the selected concept, refining it through product architecture, configuration design, and parametric design. Finally, Phase III: Detail Design transforms the refined concept into a fully specified product ready for manufacturing. Each of these phases incorporates the iterative nature of the design process, allowing for continuous refinement and improvement. By following this structured approach, engineers can systematically navigate the complexities of design,

from initial idea to final product, ensuring that all aspects of the problem are thoroughly addressed and the resulting solution meets or exceeds the identified needs and requirements.

3. Phase I: Conceptual Design

Conceptual design is the foundational phase of the engineering design process, where creativity and innovation take center stage. This critical stage involves translating customer needs and project requirements into potential solutions, setting the trajectory for the entire product development journey (Ulrich & Eppinger, 2020). During this phase, engineers and designers explore a wide range of ideas, focusing on the core functionality and overall structure of the product without getting bogged down in specific details. The goal is to generate multiple concepts that address the identified problem or opportunity, providing a solid basis for further development and refinement.

The conceptual design phase is characterized by its emphasis on divergent thinking and the exploration of diverse solutions. It typically involves activities such as problem definition, information gathering, idea generation, and concept evaluation (Dieter & Schmidt, 2021). This stage is crucial for innovation, as it allows for the consideration of novel approaches and technologies that might lead to breakthrough solutions. By investing time and effort in conceptual design, engineering teams can significantly influence the final product's performance, cost-effectiveness, and market success, while also reducing the likelihood of costly changes in later stages of development (Pahl et al., 2007).

3.1. Problem Definition

Problem definition is the critical first step in the engineering design process, serving as the foundation upon which all subsequent stages are built. It involves clearly articulating the issue or need that the project aims to address, ensuring that all stakeholders have a shared understanding of the challenge at hand. According to Dieter and Schmidt (2021), a well-defined problem statement not only guides the entire design process but also significantly influences the quality and effectiveness of the final solution.

The process of problem definition encompasses several key components: identifying customer needs, gathering information, generating engineering specifications, and developing a Product Design Specification (PDS). These elements work together to create a comprehensive framework that guides engineers through the design process, helping them to focus their efforts on developing solutions that truly meet the needs of end-users and stakeholders. As Ullman (2015) notes, a clear and concise problem definition minimizes the potential for misinterpretation and ensures that all team members are working towards the same goal.

3.1.1. Identifying Customer Needs

Identifying customer needs is a crucial step in problem definition, ensuring that the final product or solution addresses the actual requirements of end-users. This process involves engaging with various stakeholders to understand their explicit and implicit needs, preferences, and pain points, which can lead to products that are more likely to succeed in the market and provide higher customer satisfaction. Engineers can employ various methods such as

interviews, focus groups, surveys, and observation of product use in real-world settings to gather this information. For example, when designing a new electric vehicle, engineers might conduct interviews with potential users to understand their concerns about range anxiety, charging time, and performance expectations, observe how current electric vehicle owners interact with their cars to identify pain points in the user experience, and use surveys to gather quantitative data on preferences for specific features or price points. The ultimate goal is to create a comprehensive list of customer needs that can be translated into actionable design requirements, ensuring that the final product meets the actual needs and expectations of its intended users.

3.1.2. Collecting Information

Once customer needs are identified, the next step is to gather relevant information to inform the design process, involving thorough research on existing technologies, market trends, competitor products, and relevant regulations or standards. This comprehensive information gathering helps engineers avoid reinventing the wheel and allows them to build upon existing knowledge and best practices. The process can take many forms, including literature reviews, patent searches, benchmarking studies, and consultations with subject matter experts. For instance, in the electric vehicle example, engineers might review academic papers on battery technology advancements, analyze patents related to charging systems, benchmark competitor vehicles for performance and features, consult with materials scientists to understand the latest developments in lightweight materials for improved vehicle efficiency, and review industry standards and government

regulations to ensure compliance and identify potential design constraints. This thorough approach to information gathering ensures that engineers have a solid foundation of knowledge to inform their design decisions and ultimately create more innovative and effective solutions.

3.1.3. Generating Engineering Specifications

Generating engineering specifications involves translating customer needs and gathered information into measurable, quantifiable parameters that will guide the design process. This step bridges the gap between qualitative customer requirements and concrete design targets. According to Otto and Wood (2001), well-defined engineering specifications provide a clear set of objectives for the design team and serve as criteria for evaluating design concepts.

Engineering specifications should be specific, measurable, achievable, relevant, and time-bound (SMART). For the electric vehicle example, engineering specifications might include:

- Range: Minimum 500 km on a single charge
- Charging time: 80% charge in 30 minutes or less
- Acceleration: 0-100 kph in under 5 seconds
- Energy efficiency: At least 7 km per kWh
- Safety rating: 5-star NCAP rating

These specifications provide clear, quantifiable targets for the design team to work towards. Tools like Quality Function Deployment (QFD) can be used to systematically translate customer needs into engineering specifications, ensuring that each

specification is directly linked to one or more customer requirements (Hauser & Clausing, 1988).

3.1.4. Developing Product Design Specification (PDS)

The Product Design Specification (PDS) is a comprehensive document that consolidates all the information gathered in the previous steps into a single, authoritative reference for the design project, serving as a "contract" between the design team and stakeholders by clearly defining what the product must achieve and within what constraints. A well-developed PDS typically includes sections such as product identification and description, performance requirements, environmental conditions and constraints, life cycle considerations, safety and regulatory requirements, ergonomic and aesthetic considerations, and cost and schedule constraints. For an electric vehicle project, the PDS might include specific details like target market segment and price point, expected production volume and manufacturing constraints, sustainability goals, compatibility with existing charging infrastructure, noise and vibration limits, and expected product lifespan and warranty terms. As a living document, the PDS should be updated as new information becomes available or as project requirements evolve, serving as a central reference point throughout the design process to ensure that all team members and stakeholders have a shared understanding of the project goals and constraints (Dieter & Schmidt, 2021).

3.2. Research - Information Gathering

Information gathering is a critical step in the engineering design process, serving as the foundation for informed decision-making and innovative problem-solving. This phase involves

systematically collecting and analyzing relevant data from various sources to gain a comprehensive understanding of the problem at hand, existing solutions, and potential opportunities for innovation. According to Ulrich and Eppinger (2020), effective information gathering can significantly enhance the quality of design outcomes and reduce the risk of costly mistakes in later stages of development.

The process of information gathering is not a one-time event but rather an ongoing activity throughout the design process. As engineers delve deeper into the problem and generate potential solutions, they often need to revisit and expand their information base. This iterative approach allows for continuous refinement of ideas and ensures that the final design is grounded in a solid understanding of both the problem context and the latest technological advancements (Dieter & Schmidt, 2021).

3.2.1. Types and Sources of Information

The types of information needed in engineering design can be broadly categorized into technical, market, and regulatory domains. Technical information includes domain-specific knowledge, existing technologies, and scientific principles relevant to the problem. Market information encompasses customer needs, competitor products, and industry trends. Regulatory information covers standards, patents, and legal requirements that may impact the design (Pahl et al., 2007).

Sources of technical information include:

Scientific journals and conference proceedings: These provide cutting-edge research findings and technological advancements. For example, the Journal of Mechanical Design or

IEEE Transactions on Engineering Management offer valuable insights into the latest developments in mechanical engineering and engineering management, respectively.

Technical handbooks and textbooks: These serve as comprehensive references for established engineering principles and practices. The "Mechanical Engineer's Handbook" by Kutz (2015) is an excellent example of a resource covering a wide range of mechanical engineering topics.

Patent databases: These offer insights into existing solutions and can inspire new ideas. The United States Patent and Trademark Office (USPTO) database is a valuable resource for engineers to explore patented technologies.

Industry standards and specifications: Organizations like ASTM International, ISO, and IEEE provide standards that ensure compatibility, safety, and quality in engineering designs.

Market information can be gathered from:

Market research reports: These provide insights into industry trends, customer preferences, and market size. Reports from firms like Frost & Sullivan or IBISWorld can offer valuable market intelligence.

Customer surveys and interviews: Direct interaction with potential users can reveal unmet needs and preferences. Tools like SurveyMonkey or Qualtrics can be used to conduct online surveys efficiently.

Trade shows and exhibitions: These events showcase the latest products and technologies in specific industries, offering opportunities for benchmarking and networking.

Competitor product analysis: Examining existing products in the market can provide insights into current solutions and potential areas for improvement. Techniques like reverse engineering can be employed for in-depth analysis (Otto & Wood, 2001).

Regulatory information sources include:

Government agencies: Organizations like the Environmental Protection Agency (EPA) or the Occupational Safety and Health Administration (OSHA) provide regulations and guidelines that may impact product design.

Legal databases: Resources like LexisNexis or Westlaw offer access to legal documents, including regulations and case law relevant to product liability and safety.

Professional associations: Organizations such as the American Society of Mechanical Engineers (ASME) or the Institute of Electrical and Electronics Engineers (IEEE) often provide industry-specific guidelines and best practices.

Consultants and experts: Specialists in areas such as intellectual property law or environmental regulations can provide valuable insights into complex regulatory landscapes.

Effective information gathering often involves a combination of these sources, tailored to the specific needs of the project. Engineers must critically evaluate the reliability and relevance of each source, considering factors such as the credibility

of the author or organization, the recency of the information, and its applicability to the current design problem (Cross, 2008).

3.3. Project Planning

Project planning is a critical phase in the engineering design process that sets the foundation for successful project execution. It involves identifying key activities, establishing timelines, allocating resources, and creating a roadmap for achieving project objectives. According to Kerzner (2017), effective project planning is essential for minimizing risks, optimizing resource utilization, and ensuring that projects are completed on time and within budget.

In the context of engineering design, project planning takes on added significance due to the complex and often interdisciplinary nature of design projects. It requires a systematic approach that considers not only technical aspects but also organizational, financial, and human resource factors. As noted by Nicholas and Steyn (2017), a well-structured project plan serves as a communication tool, aligning team members and stakeholders around common goals and expectations.

3.3.1. Planning and Scheduling Techniques

Planning and scheduling techniques are methodologies used to organize project activities, establish timelines, and allocate resources effectively. These techniques help project managers and team members visualize the project's workflow, identify critical tasks, and manage dependencies between different project elements.

One commonly used planning technique is the Work Breakdown Structure (WBS). The WBS is a hierarchical decomposition of the project into smaller, more manageable

components. It provides a visual and textual representation of the project scope, breaking down complex tasks into simpler, actionable items. For example, in designing a new electric vehicle, the WBS might include top-level categories such as "Powertrain Design," "Body Design," and "Interior Design," each further broken down into specific tasks and subtasks (Project Management Institute, 2017).

Another important planning technique is the Critical Path Method (CPM), which identifies the sequence of dependent tasks that determine the minimum time needed to complete the project. By focusing on these critical tasks, project managers can prioritize resources and manage potential delays more effectively. For instance, in a building construction project, the critical path might include tasks such as site preparation, foundation laying, structural work, and finishing, with each task dependent on the completion of the previous one (Meredith et al., 2017).

3.3.2. Project Management Tools (Gantt Charts, CPM, PERT)

Project management tools are essential for visualizing, tracking, and controlling project progress. They provide a structured approach to managing complex projects and facilitate communication among team members and stakeholders.

Gantt charts are one of the most widely used project management tools. Developed by Henry Gantt in the early 20th century, these charts provide a graphical representation of project tasks over time. Each task is represented by a horizontal bar, with the length of the bar indicating the task's duration. Gantt charts allow project managers to visualize task dependencies, track progress, and

identify potential scheduling conflicts. For example, in a software development project, a Gantt chart might show tasks such as requirements gathering, design, coding, testing, and deployment, with their respective timelines and dependencies clearly illustrated (Lock, 2013).

The Critical Path Method (CPM) is both a planning technique and a project management tool. As a tool, CPM uses network diagrams to represent project activities and their dependencies. It calculates the longest path of planned activities to the end of the project, determining the earliest and latest start dates for each activity. This helps in identifying which activities are "critical" (i.e., they must be completed on time for the project to finish on schedule) and which have "float" (i.e., they can be delayed without affecting the project end date). For instance, in a product development project, CPM might reveal that prototype testing is on the critical path, while packaging design has some float (Kerzner, 2017).

The Program Evaluation and Review Technique (PERT) is another network-based tool that is particularly useful for projects with uncertain activity times. PERT uses probabilistic time estimates (optimistic, most likely, and pessimistic) for each activity to calculate the expected project duration. This makes it especially valuable for research and development projects where task durations are often difficult to predict accurately. For example, in a pharmaceutical drug development project, PERT could be used to estimate the overall project timeline considering the uncertainties in clinical trial durations (Nicholas & Steyn, 2017).

Modern project management software often integrates these tools, allowing for dynamic updating and real-time collaboration. Tools like Microsoft Project, Primavera, or web-based platforms like Asana or Trello provide comprehensive project management capabilities, combining Gantt charts, CPM, and resource allocation features in user-friendly interfaces. These digital tools enable project managers to quickly update schedules, track progress, and generate reports, enhancing overall project visibility and control (Schwalbe, 2015).

3.4. Concept Generation

Concept generation is a critical phase in the engineering design process where creativity and innovation take center stage. This stage involves the systematic exploration and creation of potential solutions to the defined problem or need. According to Ulrich and Eppinger (2020), effective concept generation can significantly influence the success of the final product, as it sets the foundation for all subsequent design activities.

During concept generation, engineers and designers aim to produce a wide range of diverse ideas, focusing on quantity rather than quality initially. This approach, often referred to as divergent thinking, allows for the exploration of novel and unconventional solutions that might otherwise be overlooked. As noted by Cross (2008), the goal is to create a rich pool of concepts from which the most promising ideas can be selected and further developed in later stages of the design process.

3.4.1. Creativity Methods (Brainstorming, 6-3-5 Method, Synectics)

Creativity methods are structured techniques used to stimulate innovative thinking and generate a large number of diverse ideas. These methods help overcome mental blocks and encourage thinking beyond conventional solutions.

Brainstorming is one of the most widely used creativity techniques. Developed by Alex Osborn in the 1950s, it involves a group of people generating ideas spontaneously to solve a specific problem. The key principles of brainstorming include deferring judgment, encouraging wild ideas, building on others' ideas, and focusing on quantity (Osborn, 1963). For example, a team designing a new electric vehicle might brainstorm ideas for improving battery efficiency, such as using solar panels, kinetic energy recovery systems, or even wireless charging roads.

The 6-3-5 Method, also known as Brainwriting, is a more structured approach to idea generation. In this method, six participants are asked to write down three ideas in five minutes, then pass their sheet to the next person who builds on or adds new ideas. This process continues until each sheet has been seen by all participants. This method encourages individual creativity and builds upon others' ideas without the potential for dominant personalities to overshadow quieter team members (Rohrbach, 1969). For instance, in a project to design a sustainable packaging solution, participants might generate ideas ranging from biodegradable materials to reusable containers to edible packaging.

Synectics is a problem-solving approach that uses analogies and metaphors to generate creative ideas. Developed by William J.J. Gordon in the 1960s, it involves making the familiar strange and the strange familiar (Gordon, 1961). This method often uses four types of analogies: direct (comparing to similar situations), personal (imagining oneself as the product), symbolic (using abstract comparisons), and fantasy (imagining impossible solutions). For example, when designing a new shock absorption system for a vehicle, engineers might draw inspiration from a kangaroo's legs (direct analogy), imagine being the shock absorber (personal analogy), think of the system as a sponge (symbolic analogy), or envision a car that floats above the road (fantasy analogy).

3.4.2. Functional Decomposition

Functional decomposition is a systematic approach to breaking down the overall function of a product or system into smaller, more manageable sub-functions. This method helps designers understand the complexity of the problem and identify potential solution principles for each sub-function.

The process typically begins by defining the overall function of the product in terms of its inputs and outputs. This is often represented as a "black box" model. For example, the function of a coffee maker might be "convert water and coffee grounds into brewed coffee." The next step is to break this down into sub-functions, such as "heat water," "mix water with coffee grounds," "filter brewed coffee," and "keep coffee warm" (Pahl et al., 2007).

Once the sub-functions are identified, they are typically arranged in a function structure diagram, showing the flow of

energy, material, and information between sub-functions. This visual representation helps designers identify key interfaces and potential areas for innovation. It also allows for the exploration of different ways to achieve the overall function by considering alternative arrangements or combinations of sub-functions (Ullman, 2015).

3.4.3. Morphological Method

The morphological method, developed by Fritz Zwicky in the 1960s, is a systematic approach to generating many potential solutions by combining different means of achieving each sub-function identified in the functional decomposition (Zwicky, 1969).

The process begins with creating a morphological chart, also known as a morphological box. This chart lists the sub-functions in one column and possible solutions (or means) for each sub-function in the corresponding row. For example, in designing a personal transportation device, the sub-functions might include "provide power," "control direction," and "support user." For each of these, various means might be listed:

- Provide power: electric motor, internal combustion engine, human power, compressed air

- Control direction: steering wheel, joystick, body lean, voice control

- Support user: seat, standing platform, harness, exoskeleton

The next step is to generate complete concepts by selecting one means from each row, creating different combinations. This can result in many potential solutions, some of which may be innovative or unexpected. For instance, combining "electric motor," "body

lean," and "standing platform" might result in a concept like an electric skateboard or hoverboard.

The morphological method is particularly useful for exploring a wide range of possibilities and identifying novel combinations that might not have been considered otherwise. However, it's important to note that not all combinations will be feasible or desirable, and further evaluation is necessary to select the most promising concepts (Ulrich & Eppinger, 2020).

3.5. Concept Evaluation and Selection

Concept evaluation and selection is a critical phase in the engineering design process that follows concept generation. This stage involves systematically assessing and comparing the generated concepts to identify the most promising solution(s) for further development. According to Ulrich and Eppinger (2020), effective concept selection can significantly influence the success of the final product, as it ensures that resources are focused on the most viable and potentially successful ideas.

During concept evaluation and selection, engineers employ various structured methods to objectively compare concepts against predetermined criteria. These methods help to minimize bias and ensure that decisions are based on a comprehensive assessment of each concept's strengths and weaknesses. As noted by Dieter and Schmidt (2021), the goal is not only to select the best concept but also to improve and combine concepts, potentially leading to even better solutions than those initially generated.

3.5.1. Pugh's Concept Selection Method

Pugh's Concept Selection Method, developed by Stuart Pugh in the 1980s, is a structured approach to concept evaluation that uses a matrix to compare multiple concepts against a set of criteria. This method is particularly useful for its simplicity and ability to handle many concepts (Pugh, 1991).

The process typically involves the following steps:

Choose evaluation criteria: These are typically derived from the product requirements and specifications.

Select a datum concept: This is usually an existing product or a well-understood concept that serves as a reference point.

Rate each concept: Concepts are compared to the datum using simple symbols (+, -, or S) for better, worse, or the same performance against each criterion.

Calculate scores: The number of +, -, and S ratings are tallied for each concept.

Rank the concepts: Based on the scores, concepts are ranked.

Combine and improve concepts: Insights from the evaluation are used to refine and potentially combine concepts.

Repeat the process: The evaluation is often repeated with a new datum or refined concepts.

For example, in designing a new electric toothbrush, criteria might include cleaning effectiveness, battery life, ergonomics, and cost. Concepts could be rated against a leading competitor's product

(the datum). A concept might receive a '+' for better battery life, a '-' for higher cost, and an 'S' for similar cleaning effectiveness.

One of the strengths of Pugh's method is its ability to highlight the relative strengths and weaknesses of each concept, facilitating concept improvement. However, it does not account for the relative importance of different criteria, which can be a limitation in some cases (Burge, 2009).

3.5.2. Weighted Decision Matrix

The Weighted Decision Matrix, also known as the Decision Matrix Method or Pugh Matrix, is an enhanced version of Pugh's method that incorporates the relative importance of evaluation criteria. This method is particularly useful when some criteria are more critical to the success of the product than others (Ulrich & Eppinger, 2020).

The process for creating and using a Weighted Decision Matrix typically involves:

Identify evaluation criteria: Like Pugh's method, these are derived from product requirements.

Assign weights to criteria: Each criterion is given a numerical weight based on its importance.

Establish rating scale: A numerical scale (e.g., 1-5 or 1-10) is defined for rating concepts against each criterion.

Rate each concept: Each concept is rated against each criterion using the established scale.

Calculate weighted scores: The rating for each criterion is multiplied by its weight, and these are summed for each concept.

Rank concepts: Concepts are ranked based on their total weighted scores.

For example, in designing a new smartphone, criteria might include battery life (weight: 0.3), camera quality (weight: 0.25), processing speed (weight: 0.2), durability (weight: 0.15), and aesthetics (weight: 0.1). Each concept would be rated on a scale of 1-5 for each criterion, and these ratings would be multiplied by the respective weights to calculate a total score.

The Weighted Decision Matrix provides a more nuanced evaluation than Pugh's method, as it accounts for the varying importance of different criteria. However, it requires more upfront effort to establish weights and can be more time-consuming for many concepts (Burge, 2009).

Both Pugh's method and the Weighted Decision Matrix are valuable tools in concept evaluation and selection. The choice between them often depends on the complexity of the design problem, the number of concepts being evaluated, and the need for differentiation between criteria importance. In many cases, designers may use Pugh's method for initial screening of many concepts, followed by a Weighted Decision Matrix for more detailed evaluation of the most promising options (Dieter & Schmidt, 2021).

4. Phase II: Embodiment Design

Embodiment design is a crucial phase in the product development process that bridges the gap between conceptual design

and detailed design. It involves transforming abstract concepts into concrete, feasible product structures while considering technical and economic criteria. According to Pahl and Beitz (2007), embodiment design aims to develop the design concept to a stage where subsequent detailed design can lead directly to production.

During this phase, engineers and designers work on refining the chosen concept, determining the overall layout of the product, and making key decisions about materials, manufacturing processes, and component interactions. The embodiment design phase is characterized by its iterative nature, as designers continuously evaluate and optimize the product structure to meet performance requirements, cost constraints, and manufacturability criteria (Ullman, 2015). This stage typically encompasses three main aspects: product architecture, configuration design, and parametric design.

4.1. Product Architecture

Product architecture refers to the arrangement of functional elements into physical chunks and the specification of interfaces between these chunks (Ulrich & Eppinger, 2020). It is a critical aspect of embodiment design that significantly influences product performance, variety, and manufacturability.

The process of defining product architecture typically involves:

Creating a schematic of the product

Clustering elements of the schematic

Creating a rough geometric layout

Identifying fundamental and incidental interactions

For example, in designing a new smartphone, the product architecture would involve decisions about the placement of components like the battery, processor, camera modules, and display. The designer might choose a modular architecture where components can be easily replaced or upgraded, or an integral architecture for a slimmer profile and potentially better performance.

Product architecture also plays a crucial role in product family design. For instance, Black & Decker revolutionized its power tool line by adopting a modular architecture with a common motor and handle design across various tools. This approach allowed for significant cost savings in manufacturing and increased product variety (Meyer & Lehnerd, 1997).

4.2. Configuration Design

Configuration design focuses on determining the general shape and relative positioning of components within the product. This stage involves establishing spatial constraints, creating and refining interfaces between components, and beginning to consider manufacturing processes (Dieter & Schmidt, 2021).

Key activities in configuration design include:

Determining the spatial arrangement of components

Defining critical dimensions

Selecting materials

Considering assembly and manufacturing processes

For example, in the design of an electric vehicle, configuration design would involve decisions about the placement of the battery pack, motor(s), and power electronics. The designer must consider factors such as weight distribution, thermal management, and crash safety while arranging these components.

Another example is the configuration design of a laptop computer. The designer must determine how to arrange components like the motherboard, battery, cooling system, and various ports within the limited space of the chassis. This involves careful consideration of heat dissipation, user ergonomics, and manufacturing constraints.

4.3. Parametric Design

Parametric design involves defining and manipulating the key parameters that control the product's geometry and performance. This approach allows for rapid exploration of design alternatives and optimization of the product's characteristics (Woodbury, 2010).

In parametric design, designers typically:

Identify key design parameters

Establish relationships between parameters

Create a parametric model

Explore design variations by adjusting parameters

For example, in the design of an aircraft wing, parametric design would allow engineers to easily adjust parameters such as wingspan, chord length, and airfoil shape. By linking these parameters to performance metrics like lift, drag, and structural

integrity, designers can quickly evaluate numerous design iterations to find the optimal configuration.

Another application of parametric design can be seen in architecture. For instance, the Beijing National Stadium (Bird's Nest) for the 2008 Olympics used parametric design to optimize the complex steel structure. The designers created a parametric model that allowed them to adjust the density and arrangement of the steel members while maintaining structural integrity and achieving the desired aesthetic effect (Kolarevic, 2005).

Parametric design is particularly powerful when combined with optimization algorithms. For instance, in the automotive industry, engineers use parametric models of car bodies coupled with computational fluid dynamics (CFD) simulations to optimize aerodynamics. By automatically adjusting parameters like hood angle, windshield rake, and rear spoiler geometry, they can find configurations that minimize drag while maintaining other design constraints (Yang et al., 2018).

5. Phase III: Detail Design

Detail design is the final phase of the engineering design process, where the conceptual and embodiment designs are transformed into a complete and precise description of the product. This stage involves creating comprehensive documentation that will guide the manufacturing, assembly, and quality control processes. According to Dieter and Schmidt (2021), detail design is critical for ensuring that the product can be manufactured efficiently, meets all specifications, and performs as intended.

During the detail design phase, engineers focus on specifying every aspect of the product, including exact dimensions, tolerances, materials, surface finishes, and manufacturing processes. This phase requires close collaboration between design engineers, manufacturing engineers, and suppliers to ensure that the design is optimized for production. As noted by Ullman (2015), the success of a product in the market often hinges on the quality and thoroughness of the detail design phase.

5.1. Preparation of Detailed Technical Drawings

Detailed technical drawings, also known as engineering drawings or working drawings, are the primary means of communicating design information to manufacturing teams. These drawings provide a complete and unambiguous description of each part and assembly in the product (Bertoline & Wiebe, 2009).

Key elements of detailed technical drawings include:

Orthographic projections: Multiple views (front, top, side) showing the exact shape of the part.

Dimensions and tolerances: Precise measurements and allowable variations for each feature.

Surface finish specifications: Indications of required surface texture and quality.

Material specifications: Clear identification of the material for each part.

Assembly drawings: Illustrations showing how individual parts fit together.

For example, in the design of a bicycle crankset, the detailed drawing would include:

- Multiple views of the crank arm, chainrings, and bottom bracket

- Precise dimensions for the crank length, bolt circle diameter, and spindle interface

- Tolerances for critical features like the pedal thread and bottom bracket interface

- Surface finish requirements for the crank arm faces and chainring teeth

- Material specifications (e.g., 7075-T6 aluminum for the crank arms)

- Assembly drawing showing how the crank arms, chainrings, and bottom bracket fit together

Modern detail design often utilizes 3D CAD software, which can generate both 3D models and 2D drawings. This approach allows for easier visualization, interference checking, and revision management (Narayan et al., 2008).

5.2. Material Information and Bill of Materials

The Bill of Materials (BOM) is a comprehensive list of all parts, components, assemblies, and materials required to manufacture a product. It serves as a critical document for procurement, manufacturing planning, and inventory management (Stark, 2015).

A typical BOM includes:

Part number: A unique identifier for each component

Part name: A descriptive name for each item

Quantity: The number of each part required per assembly or product

Unit of measure: The unit used for quantifying each item (e.g., pieces, meters, kilograms)

Material specification: Detailed description of the material for each part

Supplier information: For purchased components or materials

Revision level: To track changes and ensure the correct version is used

For example, a BOM for an electric scooter might include:

- Frame assembly (1 pc, aluminum alloy 6061-T6)

- Lithium-ion battery pack (1 pc, 36V 10Ah)

- Brushless DC motor (1 pc, 350W)

- Controller (1 pc)

- Wheels (2 pcs, 8.5-inch pneumatic tires)

- Brake system (1 set, disc brakes)

- Handlebar assembly (1 pc, includes grips and controls)

- Fasteners (various types and quantities)

Material information in the BOM should be detailed enough to ensure that the correct materials are procured and used in

manufacturing. This may include specific grades, heat treatments, or other processing requirements. For instance, the frame material might be specified as "Aluminum alloy 6061-T6, extruded and heat-treated to achieve minimum yield strength of 240 MPa" (Ashby, 2016).

5.3. Manufacturing Operations and Process Sheets

Manufacturing operations and process sheets provide detailed instructions for producing each part and assembling the final product. These documents bridge the gap between design and manufacturing, ensuring that the product can be produced efficiently and consistently (Groover, 2019).

A typical process sheet includes:

Part identification (name, number, revision)

Raw material specification

Sequence of operations

Machine or equipment to be used for each operation

Tooling requirements

Setup instructions

Process parameters (e.g., cutting speeds, feed rates, temperatures)

Inspection requirements and quality control checks

For example, a process sheet for manufacturing a bicycle frame tube might include:

Cut 6061-T6 aluminum tubing to length (1000mm ±0.5mm) using a circular saw

Deburr cut ends using a bench grinder

CNC machine miter joints at both ends (setup details and G-code program reference)

Clean and degrease the tube

Perform heat treatment (solution treat at 530°C for 1 hour, water quench, age at 175°C for 8 hours)

Inspect dimensions and surface finish

Apply surface treatment (anodize to Type II, Class 1 specification)

In modern manufacturing environments, process planning is often aided by Computer-Aided Process Planning (CAPP) systems. These systems can automatically generate process plans based on part geometry, material properties, and available manufacturing resources, significantly reducing planning time and improving consistency (Wang, 2013).

6. Advanced Concepts in Engineering Design

As engineering design has evolved, several advanced concepts and methodologies have emerged to enhance the efficiency, quality, and innovation of the design process. These concepts go beyond traditional sequential design approaches, leveraging interdisciplinary collaboration, computational power, and advanced technologies to address the increasing complexity of modern engineering challenges. According to Prasad (1996), these advanced concepts aim to reduce time-to-market, improve product

quality, and optimize resource utilization throughout the product lifecycle.

The integration of advanced concepts such as Concurrent Engineering, Modeling and Simulation, Optimization Techniques, and Computer-Aided Design and Manufacturing (CAD/CAM) has revolutionized the engineering design landscape. These approaches enable engineers to make more informed decisions earlier in the design process, predict product performance with greater accuracy, and streamline the transition from design to manufacturing. As noted by Suh (2001), these advanced concepts collectively contribute to a more holistic and efficient design process, allowing for the creation of more innovative and competitive products.

6.1. Concurrent Engineering

Concurrent Engineering (CE) is an approach that emphasizes the parallelization of tasks and integration of various aspects of product development, including design, manufacturing, and support. This methodology aims to reduce the time and cost of product development while improving quality by considering all elements of the product lifecycle from the outset (Prasad, 1996).

Key principles of Concurrent Engineering include:

Cross-functional teams: Bringing together experts from different disciplines to collaborate from the early stages of design.

Parallel activities: Conducting various development tasks simultaneously rather than sequentially.

Early consideration of manufacturing and lifecycle issues: Addressing potential production and support challenges during the design phase.

For example, in the automotive industry, CE has been widely adopted to reduce development time and costs. When designing a new vehicle model, teams of designers, engineers, manufacturing specialists, and marketing professionals work together from the concept stage. This allows for simultaneous consideration of aesthetics, performance, manufacturability, and market requirements. Issues that might traditionally be discovered late in the process, such as assembly difficulties or maintenance challenges, can be identified and addressed early on, leading to a more optimized final product (Sapuan, 2005).

Another example of CE implementation can be seen in the aerospace industry. When developing new aircraft, companies like Boeing use Integrated Product Teams (IPTs) that bring together experts from various disciplines. These teams work concurrently on different aspects of the aircraft, such as aerodynamics, structures, systems, and manufacturing. This approach allows for rapid iteration and problem-solving, ensuring that design decisions consider impacts across all areas of the aircraft's lifecycle (Pardessus, 2004).

6.2. Modeling and Simulation

Modeling and Simulation (M&S) are powerful tools in engineering design that allow for the virtual representation and analysis of products, systems, and processes before physical prototypes are built. These techniques enable engineers to predict

performance, identify potential issues, and optimize designs in a cost-effective and time-efficient manner (Banks et al., 2010).

Types of modeling and simulation in engineering design include:

Computer-Aided Engineering (CAE): Using computer software to analyze the geometry of parts and assemblies to simulate real-world physical behavior.

Finite Element Analysis (FEA): A numerical method for solving problems of engineering and mathematical physics, particularly useful for structural analysis.

Computational Fluid Dynamics (CFD): Simulation of fluid flows and heat transfer.

Multibody Dynamics: Simulation of the motion of interconnected rigid or flexible bodies.

An example of M&S in action is the use of FEA in the design of aircraft components. Engineers can create detailed models of structural elements like wings or fuselage sections and subject them to simulated loads representing different flight conditions. This allows for the optimization of material usage and structural design without the need for extensive physical testing, significantly reducing development time and costs (Rao, 2018).

Another example is the use of CFD in automotive design. Engineers can simulate airflow around vehicle bodies to optimize aerodynamics, reducing drag and improving fuel efficiency. For instance, Formula 1 teams extensively use CFD to refine the aerodynamic properties of their race cars, testing hundreds of design

iterations virtually before building physical prototypes (Hucho, 2013).

6.3. Optimization Techniques

Optimization techniques in engineering design involve the systematic selection of the best solution from a set of available alternatives, based on specific criteria or objectives. These methods aim to maximize performance, minimize costs, or achieve the best trade-off between multiple competing objectives (Arora, 2016).

Common optimization techniques in engineering design include:

Gradient-based methods: Such as steepest descent or Newton's method, used for continuous optimization problems.

Genetic Algorithms: Evolutionary algorithms inspired by natural selection, useful for complex, non-linear problems.

Particle Swarm Optimization: A population-based stochastic optimization technique inspired by social behavior of bird flocking or fish schooling.

Topology Optimization: A method that optimizes material layout within a given design space, for a given set of loads and boundary conditions.

An example of optimization in engineering design is the use of topology optimization in aerospace structural design. Engineers can define a design space, loads, and constraints, and the algorithm will determine the optimal distribution of material to achieve the lightest possible structure that meets all strength and stiffness

requirements. This approach has led to the development of highly efficient, lightweight components in aircraft and spacecraft design (Bendsøe & Sigmund, 2003).

Another example is the use of multi-objective optimization in automotive powertrain design. Engineers might seek to simultaneously optimize fuel efficiency, performance, and emissions. Genetic algorithms can be employed to explore a vast design space, considering variables such as engine geometry, transmission ratios, and control strategies. This approach allows for the discovery of non-intuitive solutions that balance multiple competing objectives (Deb, 2001).

6.4. Computer-Aided Design (CAD) and Manufacturing (CAM)

Computer-Aided Design (CAD) and Computer-Aided Manufacturing (CAM) are technologies that use computer systems to aid in the creation, modification, analysis, and optimization of a design (CAD) and to plan, manage, and control manufacturing operations (CAM). The integration of CAD and CAM systems has revolutionized the product development process, enabling seamless transition from design to production (Groover & Zimmers, 1983).

Key aspects of CAD/CAM include:

3D Modeling: Creation of detailed three-dimensional representations of parts and assemblies.

Parametric Design: Ability to define relationships between design elements, allowing for easy modifications and design variations.

Simulation and Analysis: Integration with CAE tools for performance prediction and optimization.

Automated Manufacturing: Generation of toolpaths and machine instructions directly from CAD models.

An example of CAD/CAM integration can be seen in the mold-making industry. Engineers use CAD software to design complex plastic parts, complete with detailed features like ribs, bosses, and snap-fits. The CAD model is then used directly in CAM software to generate toolpaths for CNC machining of the mold. This seamless integration ensures that the manufactured mold accurately reflects the intended design, reducing errors and iterations in the mold-making process (Kuang-Hua, 2018).

Another example is in the aerospace industry, where CAD/CAM integration is crucial for manufacturing complex components like turbine blades. Engineers use advanced CAD software to design airfoil shapes optimized for aerodynamic performance. These designs are then directly translated into CAM instructions for five-axis CNC machining or additive manufacturing processes. This integration allows for the production of highly complex geometries that would be extremely difficult or impossible to manufacture using traditional methods (Kalpakjian & Schmid, 2014).

In the field of mechanical engineering, advanced concepts play a vital role in enhancing the efficiency and effectiveness of the design process. These concepts, which include Concurrent Engineering, Modeling and Simulation, Optimization Techniques, and Computer-Aided Design and Manufacturing (CAD/CAM),

allow engineers to address the complexities of modern product development. By integrating these methodologies, engineers can streamline workflows, reduce time-to-market, and improve product quality. The incorporation of these advanced techniques not only fosters innovation but also ensures that products are designed with a comprehensive understanding of their lifecycle, from conception to retirement.

Understanding and implementing these advanced concepts is essential for mechanical engineering students as they prepare for their graduation projects and future careers. Each of these methodologies offers unique advantages that can significantly impact the overall success of a project. For instance, Concurrent Engineering promotes collaboration across disciplines, enhancing communication and reducing design iterations. Meanwhile, Modeling and Simulation provide valuable insights into product performance before physical prototypes are built, allowing for better decision-making. Optimization Techniques enable engineers to refine designs for maximum efficiency, while CAD/CAM systems facilitate seamless transitions from design to manufacturing. Mastering these concepts equips students with the skills necessary to tackle real-world engineering challenges effectively.

As the students embark on their engineering design journey, it is crucial to embrace these advanced concepts and apply them to their graduation projects. By doing so, they will not only enhance the quality and functionality of their designs but also develop a deeper understanding of the engineering process as a whole. One has to remember that the iterative nature of engineering design allows for continuous improvement and learning, so the students should be

open to revisiting and refining their ideas. Ultimately, the knowledge and experience gained from applying these advanced methodologies will serve as a strong foundation for their future endeavors in the field of mechanical engineering.

7. Conclusion

The engineering design process is a structured, iterative approach that guides mechanical engineering students through the complex journey of product development. From problem identification to final implementation, this process provides a systematic framework for addressing engineering challenges. As we have explored in this chapter, the process begins with a thorough understanding of customer needs and problem definition, progresses through creative concept generation and rigorous evaluation, and culminates in detailed design and production planning. Each phase builds upon the previous one, with continuous refinement and improvement at every step. The integration of advanced concepts such as concurrent engineering, modeling and simulation, and computer-aided design and manufacturing further enhances the efficiency and effectiveness of the design process.

Throughout this chapter, we have emphasized the importance of a holistic approach to engineering design. This includes not only the technical aspects of product development but also considerations for manufacturing, distribution, use, and eventual retirement of the product. By adopting this comprehensive perspective, engineers can create solutions that are not only functionally superior but also economically viable, environmentally sustainable, and user-friendly. The various tools and techniques discussed, from quality function deployment to morphological analysis and decision matrices,

provide students with a robust toolkit for tackling complex design challenges. These methodologies foster critical thinking, creativity, and systematic problem-solving skills that are essential for success in the field of mechanical engineering.

As mechanical engineering students embark on their graduation projects, the principles and practices outlined in this chapter serve as a valuable guide. However, it's crucial to remember that engineering design is not a rigid, linear process but a flexible and iterative one. Real-world design challenges often require engineers to revisit and refine earlier stages as new information becomes available or unexpected obstacles arise. The ability to navigate this iterative process, to learn from failures, and to continuously improve designs is what distinguishes successful engineers. By applying these concepts to their graduation projects, students not only create innovative solutions but also develop the critical skills and mindset necessary for their future careers in mechanical engineering. As they move forward, students are encouraged to embrace the challenges, remain curious, and continue to refine their design skills through practice and lifelong learning.

References

Arora, J. S. (2016). *Introduction to optimum design* (4th ed.). Academic Press.

Ashby, M. F. (2016). *Materials selection in mechanical design* (5th ed.). Butterworth-Heinemann.

Banks, J., Carson II, J. S., Nelson, B. L., & Nicol, D. M. (2010). *Discrete-event system simulation* (5th ed.). Prentice Hall.

Bendsøe, M. P., & Sigmund, O. (2003). *Topology optimization: Theory, methods, and applications*. Springer.

Bertoline, G. R., & Wiebe, E. N. (2009). *Fundamentals of graphics communication* (6th ed.). McGraw-Hill.

Burge, S. (2009). *The systems engineering tool box - Pugh matrix*. Burge Hughes Walsh.

Chakrabarti, A., & Blessing, L. T. (2014). *An anthology of theories and models of design: Philosophy, approaches and empirical explorations*. Springer.

Chandrasegaran, S. K., Ramani, K., Sriram, R. D., Horváth, I., Bernard, A., Harik, R. F., & Gao, W. (2013). The evolution, challenges, and future of knowledge representation in product design systems. *Computer-Aided Design*, 45(2), 204-228.

Cross, N. (2008). *Engineering design methods: Strategies for product design* (4th ed.). John Wiley & Sons.

Dieter, G. E., & Schmidt, L. C. (2021). *Engineering design* (6th ed.). McGraw-Hill Education.

Dym, C. L., Agogino, A. M., Eris, O., Frey, D. D., & Leifer, L. J. (2005). Engineering design thinking, teaching, and learning. *Journal of Engineering Education, 94*(1), 103-120.

Gordon, W. J. J. (1961*). Synectics: The development of creative capacity*. Harper & Row.

Groover, M. P. (2010). *Fundamentals of modern manufacturing: Materials, processes, and systems* (4th ed.). John Wiley & Sons.

Hauser, J. R., & Clausing, D. (1988). The house of quality. *Harvard Business Review, 66*(3), 63-73.

Hucho, W. H. (2013). *Aerodynamics of road vehicles: From fluid mechanics to vehicle engineering*. Butterworth-Heinemann.

Juran, J. M., & De Feo, J. A. (2010). *Juran's quality handbook: The complete guide to performance excellence* (6th ed.). McGraw-Hill Education.

Kalpakjian, S., & Schmid, S. R. (2014). *Manufacturing engineering and technology* (7th ed.). Pearson.

Kerzner, H. (2017). *Project management: A systems approach to planning, scheduling, and controlling* (12th ed.). John Wiley & Sons.

Kolarevic, B. (2005). *Architecture in the digital age: Design and manufacturing*. Taylor & Francis.

Kuang-Hua, C. (2018). *e-Design: Computer-aided engineering design*. Academic Press.

Lock, D. (2013). *Project management* (10th ed.). Gower Publishing, Ltd.

Meredith, J. R., Shafer, S. M., & Mantel Jr, S. J. (2017). *Project management: A strategic managerial approach* (10th ed.). John Wiley & Sons.

Meyer, M. H., & Lehnerd, A. P. (1997). *The power of product platforms*. Free Press.

Narayan, K. L., Rao, K. M., & Sarcar, M. M. M. (2008). *Computer aided design and manufacturing*. Prentice Hall of India.

National Academy of Engineering. (2004). *The engineer of 2020: Visions of engineering in the new century*. National Academies Press.

Nicholas, J. M., & Steyn, H. (2017). *Project management for engineering, business and technology* (5th ed.). Routledge.

Otto, K. N., & Wood, K. L. (2001). *Product design: Techniques in reverse engineering and new product development*. Prentice Hall.

Osborn, A. F. (1963). *Applied imagination: Principles and procedures of creative problem solving* (3rd ed.). Charles Scribner's Sons.

Pahl, G., Beitz, W., Feldhusen, J., & Grote, K. H. (2007). *Engineering design: A systematic approach* (3rd ed.). Springer.

Pardessus, T. (2004). Concurrent engineering development and practices for aircraft design at Airbus. *In Proceedings of the 24th ICAS Conference*, Yokohama, Japan (pp. 1-8).

Prasad, B. (1996). *Concurrent engineering fundamentals (Vol. 1)*. Prentice Hall.

Project Management Institute. (2017). *A guide to the project management body of knowledge (PMBOK guide)* (6th ed.). Project Management Institute.

Pugh, S. (1991). *Total design: Integrated methods for successful product engineering.* Addison-Wesley.

Rao, S. S. (2018). *The finite element method in engineering* (6th ed.). Butterworth-Heinemann.

Rohrbach, B. (1969). Kreativ nach Regeln – Methode 635, eine neue Technik zum Lösen von Problemen. *Absatzwirtschaft, 12(19)*, 73-75.

Sapuan, S. M. (2005). Concurrent engineering in the automotive industry. In A. Y. C. Nee, S. K. Ong, & Y. F. Zhang (Eds.), *Advanced concurrent engineering* (pp. 39-46). World Scientific.

Schwalbe, K. (2015). *Information technology project management* (8th ed.). Cengage Learning.

Stark, J. (2015). *Product lifecycle management (Volume 1): 21st century paradigm for product realisation* (3rd ed.). Springer.

Suh, N. P. (2001). *Axiomatic design: Advances and applications*. Oxford University Press.

Ullman, D. G. (2015). *The mechanical design process* (5th ed.). McGraw-Hill Education.

Ulrich, K. T., & Eppinger, S. D. (2020). *Product design and development* (7th ed.). McGraw-Hill Education.

Wang, L. (2013). Machine availability monitoring and machining process planning towards Cloud manufacturing. *CIRP Journal of Manufacturing Science and Technology, 6*(4), 263-273.

Woodbury, R. (2010). *Elements of parametric design*. Routledge.

Yang, X., Xia, Y., Luo, Q., & Guo, X. (2018). Aerodynamic shape optimization for high-speed train using parametric design. *Journal of Wind Engineering and Industrial Aerodynamics*, 175, 177-186.

Zwicky, F. (1969). *Discovery, invention, research through the morphological approach*. Macmillan.


BİDGE